INVESTIGATIONS OF MULTILAYERED III-V COMPOUND STRUCTURES GROWN BY LIQUID PHASE EPITAXY

A Thesis submitted
to the
University of Mumbai
for the

Ph. D. (Science) Degree
in Physics

Submitted By

Shri S. S. CHANDVANKAR

Under the Guidance of

Prof. B. M. Arora

Tata Institute of Fundamental Research
Homi Bhabha Road, Mumbai – 400 005

December 2004

STATEMENT BY THE CANDIDATE

As required by the University Ordinance 770, I wish to state that the work embodied in this thesis titled **“ Investigations of multilayered III-V compound structures grown by liquid phase epitaxy ”** forms my own contribution to the research work carried out under the guidance of Prof. B. M. Arora at the Department of Condensed Matter Physics and Materials Science, Tata Institute of Fundamental Research, Mumbai this work has not been submitted for any other degree of this or any other University. Whenever references have been made to previous works of others, it has been clearly indicated as such and included in the Bibliography.

Signature of candidate

Name - Shri S. S. Chandvankar

Certified by

Signature of Guide

Name - Prof. B. M. Arora

Statement required under ordinance 771

This thesis describes results obtained during the " Investigations of multilayered III-V compound structures grown by liquid phase epitaxy ". The new facts that have emerged from this work are:

1] AlGaAs based strained heterostructures could be grown using low temperature liquid phase epitaxy. A piston graphite boat is found suitable for low temperature (700^0-400^0C) liquid phase epitaxy.

2] Thin epitaxial layers (about 50nm thick), for the active layer of laser diodes can be synthesized reproducibly using this technique.

3] Fully strained, defect-free, thin pesudomorphic layers such as GaAsP and GaAsSb could be synthesized on GaAs substrates using LPE. These layers are of device quality and can be used for the active region of strained-layer laser diodes.

4] A disadvantage of piston boat is an unavoidable mixing of successive solutions with the preceding ones. About 3-7% Al is incorporated in GaAs grown from a solution that displaces the solution used for growing $Al_{0.3}Ga_{0.7}As$ layer.

5] Emission wavelength of laser diode fabricated from such heterostructure with GaAs active layer is in 820-850nm range. This variation is due to aluminium incorporation in the active layer because of solution intermixing.

6] Incorporation of P produces tensile strain whereas compressive strain is produced by incorporation of Sb. Thus, with P incorporation lasers emitting at 795, 818, 830 and 833nm are obtained whereas with Sb incorporation, lasers emitting at 855, 870, 880 and 900nm are obtained. It is shown by x-ray measurements that the layers are pseudomorphically strained.

Dedicated to

My Parents, Family Members,
Teachers
And Colleagues at TIFR

Contents

Acknowledgements
List of publications

Chapter 1: Semiconductor heterostructures and applications

1.1 Multilayered heterostructures and III-V compounds 1
1.2 Development of heterostructures for semiconductor lasers 3
1.3 Growth of ultrathin (quantum well) and strained layers using LPE 6
1.4 Current status of LPE in industry 7
    References 8

Chapter 2: Experimental techniques

2.1 Epitaxy 10
2.2 Methods of LPE 11
2.3 LPE growth techniques 13
2.4 Heterostructures grown by LPE 15
2.5 LPE work at TIFR 16
    2.5.1 Graphite boat fabricated at TIFR 17
    2.5.2 Graphite boat fabricated at Ioffe Institute, Russia 18
    2.5.3 Benefits and shortcomings of a piston boat 20
2.6 Growth reactor used for LPE work 21
2.7 Growth of single layers: GaAs and AlGaAs 23
2.8 Synthesis of heterostructures 24
2.9 Phase diagram information and analysis 24
    2.9.1 Phase diagram calculations for GaAs-GaP 25
    2.9.2 Phase diagram calculations for GaAs-GaSb 27
2.10 Characterization techniques for epitaxial layers and heterostructures 28
    2.10.1 Surface morphology and layer thickness 28
    2.10.2 Hall measurements 29
    2.10.3 ECV profile measurements 30
    2.10.4 Photoluminescence measurements 32

2.10.5 X-ray measurements 34
2.11 Fabrication of laser diodes 40
References 42

Chapter 3: Growth experiments and materials characterization.

3.1 Growth experiments 45
3.2 Growth experiments using graphite boat made at TIFR 46
3.2.1 Growth of single layers of undoped GaAs 46
3.2.2 Growth of single layers of p-doped GaAs 47
3.2.3 Growth of single layers of n and p-doped AlGaAs 48
3.2.4 Attempts to synthesize multilayered structures 49
3.3 Growth experiments using graphite boat made at Ioffe Institute, Russia 50
3.3.1 Growths of single layers 50
3.3.2 Growth of DH structures 50
3.3.3 Growth of SCH laser structures 50
3.3.4 Growth of strained SCH laser structures 52
3.4 Results of characterization of the materials/heterostructures 53
3.4.1 Surface morphology 53
3.4.2 Thickness of the epi layers 55
3.4.3 Electrical measurements 56
3.4.4 Electrochemical voltage etch profile measurements 59
3.4.5 Optical measurements 60
3.4.6 X-ray measurements 65
References 70

Chapter 4: Electro-optic characterization of heterostructures and laser diodes.

4.1 (L-I) - Light output-current characteristics of laser diodes 71
4.2 EL – Electroluminescence characteristics of laser diodes 73
4.3 Wavelength tuning by incorporating Sb or P in the active layer 75

4.4 Change in band gap due to strain in the heterostructures 76
4.5 Estimation of composition of active layers: problem of mixing of solutions 77
4.6 Incorporation of P/Sb in the active layer 78
4.7 Effect of strain on growth process 80
References 81

Chapter 5: Summary and scope for further work

5.1 Summary 82
5.2 Scope for further work 83

Bibliography 84

Synopsis 89

Acknowledgements

I am deeply indebted to Prof. B. M. Arora for the guidance and support in this work. He suggested this rather challenging problem to me and helped me at every stage of the work. I am thankful to Dr. S. Subramanian for introducing me to the art and science of liquid phase epitaxy (LPE). He trained me in handling the experimental set up used for liquid phase epitaxy in our laboratory.

I am thankful to Mr. Jhanje and Mr. Panchal of glass blowing section who fabricated the graphite boat used in early stage of this work. Dr. V. P. Khvostikov, of A. F. Ioffe Physico-Technical Institute, St. Petersburg, Russia visited our laboratory in May 1997 and gave me several hints and suggestions in synthesizing the laser structures using the graphite piston boat made in TIFR. During my visit to A. F. Ioffe Physico-Technical Institute in November 1997, Dr. V. P. Khvostikov, Dr. V. R. Larionov, Prof. V. M. Andreev and his colleagues helped me in designing and fabricating the piston boat. I am very much thankful to them all.

Special thanks are due to my colleagues at TIFR who have helped me in many ways. Mrs. A. A. Sardesai, Mrs. A. D. Deorukhkar, and Mrs. Veera Mistry helped me in sample preparation for growth experiments, and in lapping the samples for devices. Mr. Amit Shah helped in Hall measurements, device fabrication and characterization of laser diodes. Dr. Sonali Banerjee helped in carrying out photoluminescence measurements on samples grown using boat fabricated in TIFR. Mr. Mahesh Gokhale and Prof. K. S. Chandrasekaran helped in XRD measurements and analysis of the data. Mr. Subhash Lokhre, Dr. Milind Purandare and Mrs. Shilpa Chalke helped in recording SEM images and EDX measurements. I am especially thankful to Dr. Arnab Bhattacharya for developing the process for laser diode fabrication. Thanks to Prof. K. L. Narsihman and Dr. Sandeep Ghosh for discussions and useful suggestions.

List of Publications

In Journals -

1] Doping and surface morphology of AlGaAs/GaAs grown at low temperature by liquid phase epitaxy.
S. S. Chandvankar, A. P. Shah and B. M. Arora,
Journal of Crystal Growth, 186 (1998) 329.

2] Synthesis of AlGaAs based strained separately confined heterostructure laser diodes by low temperature liquid-phase epitaxy.
S. S. Chandvankar, A. P. Shah, A. Bhattacharya, K. S. Chandrasekaran, and B. M. Arora,
Journal of Crystal Growth, 260 (2004) 348.

In Proceedings -

1] Synthesis of device quality strained heterostructure $Al_{0.3}Ga_{0.7}As$/GaAsSb/ $Al_{0.3}Ga_{0.7}As$ by liquid phase epitaxy.
S. S. Chandvankar, S. Banerjee, G. Fernandes, A. K. Srivastava and B. M. Arora,
Proceedings of the Conference on Emerging Optoelectronic Technologies (CEOT-94), Bangalore, (1994) 377.

2] Synthesis of 730-850 nm SCH laser diodes by low temperature liquid phase epitaxy.
S. S. Chandvankar, A. P. Shah, A. Bhattacharya, K. S. Chandrasekaran, and B. M. Arora,
Proceedings: Photonics-2000, International Conference on Fiber Optics and Photonics, Calcutta, Vol. 1, (2000) 203.

3] An attempt to synthesize 850-900nm SCH laser diodes by low temperature liquid phase epitaxy.
S. S. Chandvankar, A. P. Shah, A. Bhattacharya, K. S. Chandrasekaran, and B. M. Arora,
Proceedings, Eleventh International Workshop on the Physics of Semiconductor Devices, New Delhi, Vol. 2, (2001) 1030.

Chapter 1

Semiconductor heterostructures and applications

1.1 Multilayered heterostructures and III-V compounds

Multilayered heterostructures using semiconductor materials are being used in number of devices such as laser diodes, detectors, solar cells and sensors. Tiny lasers are in everyday use in our homes and offices. They are present in CD/DVD players, computer drives and laser printers, displays and bar code readers, pointers and indicators, and are also used for medical and military operations. However, these lasers are barely forty years old and until about 1980 they were largely used in the laboratories. With the development of optical communication systems, these lasers were found quite useful in data transmission. Soon the commercial production was taken up in industries. It will be quite instructive to review the development of these tiny light emitters made using semiconductor heterostructures. To begin with, we shall describe in brief the semiconductor materials used in synthesizing laser diodes.

A perfect crystalline inorganic bulk semiconductor has a band of electronic states completely filled at absolute zero temperature (termed as valence band), separated from another completely empty band of electronic states (termed as conduction band) by a region of forbidden energy. At absolute zero temperature, this ideal intrinsic semiconductor is a perfect insulator. At higher temperatures, a few electrons from the valence band acquire sufficient thermal energy and are excited across the forbidden energy gap to partially fill the electronic states in the conduction band and leave empty states in the valence band. Both the electrons in the partially filled conduction band and the positively charged empty states (termed as holes) in the valence band contribute to electrical conduction in semiconductors. The conductivity of an intrinsic semiconductor can be altered and enhanced by doping with appropriate impurities which are either electron donors making it n type or electron acceptors making it p type.

Depending on the nature of constituent atoms and the crystal structure, electronic energy depends on momentum in a complex way. There are maxima and minima in energy along specific directions in the momentum space. The energy separation between the lowest conduction band minimum and the highest valence band maximum is termed as the fundamental energy gap or simply the band gap of the material. Examples of the inorganic bulk semiconductors, with different energy gaps are: (i) elemental semiconductors in which only group IV elements are assembled in a diamond lattice structure, viz. Si: 1.12eV, Ge: 0.67eV, and (ii) compound semiconductors constituting group III and group V elements of the periodic table having zinc blende or hexagonal lattice structure, viz. GaN: 3.36eV, GaP: 2.1eV, GaAs: 1.42eV, InP: 1.35eV. GaSb: 0.7eV, InAs: 0.36eV, and InSb: 0.17eV.

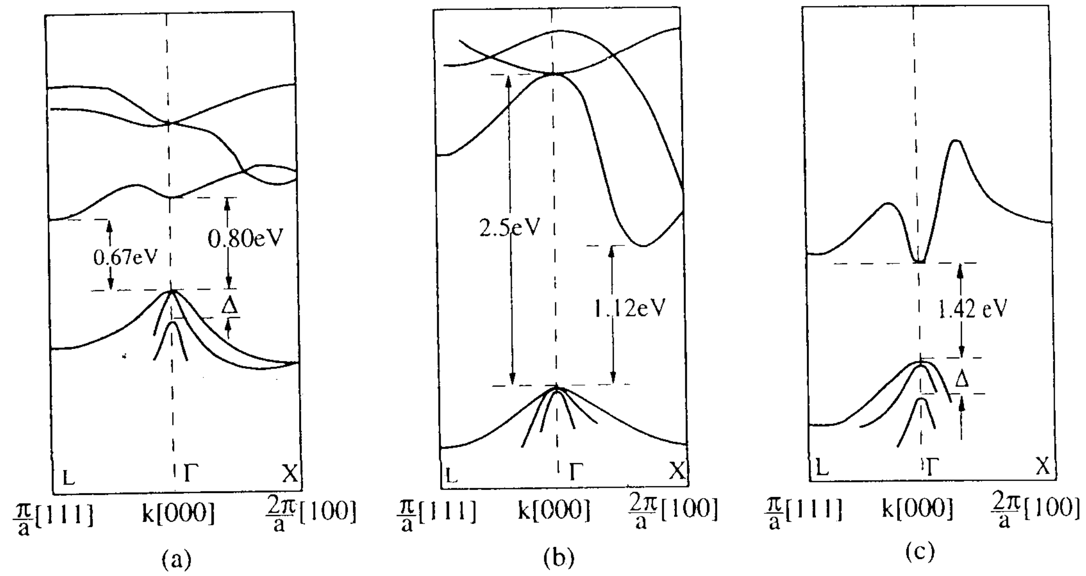

Fig. 1.1 Band diagram of (a) Germanium, (b) Silicon, and (c) GaAs

Fig. 1.1 shows the variation of electron energy with wave number (momentum) in (a) Germanium, (b) Silicon, and (c) GaAs along the [100] and [111] directions in k space [1]. As seen, if the conduction band minimum (CBM) and the valence band maximum (VBM) occur at the same wavevector k, [momentum $p = (h/2\pi)\ k$] the semiconductor is called direct gap and if the CBM and VBM occur at different points in the momentum space, the semiconductor is called indirect. The fundamental band gap of elemental semiconductors such as Si and Ge is indirect. In these, the absorption coefficient near the band edge energy is relatively low and correspondingly they are inefficient light emitters. On the other hand, several compound semiconductors (although not all) such as GaAs, InP and GaSb have direct fundamental energy gap. They have high absorption coefficients near the band edge energy and are also efficient light emitters. These binary compounds can be combined or alloyed using one or more group III elements with one or more group V elements to form mixed crystals such as ternary and quaternary materials AlGaAs, AlGaAsP, InGaAs, InGaP, InGaAsP, GaAsSb, AlGaAsSb etc. Band gap of each alloy varies with the composition and hence these materials are useful for synthesizing light emitting diodes and lasers over an extended wavelength range 650-1600nm. These ternary and quaternary compounds are typically used in the form of thin epitaxial films deposited on GaAs, InP or GaSb substrates.

1.2 Development of heterostructures for semiconductor lasers

A simple laser diode structure consists of a junction between p-type and n-type semiconductor. Under forward bias, charge carriers viz. electrons from n-type and holes from p-type are injected across the junction. These excess carriers in the junction region recombine giving rise to photon emission during the process of radiative recombination. The photon emission could be spontaneous as in the case of light emitting diodes (LED's) or stimulated as in the case of laser amplifiers respectively. In addition to light amplification by stimulated emission of radiation, the laser diode incorporates a suitable cavity structure to provide feedback so that the device behaves as an oscillator.

Initially, homojunction lasers were made by diffusing p-type dopant in n-GaAs substrates. During 1961-62, three laboratories independently developed lasers employing GaAs homojunctions [2-4]. These diodes operated at cryogenic temperatures in pulse mode and had threshold current densities over 50,000 A/cm^2. The reliability was erratic, with operating lifetimes ranging from minutes to a few hundred hours. Several other II-VI, III-V and IV-VI compounds also exhibited stimulated light emission by photo pumping. By about 1968, lasing action had been obtained, particularly by photo pumping, at low temperatures and over a broad 0.5-20μm spectral range using a variety of materials, although room temperature light emission was achieved with only few materials e.g. GaAs emitting at ~870nm.

Improvement in the laser performance had to await the concept of heterostructure in which the active layer of GaAs is sandwiched between higher band gap ternary alloy of AlGaAs. The idea was suggested by H. Kroemer [5] in the U.S. and by R. F. Kazarinov and Zh. I. Alferov [6] in the then Soviet Union. By 1970, Alferov's group [7] and Hayashi and Panish [8] demonstrated double heterostructure laser continuously operating at room temperature and with threshold current densities reduced to ~ 5000 A/cm^2. In the year 2000, Alferov shared Nobel Prize in physics with H. Kroemer for this discovery of heterostructure that has laid the foundation of modern lasers used extensively in information technology. Fig. 1.2 shows a schematic of a typical DH structure along with the band diagram, refractive index variation and optical confinement in the active region.

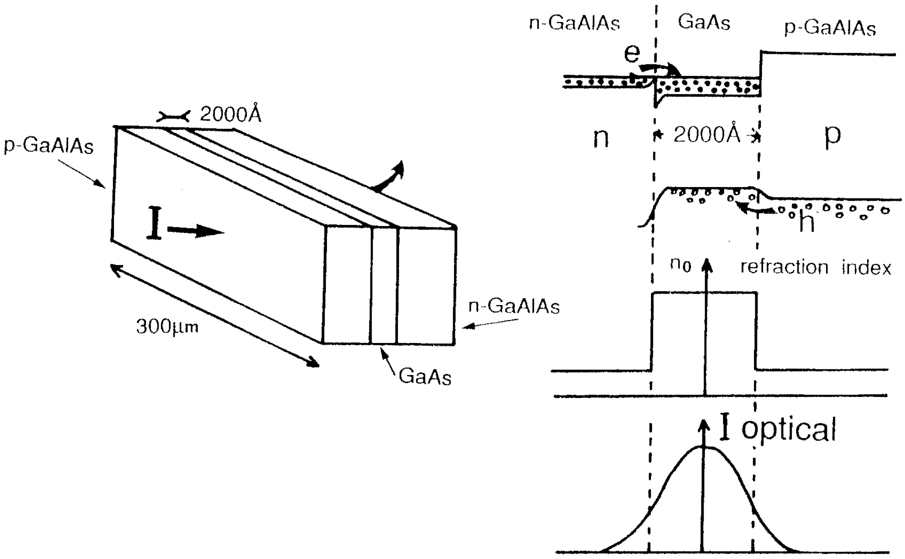

Fig. 1.2 Schematic of a typical DH structure

Typical width of the middle GaAs layer is about 1000-2000 A^0 and the emission wavelength of laser is around 870nm. Development and usage of AlGaAs/GaAs DH structures continued as these diodes had long operating lifetimes of the order of few years. One role of a double heterostructure in these devices was to provide a barrier that blocked the diffusion of carriers across the junction and confined them to narrow region (carrier confinement). It also worked as a waveguide to confine light (optical confinement). Together, these two consequences of the double heterostructure reduced the threshold current density for lasing. The materials for these heterostructures were grown by methods of vapor phase epitaxy (VPE) and liquid phase epitaxy (LPE).

In the mean time, new developments were occurring in semiconductor materials and devices. Novel structures such as superlattices, quantum wells, quantum wires and quantum dots and strained layers were suggested and studied theoretically. A whole new field of quantum structures emerged in which reduction of the size of the active layer below De Broglie wavelength of carriers, altered their energy band structures and modified electrical and optical properties, which has come to be known as quantum size effect (QSE). However, VPE/LPE techniques were not useful for growing the thin layers required for these structures. Around 1970, new techniques such as molecular beam epitaxy (MBE) and metal organic chemical vapor deposition (MOCVD) emerged and were found useful in growing ultrathin layers with much better thickness control with abrupt interfaces. These novel techniques opened up a new branch of devices employing ultra thin layers in nanometer scale. A quantum well structure is similar to a double heterostructure in which thickness of the active layer is reduced to few tens of a nanometer. Fig. 1.3 shows a schematic of a quantum well structure in which a low band gap material of thickness L_z is sandwiched between two barrier layers of high band gap material. Thus, in case of AlGaAs / GaAs materials, GaAs with band gap (E_g) forms a quantum well and AlGaAs layers with band gap ($E_{g,\ b\text{-barrier}}$) form the barrier. As seen, due to the quantum size effect, energy levels are split in conduction and valence bands. In the well region, the quantized subband electron (hole) energies e_1, e_2 (hh_1, hh_2, lh_1) are inversely proportional to L_z. For GaAs, the quantization is appreciable for $L_z < 150\ A^0$. Lasers using quantum structures were expected to give shorter emission wavelengths, lower threshold currents and weaker temperature dependence of the threshold current. In 1975, lasing from quantum states in very thin MBE grown GaAs-$Al_{0.2}Ga_{0.8}As$ multilayer structure was demonstrated [9]. In 1978, the room temperature operation of quantum well $Ga_{1-x}Al_xAs$-GaAs lasers grown by MOCVD was reported [10]. This MOCVD grown laser had a single 20nm wide quantum well. It operated in pulsed mode at a threshold current density of about 3 kA/cm^2 at 300K. In 1979, MBE grown AlGaAs injection laser containing 14 quantum wells, 13.9nm wide, with a room temperature threshold of about 2 kA/cm^2 was reported [11]. In 1982, MBE grown AlGaAs / GaAs, GRIN-SCH [Graded Index Separate Confinement Heterostructure] laser was reported [12]. These lasers had extremely low threshold current density ~160A/cm^2. Optical communication gave a boost to the research in semiconductor lasers emitting in wavelength range exceeding 1μm. Since 1985, as more and more MBE and

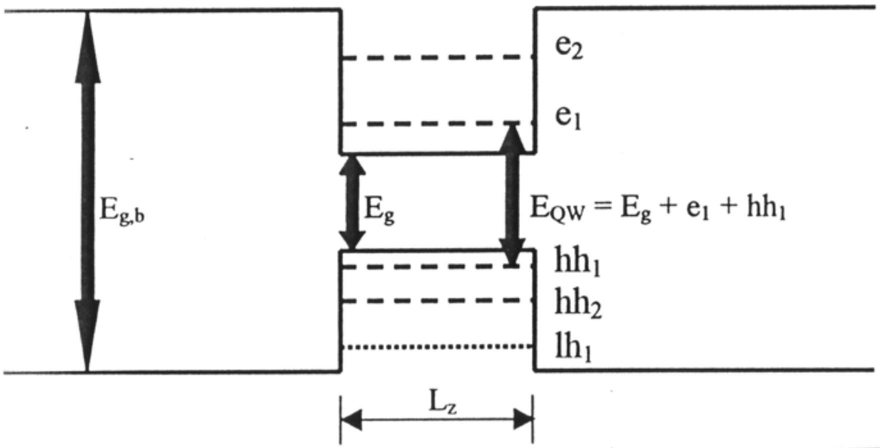

Fig. 1.3 Schematic of a quantum well structure

MOCVD machines were manufactured commercially, the research in quantum well lasers increased tremendously.

Early DH lasers and quantum well lasers used lattice matched material systems in which lattice parameter of the substrate and the layers was the same. Adams, Yablonovitch and Kane [13-14] predicted further reduction in the threshold current and improved device performance by using strained active layers. By replacing the active layer with larger (or smaller) lattice constant material, a compressive (or tensile) strain can be incorporated. This could be done easily by depositing ternary and quaternary alloys, such as InGaAs, InGaP, GaAsP, GaAsSb. InGaAsP. By controlling the thickness to a critical value (h_c), the strain could be accommodated in the structure without producing dislocations. High quality, dislocation free, pseudomorphic layer can be grown if the product of lattice mismatch times the layer thickness is less than about $200A^0$ %. Thus, for accommodating 2% strain, the critical thickness has to be in the range of $100A^0$. Such thin layers are generally grown easily using MBE and MOCVD techniques. Strained layer quantum well lasers are available commercially over a wide range of wavelengths.

1.3 Growth of ultrathin (quantum well) and strained layers using LPE.

Although LPE method is not generally used for growing ultrathin layers, several attempts have been made to synthesize superlattices and quantum wells. Early AlGaAs/GaAs DH lasers were synthesized using LPE at high temperatures [~800^0C] and hence it was very difficult to achieve thickness control. This was a serious drawback in synthesis of thin layers as needed for quantum well lasers by using LPE. Due to the difficulties in growing GaInAsP by MBE and the inadequate MOVPE technology in early 80's, LPE was used for the growth of DH-GaInAsP/InP quantum well lasers in Japan, and in USA [15-17]. These structures were grown using low growth temperatures; controlled melt supersaturation and computer controlled slider movements. When fabricated into devices, these structures yielded GaInAsP lasers emitting at 1.3μm. During 1985-95, research groups from China, Germany, and Russia could obtain quantum well structures [18-22] by employing low temperature LPE growth technique. Quantum well lasers with threshold current density of 120 A/cm^2 were reported by a Russian group [23].

In the initial stages of the present work, we concentrated on synthesizing structures which had only GaAs and AlGaAs, which are closely lattice matched. We synthesized laser structures in which the thin active layer was GaAs with a small amount (2-3%) of Al. Although quantum well lasers based on AlGaAs/GaAs heterostructures synthesized by using LPE have been reported, there is no report on the synthesis of strained active layer based lasers. In this thesis, we report on the synthesis and characterization of AlGaAs based, separately confined 'strained' heterostructures, using liquid phase epitaxy. Strain has been incorporated in the active layer by using $GaAs_xP_{1-x}$ or $GaAs_xSb_{1-x}$. The active layer that contains small amount of P is tensile strained and the one which contains Sb is compressively strained. We also report on the characterization of laser diodes fabricated using these structures.

1.4 Current status of LPE in industry

About 35 companies produce over 80-100 million units of laser diodes every year and contribute to about 400million US $ turnover [24]. Laser diodes are the only components that use all the three epitaxy techniques. Long wavelength diodes [>1300 nm] use LPE for the simpler structures and MOVPE and MBE techniques are used for more complex ones. Till the year 1996, over 65 % of LED's and laser diodes were being made using LPE [25]. Thus, LPE has continued to play an important role in industry although quantum well and strained layer lasers are not produced commercially by using LPE.

REFERENCES

[1] Pallab Bhattacharya in Semiconductor Optoelectronic Devices, Prentice Hall (1995).

[2] R.N.Hall, G. E. Fenner, J. D. Kingsley, T.J. Soltys and R.O.Carlson, Phys. Rev. Lett.9, (1962) 366

[3] M. I. Nathan, W. P. Dumke, G. Burns, F. H. Dill Jr., and G. Lasher, Appl. Phys. Lett. 1, (1962) 63.

[4] T. M. Quist, R. H. Rediker, R. J. Keyes, W. E. Krag, B. Lax, A. L. McWhorter, and H. J. Ziegler, Appl. Phys. Lett. 1, (1962) 91.

[5] H. Kroemer, Proc. IEEE 51 (1963) 1782.

[6] Zh. I. Alferov and R. F. Kazarinov, USSR Patent 181737 (1963).

[7] Zh. I. Alferov, V. M. Andreev, D. Z. Garbuzov, Yu. V. Zhilyaev, E. P. Morozov, E. L. Portnoi and V. G. Trofim, Sov. Phys. Semicond. 4, (1971) 1573.

[8] I. Hayashi, M. B. Panish, P. W. Foy and S. Sumski, Appl. Phys. Lett. 17, (1970) 109.

[9] J. P. Van Der Ziel, R. Dingle, R. C. Miller, W. Wiegmann and W. A. Nordland Jr. Appl. Phys. Lett. 26, (1975) 463.

[10] R. D. Dupuis, P. D. Dapkus, N. Holonyak, Jr. E. A. Rezek and R. Chin, Appl. Phys. Lett. 32, (1978) 295.

[11] W. T. Tsang, C. Weibuch, R. C. Millar and R. Dingle, Appl. Phys. Lett. 35, (1979) 673.

[12] W. T. Tsang, Appl. Phys. Lett. 40, (1982) 217.

[13] A. R. Adams, Electron. Lett. 22 (1986) 249.

[14] E. Yablonovitch, and E. O. Kane J. Lightwave Technol. 4 (1986) 504.

[15] Y. Sasai, N. Hasae and T. Kajiwara, Japn. J. Appl. Phys. 24, (1981) L 137.

[16] E. A. Rezek, N. Holonyak Jr., B. A. Vojak, G. F. Stillman, J. A. Rossi, D. L. Keune, and J. D. Fairing, Appl. Phys. Lett. 31 (1977) 288.

[17] E. A. Rezek, B. A. Vojak, R. Chin, N. Holonyak Jr., and E. A. Samman, J. Electron. Mater. 10 (1981) 255.

[18] Zh. I. Alferov, I. N. Arsent'ev, L. S. Vavilova, D. Z. Garbuzov and V. V. Krasovskii, Sov. Phys. Semicond, 18 (1984) 1035.

[19] D. Z. Garbuzov, I. N. Arsent'ev, L. S. Vavilova, A. V. Tikunov and E. V. Tulashvili, Sov. Phys. Semicond, 19 (1985) 83.

[20] Mu-Kuen-Chen, Tien-Chin Chang, and Hao-Hsiung Lin, J. Appl. Phys. 74 (1993) 3464

[21] K. Ketling, K. Koehler and P. Zwicknagl, Appl. Phys. Lett. 48 (1986) 157.

[22] Zh. I. Alferov, A. A. Vodnev, O. O. Ivent'eva, V. R. Laroinov and V. D. Rumyantsev, Sov. Phys. Semicond, 20 (1986) 239.

[23] V. M. Andreev, A. B. Kazantsev, V. P. Khvostikov, E. V. Paleeva, V. D. Rumyantsev and S. V. Sorokina, Materials Chemistry and Physics, 45 (1996) 130.

[24] Strategies Unlimited, [an optoelectronic market research firm based in Mountain View, CA, USA], Laser Diode review, Forecast-1996, Report OM-6.

[25] R. L. Moon, J. Cryst. Growth 170 (1997) 1.

Chapter 2

Experimental Techniques

2.1 Epitaxy

The term ‘epitaxy’ is defined as the deposition of a single crystal layer on a single crystal substrate in such a way that the crystalline structure of the substrate is continued into the layer. This requires that the crystal structure of the layer and the substrate should have the same crystallographic space group and that the lattice parameter of the layer and the substrate should be identical or closely matched.

The lattice mismatch (ε) is defined as $[\varepsilon] = [(a_l - a_s) / a_s]$ where a_l is lattice parameter of the layer and a_s is that of the substrate. As a general rule, it is found that if (ε) $\leq 10^{-3}$, then nearly lattice matched epitaxial growth will occur. If however, (ε) $> 10^{-3}$ then there is an increasing tendency towards the generation of misfit dislocations at the interface due to lattice mismatch. If the mismatch is large, then the quality of the epi-layer degrades because it contains a network of misfit dislocations.

The term ‘homoepitaxy’ means the layer and the substrate are of the same material e.g. GaAs layer on GaAs substrate. Likewise GaSb on GaSb, InP on InP etc. are other examples of homoepitaxy. In ‘heteroepitaxy’, the layer is of different material than the substrate e.g. AlGaAs on GaAs substrate or InGaAsP on InP substrate. The term ‘liquid phase epitaxy’ (LPE) means the growth from a supersaturated solution at elevated temperature. The other epitaxial growth techniques in common use are molecular beam epitaxy (MBE), and metal organic vapour phase epitaxy (MOVPE). These can support considerably larger supersaturation than is possible in LPE. As a result, it is possible to grow single crystal films on substrates with much larger mismatch [(ε)~10^{-1}] or with different crystal structures, e.g. GaAs on Si or GaAs on sapphire, albeit the epitaxial quality is poorer.

The subject of liquid phase epitaxy is relatively older and it has been reviewed extensively in the last forty years [1-10]. Despite the advent of MBE and MOVPE techniques, the semiconductor industries still use LPE method extensively for manufacturing light emitting diodes, lasers, solar cells and detectors [11], because it is relatively less expensive and safer technique. It has limitations, particularly for the growth of very thin layers ~10-100 A^0, which are used in modern semiconductor quantum well structures for which MBE and MOVPE are the preferred techniques.

2.2 Methods of LPE

In LPE, the basic requirement is to bring the substrate and the supersaturated solution in contact with one another to initiate the epitaxial layer growth and then to separate them at the end of the growth cycle. This is best achieved in graphite boats of specific designs. The choice of graphite is governed by its availability in high purity form. Graphite can be easily machined into necessary shapes to high tolerances. It is non-reactive with the normal solution constituents, not wetted by the growth solutions containing gallium and indium metals, and above all it has good thermal conductivity. However, graphite has the disadvantage of being porous, which leads to absorption of atmospheric oxygen and water vapour during loading. But this can be overcome by the use of glove box for loading and using long baking procedures for the solutions.

Three types of growth systems viz. ‘tip’, ‘dip’ and ‘slider’ are in common use. Historically, in the ‘tip system’, proposed by Nelson [1], the graphite boat is placed in the center of the quartz tube such that at the beginning of the growth experiment, the growth solution and the substrate are at two ends. The supersaturated solution is rolled over the substrate for deposition. It is then tipped off when the deposition of the layer is complete. The apparatus is extremely simple and cheap to assemble. The main drawback of the tipping technique, apart from the difficulty of growing multilayer structures, is that the removal of solution at the end of the growth period is unreliable. In the ‘dip’ system originally described by Rupprecht [12], the growth solution is held in graphite or silica crucible and the substrate is placed either vertically or horizontally in a silica holder. The substrate is ‘dipped’ in the supersaturated solution and it is removed after the layer deposition.

In the ‘slider’ system, the substrate is normally placed in a recess in the base of the boat while the growth solutions reside in wells/slots machined in movable/sliding solution carriers. Different solutions are positioned sequentially over the substrate by moving the slider and using the external push-rod arrangement to grow multilayered structures. In another variation, the solutions are held stationary and the substrate is pushed under them sequentially. An important factor in the boat design is the separation between the substrate surface and the graphite surface of the solution carrying slider. This clearance is important in the wiping action when the solution is moved away from the growth substrate. If the clearance is too large, the solution wipe off will not be efficient, while if it is too small, scratching of the substrate may occur during the slider movements. Typical clearances are 25-100μm and can be adjusted by keeping thin graphite plates below the substrate. Most systems use 'stationary substrate and moving solutions' scheme.

The origin of the use of horizontal sliding boat system is difficult to establish, but the paper by Panish et al [13] was one of the firsts. The sliding boat made biggest impact in the growth of multilayer structures where accurate control of layer thickness is important and good wipe off of solution at each stage is required. Size of a typical substrate used is few cm^2 and about 400μm thick. The solution wells are circular or oblong or rectangular and made deep enough to hold 1-10gm gallium solvent. Since the amount of the solution used is much less than in 'tip' and 'dip' systems, economical use is made of the solution materials. Growth systems employing rotary sliders [14], wipingless slider [15] and pistons [16] have been developed and used successfully to synthesize AlGaAs/GaAs and InGaAsP/InP DH lasers and detectors.

Growth experiments are carried out in quartz reactors that are heated in furnaces designed as per the requirements of the laboratories. High thermal mass furnaces are used where temperature stability is important. This can be achieved by employing bulky insulation between the heating element and the outer furnace walls. Low thermal mass furnaces are useful where rapid temperature changes are required e.g. fast rise in temperature, step cooling, supercooling during growth experiment. One such furnace uses gold coating for insulation [17]. The gold coated, semi-transparent, low thermal mass furnace consists of quartz tube coated on the inside with a thin semitransparent film of gold. By reflecting most of the IR radiation back into the tube, good temperature stability and almost uniform profile is obtained by suitable design of the heating element. This 'gold' furnace is the outcome of the research at MIT Lincoln laboratory in 1970 and these furnaces are now available commercially with Trans Temp Company, USA. The furnace design offers a unique combination of visibility of high temperature phenomena and exceptional profile control.

Ambient gas inside the quartz reactor tube is normally ultra high purity palladium-diffused hydrogen produced by commercially available purifier units [Matheson, Johnson-Matthey].

Hydrogen has the advantage of being able to reduce any metal oxides that may be present on the surface of the growth solutions. Vacuum attachments are often used with LPE systems to evacuate the quartz tube followed by back filling with nitrogen or hydrogen. These are also used for leak testing the growth apparatus or for in situ vacuum baking of the growth melts.

2.3 LPE growth techniques

Fig. 2.1 shows phase diagram of GaAs that is typical of most of the III-V binary compounds. [9]. It represents temperature (T)-composition (X) plot, where X is the atom fraction of group V element of the compound (viz. arsenic in the present case). The vertical line at X = 0.5, called 'solidus', represents GaAs solid that melts at 1238^0C. The upper curve represents the 'liquidus'. A point on this curve, e.g. 'A', represents a mixture of As and Ga of composition X_A, saturated at temperature T_A. The composition of the solid phase is given by a 'tie-line' AC. If the temperature is dropped to T_B, the equilibrium liquid phase composition is now X_B and the solid composition is again GaAs given by tie line BD. If the cooling process is carried out with a GaAs seed or substrate present under the solution, then the epitaxial deposition will occur. Phase diagram is useful in estimating the solution composition at any desired growth temperature. Fig. 2.2 shows solute profiles for a growth solution in contact with the

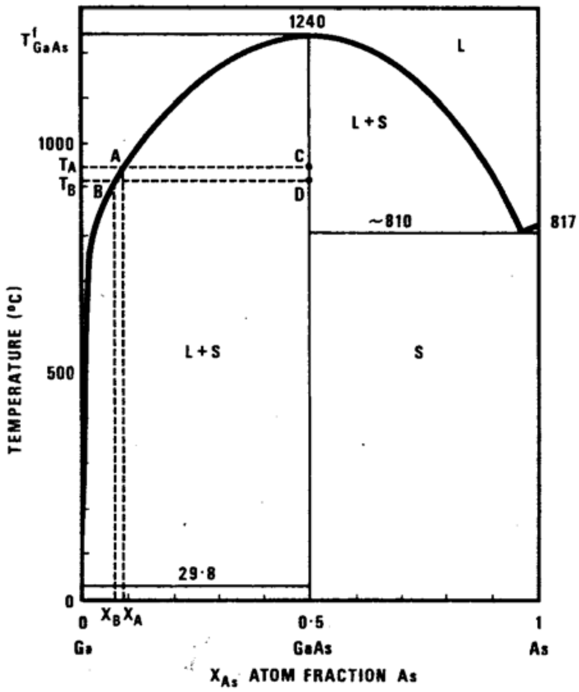

Fig. 2.1 Liquidus-solidus phase diagram for Ga-As system.

substrate at x = 0. Prior to the contact, the solution concentration C [x, t < 0] = C_0 for all x. After the contact (t = 0) and at any time t, the solute concentration at the solid-liquid interface has a value equal to the liquidus concentration $C_E(T)$ corresponding to the solution temperature. If the solution is being cooled, then at times t_1 and t_2 the concentrations are C_{E1} and C_{E2} corresponding to temperatures T_1 and T_2, $T_1 > T_2$ according to the cooling rate. As the cooling takes place, the layer of the solution next to the interface gives up its excess solute, which gets deposited on the substrate.

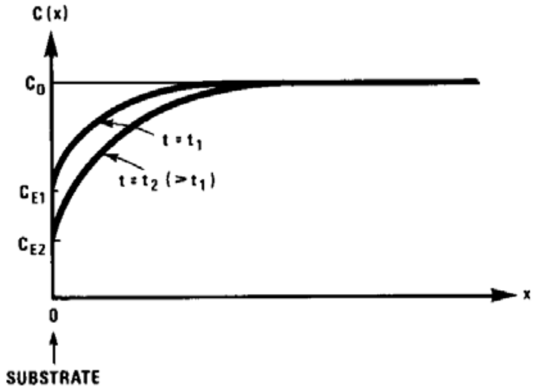

Fig. 2.2 Solute profile for semi-infinite solution

In the case of a thick solution, far away from the interface, the concentration still remains at C_0 since there is no nucleation center around. This sets up a concentration gradient of the solute in the solution and the solute diffuses towards the interface. The growth occurs due to the deposition of the excess solute at the interface caused by continuous cooling of the interface and the diffusive transport of the solute from the bulk of the solution to the interface. Thus, the basis of LPE growth is the supersaturation in the growth solution and it can be produced in number of ways. Three methods that are commonly used for cooling solutions are as follows:

1] Step cooled growth – In this method, after saturation at T_{sat}, the solution is cooled by ΔT [10-15^{0}C], below the saturation temperature, before it is brought into contact with the substrate. Growth solution is held at this temperature [T_{sat} - ΔT] during the growth period t. In this case, the thickness of the grown layer is given by $d(t) = 2\,\Delta T\,(D/\pi)^{1/2}\,(1/C_S m)\,t^{1/2}$ [18] where ΔT is the initial supersaturation in the solution, D is diffusion coefficient of solute, m is slope of the liquidus at the growth temperature and C_S is concentration of solute in the solid. This method has been widely used in thin layer growth of lattice matched AlGaAs/GaAs and GaInAsP/InP materials.

2] Ramp cooled growth - Here the temperature of the solution, saturated at T_{sat}, is lowered continuously at a rate α [^{0}C/min] from the liquidus temperature T_{sat} while in contact with the substrate during the growth period t. In this method, thickness of the grown layer is given by $d(t) = 4/3\ (D/\pi)^{1/2}\ (\alpha/C_S\ m)\ t^{3/2}$ [18], where α is the cooling rate of solution and rest of the terms are same as above. By suitable choice of α, slow or fast growth rate can be obtained This method has been widely used for depositing thick layers.

3] Supercooled growth - This method is generally used for thick growth (> 5-10μm) and it is a combination of the above two methods. Here, the temperature of the growth solution is lowered ΔT [10-15^{0}C], below the saturation temperature (T_{sat}), before the solution is contacted with the growth substrate. The solution is further cooled at a rate α [^{0}C/min] over the desired temperature range while the growth continues. The thickness in this method is given by: $d(t) = (1/C_S\ m)\ (D/\pi)^{1/2}\ [2\ \Delta T\ t^{1/2} + 4/3\ \alpha\ t^{3/2}]$ [18]. This technique has the advantage of an initial supercooling to enhance nucleation together with the ability to grow thicker layers than can be obtained by simple step cooled growth. This method has been extensively used in the heteroepitaxial growth of III-V compounds and alloys such as GaInAs on InP [19-21], GaAsSb on GaAs [22], InGaAsSb on GaSb [23-24], and InGaAsP on InP [25-26].

2.4 Heterostructures grown by LPE

Growth of heterostructures using LPE was at first studied extensively for the synthesis of diode laser structures based on AlGaAs/GaAs materials. By 1970, Zh. I. Alferov and his colleagues [27], Hayashi and Panish [28] demonstrated double heterostructure laser continuously operating at room temperature, with threshold current densities reduced to ~5000A/cm^2. Symmetric, separately confined heterostructure (SCH) was suggested by Hayashi [29] and Thompson and Kirby et al [30] to obtain lasers with low threshold current density (J_{th}) and operating at room temperature. Since 1980, some groups have reported SCH laser structures of InGaAsP/InP materials. [31-32]. Schanen et. al. [33] made complicated devices like twin-guided Distributed Feed Back (DFB) lasers grown by three step epitaxial process. Active layer in these structures was ~100-500nm thick. Use of LPE to grow quantum wells in AlGaAs/GaAs was neglected due to the ease and the success of MBE and OMVPE techniques for synthesizing such thin layers. Some research groups have however reported the LPE growth of single quantum well and QW lasers [34-36].

2.5 LPE work at TIFR

Liquid phase epitaxy of GaAs at TIFR began in early seventies. Subsequently, the work was extended for the deposition of single layers of binary, ternary and quaternary materials on GaAs, GaSb and InP substrates. Growth experiments were done using horizontal graphite slider boat, shown schematically in Fig. 2.3. This boat had the capability of holding three solutions and two substrates, one substrate for solution saturation and the other for growth. As seen, two wells contain growth and etching solutions. The technique of saturation of the growth solution using a separate saturating substrate was thus employed. A process of in situ etch-back of substrate surface prior to growth was also developed and employed successfully [37]. The inset shows the use of a graphite disc for covering sample surface to minimize thermal degradation of the substrate surface and a plug to avoid loss of solute during the initial heating for solution homogenization. Single layers of undoped GaAs, AlGaAs, GaSb, GaAsSb, InP, InGaAs, and InGaAsP were grown on respective substrates. Sn doped AlGaAs on GaAs [38] and lattice matched, Ge doped InGaAs and InGaAsP layers were deposited on InP substrates to study the behavior of these dopants [39-41]. Growth of indium thallium phosphide (InTlP) on InP substrate was also attempted

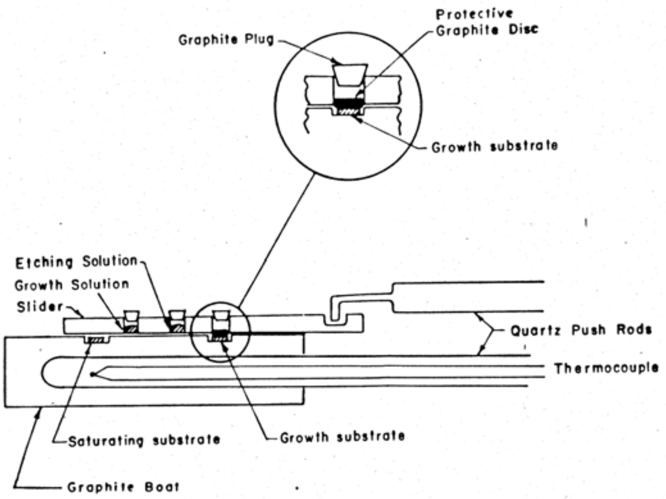

Fig. 2.3 Schematic of the slider graphite boat

[42]. Apart from these materials related studies, in 1992-93, we decided to extend the LPE work to grow multilayer heterostructures for devices such as lasers, using AlGaAs/GaAs materials. The motivation for this work was to investigate:

1] Synthesis of multilayered structures in lattice matched AlGaAs/GaAs materials.
2] Growth of a single quantum well in AlGaAs/GaAs/AlGaAs heterostructure.
3] Growth of a strained single quantum well by incorporating elements such as P or Sb in the active GaAs layer.
4] Synthesis of separately confined heterostructures for laser diodes employing strained/non-strained active layer/quantum well.

Considering the requirements of growing thin layers reliably, it was clear that growth at lower temperatures would be desirable. With due consideration to various options, we decided to use the 'piston boat', originally designed and used by Russian research scientists [16]. We have used two designs of the piston boat as described below:

2.5.1] Boat fabricated at TIFR –

Fig. 2.4 shows schematic of the graphite boat fabricated by Mr. Jhanje at the graphite shop in the Glass Blowing section of TIFR. As seen, the boat contains three parts, a substrate carrier and a disposal bin for collecting the used solutions, a piston housing for solution transfer and a tray for carrying growth solutions. The movements of the piston and the solutions are carried out externally using quartz rods extending out of the reactor tube through the stainless steel end cap. Fig. 2.5 shows photographs of the graphite parts and the assembled boat. The

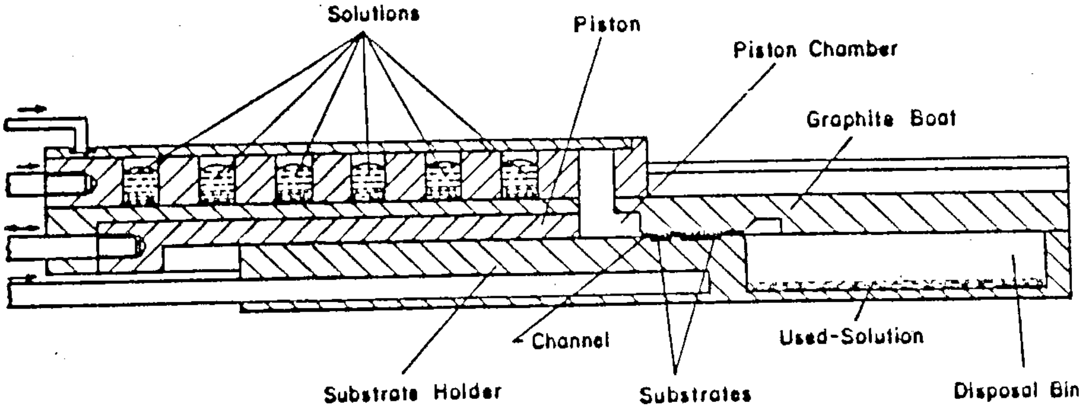

Fig. 2.4 Schematic of the piston graphite boat fabricated at TIFR.

boat is 200mm long, 30mm wide and 25mm in height. The substrate recess is made in two parts to fit two rectangular substrates of 10mm x 4mm and 10mm x 8mm size. Fig. 2.5 shows photographs of (a) assembled graphite boat and (b) dismantled boat with piston housing (top), substrate carrier with solution collection bin (middle) and solution carrier tray (bottom). High purity Poco graphite block is used for fabricating the boat and the machining is done without using any oil, grease or a coolant. The solution wells are 7mm clear circular holes spaced 15mm apart and the height of the solution well is 10mm, providing $\sim 0.4cm^{-3}$ volume for the solution. The gap between the substrate surface and the top graphite housing

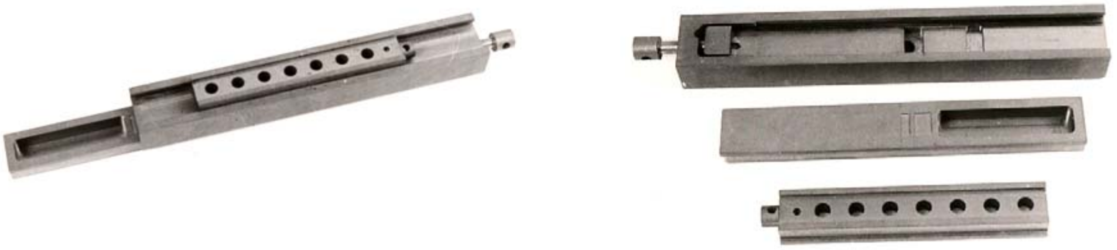

(a) Assembled boat **(b) Dismantled boat**

Fig. 2.5 Photographs of the piston boat fabricated at TIFR.

is about 0.5mm and can be changed by selecting substrates of different thickness or by using thin graphite plates. After machining, the boat was thoroughly cleaned and degreased in hot organic solvents like trichloroethylene several times and then heated in vacuum at about 1000^0C for several hours to remove volatile impurities. In this design, the growth substrate is placed in a fixed position and the last solution remained on it till the furnace cooled down to room temperature. This resulted in extra and unwanted growth from the last solution. Although we could grow the heterostructures of device quality using this boat, it was desirable to have a boat in which the substrate could be separated from the last solution while the furnace was cooled to room temperature. Such a boat was fabricated in Russia as described next.

2.5.2] Boat fabricated at A. F. Ioffe Institute at St. Petersburg, Russia.

During a visit of the author to A. F. Ioffe Institute, Russia in November 1997, another piston boat was designed, fabricated in the graphite shop of the Ioffe institute, fired in high vacuum and brought back to TIFR for further experimentation. Fig.2.6 (a) shows the photographs of this boat. Picture on left shows dismantled graphite boat parts whereas the one on the right shows the assembled boat.

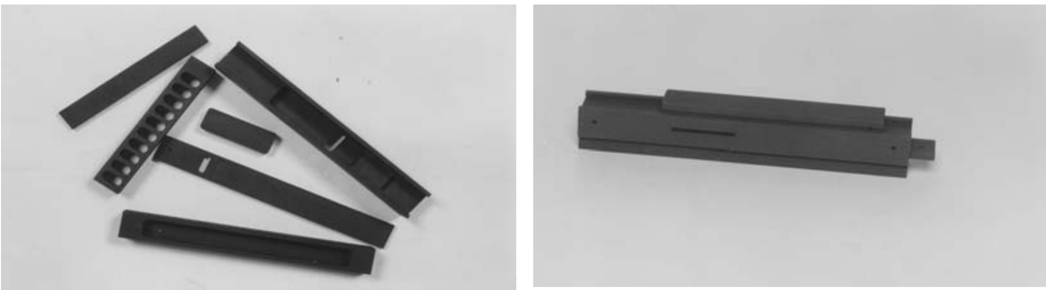

Dismantled boat **Assembled boat**

Fig. 2.6(a) Photographs of the boat fabricated at Russia.

Fig. 2.6 (b) shows schematic cross-section of this boat. As seen, it contains a solution tray, disposal bin for used solutions, piston and a substrate carrier that could be slid in and out of the entire body of the boat. The substrate carrier has a 15mm x 15mm x 0.5mm recess for placing the growth substrate. The gap between substrate surface and top graphite housing is about 0.7mm. This boat has a facility of using ten solutions, and the solution wells are 10mm x7mm x10mm, separated by 3mm from one another. The corners of the rectangular wells are rounded off to avoid sticking of the solution at sharp edges. Each well has volume of about $0.7cm^{-3}$, almost double than the boat made in TIFR. The movements of the solutions, piston and the substrate carrier are carried out using 2mm diameter molybdenum rods fitted to the

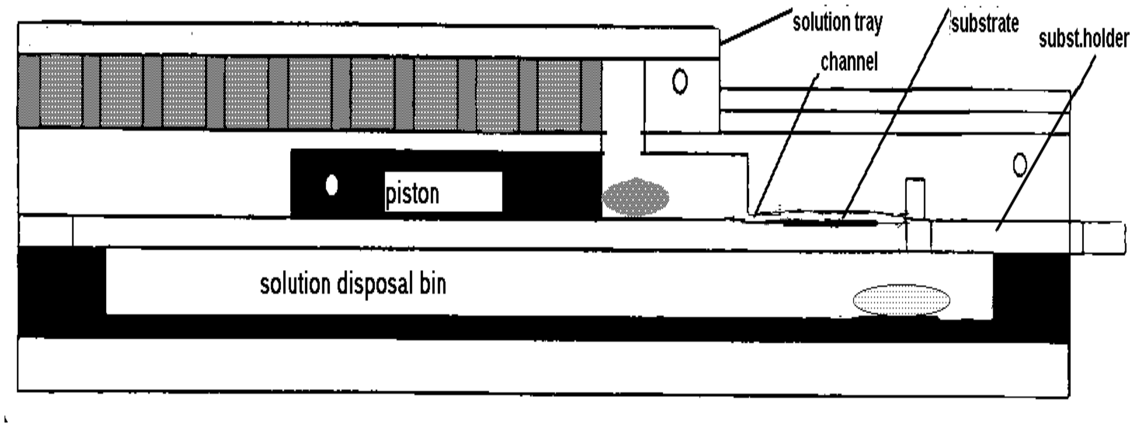

Fig. 2.6 (b) Schematic of the piston boat fabricated at A. F. Ioffe Institute, Russia

end cap fabricated for this boat. All the experiments of synthesizing multilayered heterostructures were done using this piston boat made in Russia.

2.5.3] Benefits and shortcomings of a piston boat

Multilayered growth is done using several solutions each designed to grow one layer. In conventional slider boat, the solutions are brought in contact with the growth substrate sequentially to deposit the layers. The surface of the grown layer is exposed to reactor ambient during the short period between solution transfer and may pose a serious wetting problem. In piston boat, the solution transfer takes place by displacing the solution that is already depositing a layer. Thus, after the initiation of the growth sequence the grown layer is always covered by a solution and never exposed to the reactor ambient till the end of the growth experiment. In order to grow a thin layer it is necessary to reduce the growth temperature to 600^0C or below. At low temperature, a solution containing aluminum may have a thin film of oxide covering the solution surface. This can pose a problem of non-wetting of the substrate surface, resulting in disconnected growth islands. In the piston boat design, the graphite piston forces the solution through a small gap of less than a mm above the substrate surface. As a result, due to the squeezing of the solution at the growth temperature, the oxide film is broken and removed. This clean solution deposits a smooth layer on the substrate. The solution substitution is performed by displacing (flushing out) one solution by the next one rather than by removing the previous one off the substrate and bringing in the next one, as is commonly done in the slider boat. Thus, the piston boat is useful for depositing smooth multilayer heterostructures at low temperatures.

There is however one serious shortcoming of the piston boat design. As one solution pushes out the other, there is inevitable mixing of the two solutions where they meet during the short period of transfer. This causes a serious problem since the two solutions will generally contain different materials or dopants. For example, if a solution containing gallium and arsenic (designed to grow a GaAs layer) is displacing the one that contains aluminum, gallium and arsenic (designed to grow AlGaAs layer), then small amount of aluminum gets into the new solution and the subsequent grown layer will contain some aluminium. Thus, it becomes impossible to obtain a layer of GaAs with zero Al content sandwiched between two layers of AlGaAs. This problem is encountered in synthesizing DH laser structure of AlGaAs/GaAs that may use GaAs as an active layer sandwiched between two AlGaAs layers.

A small amount of Al will always be incorporated in the active GaAs layer. Also at the end of the growth experiment, all the used melts are collected in the disposal bin, get mixed and thus can not be reused again for subsequent growth experiments.

2.6 Growth reactor used for LPE work

Fig. 2.7 shows schematic of the LPE growth apparatus used in our laboratory. The growth reactor consists of a 50cm long, 10cm diameter, gold-coated transparent furnace that can be resistively heated to over 1000^0C. It is capable of giving a constant temperature (± 2^0C) over 70% of the heating element length. The heating element (coil) is connected to Eurotherm Lilliput Thyristor unit (type 031), a temperature controller (type 093) and a programmer (type 125). Using this equipment, the current in the coil is controlled accurately.

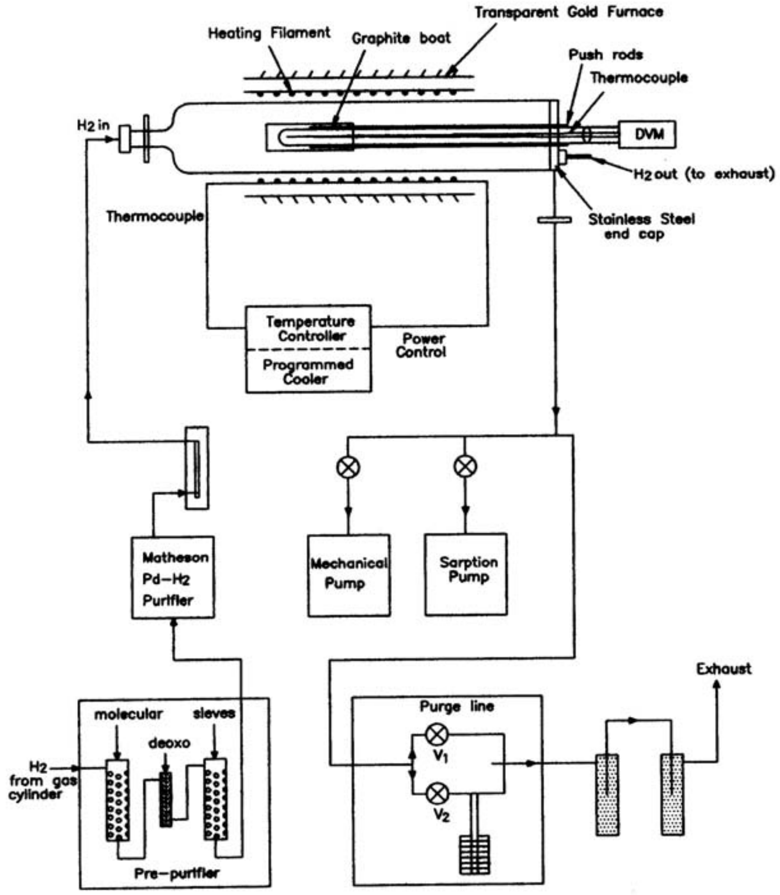

Fig. 2.7 Schematic of the LPE growth apparatus

The furnace attains the set temperature in about 20minutes. Chromel-Alumel thermocouple is placed close to the heating coil and the output of the thermocouple is connected to Eurotherm control unit. This feedback is used to control the current in the coil to maintain the temperature at the set value within ± 2.0^0C. The reactor is a 100cm long quartz tube of 50mm diameter and 3mm wall thickness. One end of the tube is narrowed down and connected to a 40mm long, 10mm diameter tube for hydrogen gas inlet. The free end of the quartz tube is used for loading and unloading the graphite boat in the furnace. Movements of the piston, substrate holder and the solution tray are carried out externally using quartz or molybdenum rods. The free ends of these rods pass through the holes made in a stainless steel end cap that fits tightly on the free end of the quartz tube. The joints between glass and metal are sealed using 'O' shaped viton rubber rings. A water cooled jacket is used to cool these rings. The end cap has an outlet for passing out hydrogen gas that is connected to exhaust. The growth experiments are done using hydrogen gas supplied by Bombay Oxygen Limited. Although it is available in high purity IOLAR grade, we need to purify it further. Hydrogen gas from the cylinder bank is fed to the pre-purifier consisting of a column of molecular sieves, a deoxo unit followed by another column of molecular sieves as shown schematically in Fig. 2.7. The first column of molecular sieve dries the incoming hydrogen. The deoxo unit has pellets covered with finely divided platinum that acts as a catalyst and causes any oxygen present in hydrogen to react forming water vapor. The second column of molecular sieve removes this water vapor from the gas before it is fed to palladium diffused hydrogen purifier (Matheson model 8372). This unit consists of a palladium diffusion cell that is heated to ~400^0C. The cell temperature is maintained using a temperature controller. Hydrogen gas diffuses through the cell where palladium membrane removes the impurities. The ultra pure gas is fed to the inlet of the reactor tube using stainless steel tube. A flow meter is connected in the gas inlet path. We use flow of about 150cc/minute during the growth experiments. A combination of a rotary and a sorption pump is used to evacuate the furnace tube and the purifier cell. The vacuum in the tube is released using pure hydrogen. A portable hand held hydrogen leak detector (Matheson gas products) is used to detect leaks (>5ppm) at various joints in the growth apparatus.

In a typical growth experiment, after loading the substrate and the solutions, the reactor is purged with hydrogen gas for several hours. The purity of the gas is checked indirectly by first heating the graphite boat at about 900^0C for several hours. There is no deposition on the boat and no graphite powder or fine particles found, indicating the good quality of the gas. Six nine pure (99.9999) Leico gallium is then put in the solution wells, in the disposal bin, and in the place next to piston and above the substrate recess. The boat is again heated at about 800-850^{0}C for about 12hours. Gallium in all the places in the boat is shiny and this again confirms the purity of the gas.

2.7 Growth of single layers: GaAs and AlGaAs

Before attempting the synthesis of heterostructures, a number of single layers of GaAs and $Al_xGa_{1-x}As$ [x = 0.3,0.6] were grown at low temperatures in 700^{0}C-500^{0}C range to obtain layers of desired properties viz. doping concentration, alloy composition and thickness. Amount of GaAs needed to saturate liquid gallium at various temperatures was obtained using binary phase diagram for GaAs. The amount of aluminum required in the growth solution was determined using the data of V. M. Andreev and V. P. Khovstikov [43] shown in Fig. 2.8. Electrical behavior of Sn, Te, Ge, Mg and Zn doped single layers was studied. In a typical growth experiment, the growth substrate was first degreased in boiling organic solvents: first in methanol, then in acetone and finally in trichloroethylene and stored back in methanol. Just before etching, it was rinsed in water and then etched for five minutes in the solution containing $5H_2O + 1H_2O_2 + 1H_2SO_4$. This removed about 5µm GaAs material from the substrate surface. Etched substrate was then dried under nitrogen jet and quickly loaded in the recess in the graphite boat and covered with top graphite housing. For a single layer growth, a solution containing gallium and undoped GaAs pieces was placed in the first

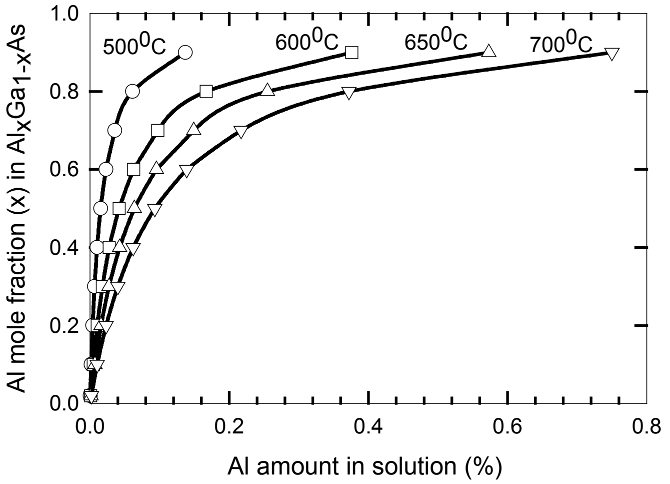

Fig. 2.8 Al incorporation in $Al_xGa_{1-x}As$

solution well. For single layer of AlGaAs growth, aluminum pieces were added to the growth solution. These aluminum pieces were cleaned using organic solvents as described above and etched in concentrated HCl for one minute, rinsed in de-ionized water and dried before use.

2.8 Synthesis of heterostructures

Synthesis of a heterostructure requires number of solutions each designed for growth of a specific layer in a heterostructure. Some layers are quite thick (~1µm), whereas some are thin (50-100nm), and hence, it was necessary to establish the growth temperature, temperature interval and the growth duration of each layer separately before attempting growth of a multilayered structure. Additionally, some layers are doped n-type and some are doped p-type, while some others are undoped. Hence it was also necessary to establish the background doping of undoped layers and the amount of particular dopant to be added to the solution to achieve a desired doping level. In going from the single layer to multilayer growth using several solutions, we experienced the problem of intermixing between the solutions. Apart from mixing, there could also be some grading and variations due to manual operation of solution displacements. Our experiments provide some measure of these aspects. For multilayer growth, the required solutions were prepared and put in different solution wells of the graphite boat.

Growth of a strained heterostructure was achieved by adding GaP or GaSb pieces to the solution used for the growth of a strained layer. Experiments have been conducted to establish the amounts of P (or Sb) source material used in the solution and the corresponding amount of P (or Sb) incorporated in the epitaxial layer. This was critical in experiments involving synthesis of GaAsP and GaAsSb layers. Since we need to grow a very thin (50-100 nm) layer, it was necessary to establish the optimum growth parameters such as growth temperature, solution supersaturation, and growth duration. Solution compositions were determined using phase diagrams as described next.

2.9 Phase diagram information and analysis.

The basis of LPE is the control of liquid-solid phase equilibrium. In the case of III-V materials, the solid phase is either 1:1 binary compound, e.g. GaAs, or an alloy of two or more compounds such as AlGaAs, while the liquid phase is normally a group III metal rich solution. For the growth, the important phase information required is:

(1) Liquidus data: gives the liquidus temperature (for a particular liquid-phase composition) at which on heating, the two phase (solid + liquid) mixture becomes a single phase (liquid). LPE growth normally occurs at or slightly below this liquidus temperature.
(2) Soildus data: provides the information about the composition of the solid phase in equilibrium with the liquid phase at the liquidus temperature.

It was necessary to establish the amounts of aluminum and arsenic to be added to liquid gallium solvent to saturate each solution at a specific temperature, and to achieve the desired aluminum content in layers to be incorporated in the heterostructure. We used the data calculated by Russian group as shown in Fig. 2.8. Typical amounts of GaAs and Al used for the saturation of 1gm gallium solvent at different growth temperatures are given in Table 2.1.

Table 2.1 Solution compositions used for single GaAs and AlGaAs layers.

Temp.	**GaAs**	**$Al_{0.3}Ga_{0.7}As$**		**$Al_{0.6}Ga_{0.4}As$**	
$T_g(^0C)$	GaAs(mg)	GaAs(mg)	Al(mg)	GaAs(mg)	Al(mg)
700	13.6	9.7	0.39	5.5	1.39
650	6.6	4.7	0.27	2.7	0.96
600	2.9	2.1	0.18	1.2	0.63
550	1.2	0.8	0.11	0.5	0.39
500	0.4	0.3	0.07	0.2	0.23

In our growth experiments, the active layer consists of (Al)GaAs, $GaAs_xP_{1-x}$ or $GaAs_xSb_{1-x}$ and it is grown at about 650^0C. Due to lack of GaAs-GaP (and GaAs-GaSb) phase diagram data at this growth temperature, we calculated solution compositions required to obtain $GaAs_xP_{1-x}$ and $GaAs_xSb_{1-x}$ [for (1-x) ~ 0-0.1].

2.9.1] Phase diagram calculations for GaAs-GaP

To compute the conditions for equilibrium between a ternary liquid solution of components A, B, C (Ga, As, P) and a quasi-binary solid solution AB-AC (GaAs-GaP), Stringfellow and Greene [44] derived the following equations:

$$RT \ln \gamma_{GaAs} (X) = RT \ln [4\, x_{Ga}^{l} x_{As}^{l} (\gamma_{Ga}^{l}\gamma_{As}^{l} / \gamma_{Ga}^{sl}\gamma_{As}^{sl})] + \Delta S^{F}_{GaAs} [T^{F}_{GaAs} - T] \qquad [1]$$

$$RT \ln \gamma_{GaP} (1-X) = RT \ln [4\, x_{Ga}^{l} x_{P}^{l} (\gamma_{Ga}^{l}\gamma_{P}^{l} / \gamma_{Ga}^{sl}\gamma_{P}^{sl})] + \Delta S^{F}_{GaP} [T^{F}_{GaP} - T] \qquad [2]$$

where γ_{GaAs} and γ_{GaP} are the activity coefficients of GaAs and GaP in the solid solution, X is the mole fraction of GaAs, x_i^l and γ_i^l (i = Ga, As and P) are the atom fractions and activity coefficients of components in the liquid solution, $\gamma_i{}^{sl}$ (i = Ga, As and P) are the activity coefficients of the stoichiometric liquid, ΔS^F, T^F, and T are respectively entropy of fusion, melting point (fusion temperature) and growth temperature. The activity coefficients γ_{GaAs} and γ_{GaP} in the solid solution are given by

$$RT \ln \gamma_{GaAs} = \beta_{GaAs\text{-}GaP} (1\text{-}X)^2$$

$$\text{and } RT \ln \gamma_{GaP} = \beta_{GaAs\text{-}GaP} (X)^2$$

where $\beta_{GaAs\text{-}GaP}$ is the interaction parameter for GaAs-GaP system, and is given to be 1000 cal/mole [45]. $T^F{}_{GaAs} = 1511$ K, $T^F{}_{GaP} = 1738$ K, $\Delta S^F{}_{GaAs} = 16.64$ e.u. , $\Delta S^F{}_{GaP} = 15.45$ e.u. With R = 1.98 cal/mol. K, and for T = 650^{0}C (923 K), equations 1 and 2 reduce to,

$X \exp [0.55(1\text{-}X)^2] = 838 [x_{Ga}{}^1 x_{As}{}^1 (\gamma_{Ga}{}^1 \gamma_{As}{}^1 / \gamma_{Ga}{}^{sl} \gamma_{As}{}^{sl})]$ [3]

$(1\text{-}X) \exp [0.55(X)^2] = 3991 [x_{Ga}{}^1 x_P{}^1 (\gamma_{Ga}{}^1 \gamma_P{}^1 / \gamma_{Ga}{}^{sl} \gamma_P{}^{sl})]$ [4]

In the stoichiometric liquid of Ga and As, $x_{Ga}{}^1 = x_{As}{}^1 = 0.5$, and hence from above equations, $\gamma_{Ga}{}^{sl} = \gamma_{As}{}^{sl} = 0.6267$. Similarly for, stoichiometric liquid of Ga and P, $x_{Ga}{}^1 = x_P{}^1 = 0.5$, and hence $\gamma_{Ga}{}^{sl} = \gamma_P{}^{sl} = 0.6847$. The activity coefficients γ's in the solution are given as:

$RT \ln \gamma_{Ga}{}^1 = \alpha_{Ga\text{-}As} (x_{As}{}^1)^2 + \alpha_{Ga\text{-}P} (x_P{}^1)^2 + [\alpha_{Ga\text{-}As} + \alpha_{Ga\text{-}P} - \alpha_{As\text{-}P}]\, x_P{}^1 x_{As}{}^1$

$RT \ln \gamma_{As}{}^1 = \alpha_{As\text{-}Ga} (x_{Ga}{}^1)^2 + \alpha_{As\text{-}P} (x_P{}^1)^2 + [\alpha_{As\text{-}Ga} + \alpha_{As\text{-}P} - \alpha_{Ga\text{-}P}]\, x_P{}^1 x_{Ga}{}^1$

$RT \ln \gamma_P{}^1 = \alpha_{P\text{-}Ga} (x_{Ga}{}^1)^2 + \alpha_{P\text{-}As} (x_{As}{}^1)^2 + [\alpha_{P\text{-}Ga} + \alpha_{P\text{-}As} - \alpha_{Ga\text{-}As}]\, x_{As}{}^1 x_{Ga}{}^1$

where $\alpha_{i,j}$ are the interaction energies of the various binary systems. These are given by Antypas et. al. [45], $\alpha_{Ga\text{-}As} = \alpha_{As\text{-}Ga} = -3.7$ T cal/mole, $\alpha_{Ga\text{-}P} = \alpha_{P\text{-}Ga} = -3.0$ T cal/mole, and $\alpha_{As\text{-}P} = \alpha_{P\text{-}As} = 2000$ cal/mole. For T = 650^{0}C (923 K), equations for γ's reduce to:

$\ln \gamma_{Ga}{}^1 = -\ 1.8691\, (x_{As}{}^1)^2 - 1.5152\, (x_P{}^1)^2 - 4.4786\, x_P{}^1 x_{As}{}^1$
$\ln \gamma_{As}{}^1 = -\ 1.8691\, (x_{Ga}{}^1)^2 + 1.0944\, (x_P{}^1)^2 - 0.7406\, x_P{}^1 x_{Ga}{}^1$
$\ln \gamma_P{}^1 = -\ 1.5152\, (x_{Ga}{}^1)^2 + 1.0944\, (x_{As}{}^1)^2 - 1.4482\, x_{As}{}^1 x_{Ga}{}^1$

Binary phase diagrams for GaAs and GaP at 650^{0}C give arsenic and phosphorus atom fractions in the solution as $x_{As}{}^1 = 0.003$ and $x_P{}^1 = 0.0002$. Using these values in above set of equations, the estimated activity coefficients are: $\gamma_{Ga}{}^1 = 0.9999$, $\gamma_{As}{}^1 = 0.1561$ and $\gamma_P{}^1 = 0.5875$. Substituting these various values of ($\gamma_i{}^1$) in equations 3 & 4, we obtain,

$X \exp [0.55(1\text{-}X)^2] = 333 (x_{Ga}{}^1 x_{As}{}^1)$ [5]

$(1\text{-}X) \exp [0.55(X)^2] = 5000 (x_{Ga}{}^1 x_P{}^1)$ [6]

Equations 5 and 6 together with the restriction, $x_{Ga}^{l} + x_{As}^{l} + x_{P}^{l} = 1$ are solved and the results are shown in Fig. 2.9. It gives the calculated solidus-liquidus of P incorporation. As seen, the amount of phosphorus required in the solution is too small to handle. Also, phosphorus in the GaP evaporates rapidly during homogenization of the growth solution. Hence, in the actual growth experiments, amount of GaP used is more than an order of magnitude larger than obtained from these calculations.

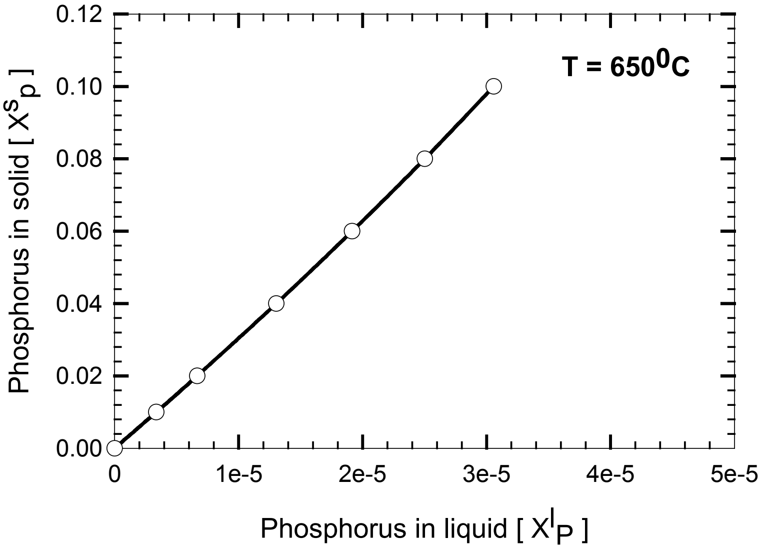

Fig. 2.9 Calculated solidus-liquidus of P incorporation

2.9.2] Phase diagram calculations for GaAs-GaSb:

M. Quillec et. al. [46] have computed GaAs-GaSb phase diagram over the whole range of x, $0<x<1$, and over a lower range of temperatures, 575-750^{0}C. They have followed the formalism and the parameter values given by Nahory et. al. [47], except in some cases where the solidus interaction parameter $\beta_{GaAs\text{-}GaSb}$ was varied from 2750-4250 cal/mole. We have checked these calculations using similar equations as used for GaAs-GaP system described above. The equations used for the calculations are,

$X \exp[1.5047(1-X)^2] = 2156\,[(x_{Ga}^{l} x_{As}^{l})(\gamma_{Ga}^{l}\gamma_{As}^{l})]$ [7]

$(1-X) \exp[1.5047(X)^2] = 6.96\,[(x_{Ga}^{l} x_{Sb}^{l})(\gamma_{Ga}^{l}\gamma_{Sb}^{l})]$ [8]

with $\beta_{GaAs\text{-}GaSb} = 2750$ cal/mole, $T = 650^0$C (923 K), $T^F_{GaAs} = 1511$ K, $T^F_{GaSb} = 985$ K, $\Delta S^F_{GaAs} = 16.64$ e.u., $\Delta S^F_{GaSb} = 12.3$ e.u., $R = 1.98$ cal/mol.K. The equations for the activity coefficients for GaAs-GaSb system at $T = 650^0$C (923 K) are:

$\ln \gamma_{Ga}^{1} = -\ 1.8691\ (x_{As}^{1})^2\ -\ 0.2732\ (x_{Sb}^{1})^2 - 3.4551\ x_{Sb}^{1}\ x_{As}^{1}$
$\ln \gamma_{As}^{1} = -\ 1.8691\ (x_{Ga}^{1})^2\ +\ 1.3131\ (x_{Sb}^{1})^2 - 0.2822\ x_{Sb}^{1}\ x_{Ga}^{1}$
$\ln \gamma_{Sb}^{1} = -\ 0.2732\ (x_{Ga}^{1})^2\ +\ 1.3131\ (x_{As}^{1})^2 - 2.9091\ x_{As}^{1}\ x_{Ga}^{1}$

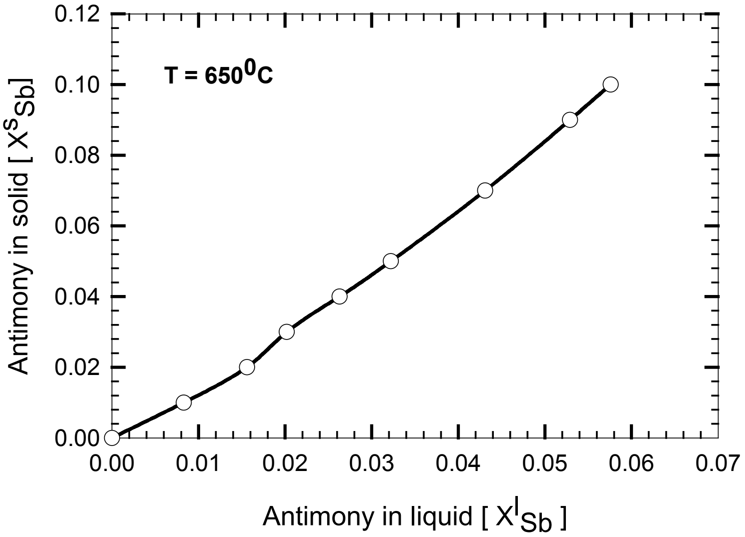

Fig. 2.10 Calculated solidus-liquidus of Sb incorporation

Binary phase diagrams for GaAs and GaSb at 650^{0}C, give arsenic and antimony atom fraction in the solution as $x_{As}^{1} = 0.003$ and $x_{Sb}^{1} = 0.2$. This gives an estimate of the activity coefficients as, $\gamma_{Ga}^{1} = 0.9999$, $\gamma_{As}^{1} = 0.1561$ and $\gamma_{Sb}^{1} = 0.77$. Using these values we get,

$X \exp [1.5047(1-X)^2] = 336\ (x_{Ga}^{1} x_{As}^{1})$ [9]

$(1-X) \exp [1.5047(X)^2] = 5.36\ (x_{Ga}^{1} x_{Sb}^{1})$ [10]

Equations 9 and 10 together with the restriction, $x_{Ga}^{1} + x_{As}^{1} + x_{Sb}^{1} = 1$, are solved and the results are shown in Fig. 2.10. It gives the calculated solidus-liquidus of Sb incorporation. Comparing figures 2.9 and 2.10, we see that for similar atom fraction of Sb (in GaAsSb) as of P (in GaAsP), the amount of GaSb required in the solution is about 100 times more than the amount of GaP. This is quite reasonable considering that the melting point of GaP (1465^{0}C) is much larger than that of GaSb (710^{0}C).

2.10 Characterization techniques for epitaxial layers and heterostructures.

Following techniques are used to characterize single layers and multilayer structures:

2.10.1] Surface morphology and layer thickness: Surface morphology of the single layer and the topmost layer in the multi-layer structure is at first examined using Nomarski interference contrast optical microscope. Peculiar surface features are recorded using both optical microscope and scanning electron microscope (SEM). For measuring the thickness of the grown layer/layers, a small piece of the sample is cleaved. Chemical solution used for delineating the junctions is known as A-B etchant [48] and consists of [A] - 40c.c.H_2O + 0.3gm $AgNO_3$ + 40c.c.HF and [B] - 40gmCrO_3 + 40c.c.H_2O. Solutions A and B are stored in separate plastic squeeze bottles. The etchant is mixed by squeezing out equal parts of A and B into a plastic container just before use. The cleaved piece is dipped in the solution for few seconds, rinsed in water and then examined using optical and/or scanning electron microscope (SEM).

2.10.2] Hall measurements: Electrical properties such as mobility, carrier concentration (doping density) and the carrier type, are determined using Hall measurements. For this, a single layer of the desired material is grown on a semi-insulating GaAs substrate. Hall measurements are made using Van der Pauw technique [49]. In this method, specific resistivity and Hall effect of flat samples of arbitrary shape can be measured if the contacts are sufficiently small and located at the circumference of the sample. For this purpose, the sample is cut into a square plate of about 5x5 mm and four indium balls are alloyed at corners by heating in high purity hydrogen at ~ 400^0C for one minute. Fig. 2.11 shows a typical sample with four contacts A, B, C and D alloyed on the epi side of the sample under test. Current is passed through one pair of contacts and the voltage is measured across the other. Thus, $R_{AB, CD}$ = [potential difference between C and D / current through A and B]. Similarly $R_{BC, DA}$ is measured with voltage measured across DA due to current passing through contacts B and C. We obtain $R'_{AB, CD} = (R_{AB, CD} + R_{CD, AB}) / 2$ and $R'_{BC, DA} = (R_{BC, DA} + R_{DA, BC}) / 2$.

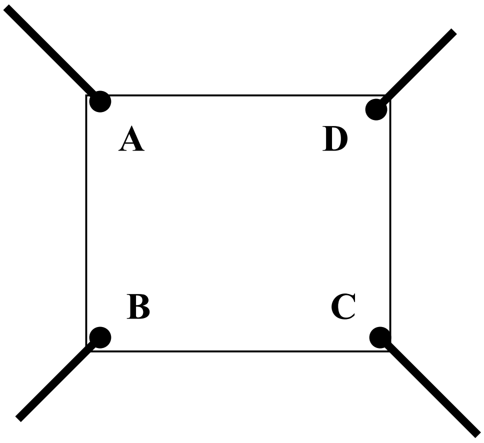

Fig. 2.11 Van der Pauw geometry with four alloyed (In) contacts for Hall measurements

Specific resistivity of the sample is given by

$\rho = [\pi d / \ln 2] [(R'_{AB, CD} + R'_{BC, DA}) / 2] f [R'_{AB, CD} / R'_{BC, DA}]$, where d is thickness of epi layer, and f is the geometrical correction factor which depends on the ratio $R'_{AB, CD} / R'_{BC, DA}$ (this ratio is always made greater than unity by keeping the larger of the two terms in the numerator). For $R'_{AB, CD} = R'_{BC, DA}$, f is unity. For the ratio $(R'_{AB, CD} / R'_{BC, DA}) > 1$, the correction factor f varies from 0.2 to 0.9 for ratio values ranging from 1000 to 3 respectively and its graphical form is given in the Van der Pauw article [49]. For reliable results, low ratio values 1 to 3 are desirable.

Hall mobility is determined by measuring the resistance $R_{BD, AC}$ and $R_{AC, BD}$ (obtained when current is passed through one pair of diagonally opposite contacts and voltage is measured across the other pair of contacts) with and without magnetic field B applied perpendicular to the sample. Hall mobility μ_H is obtained from the difference in the two readings with the field B and with B = 0. Thus, $\Delta R_{AC, BD} = [R_{AC, BD} (B) - R_{AC, BD} (0)]$ and $\Delta R_{BD, AC} = [R_{BD, AC} (B) - R_{BD, AC} (0)]$. The Hall voltage ΔV is measured in the magnetic field B of about 3 kilogauss. The carrier density and mobility are obtained by using the relations, $n_H = (1 / e \rho \mu_H)$, where e is charge of electron, ρ is specific resistivity and $\mu_H = (d/B) [(\Delta R_{AC, BD} + \Delta R_{BD, AC} / 2 \rho]$. Thus, from Hall measurements electrical parameters such as carrier density and mobility are obtained to ascertain the quality of the materials grown. The sign of the Hall voltage gives the carrier (n/p) type.

2.10.3] ECV profile measurements: A multilayer structure consists of number of layers of different compositions, thickness and doping concentrations. It is desirable to know the carrier type and the profile as a function of thickness. For single layers, capacitance voltage [C-V] measurements are used [50]. For this, Au-Ge-Ni ohmic contact is deposited by vacuum evaporation and alloyed at the back of n+ GaAs substrate upon which the desired epi layer is already grown. Usually Au Schottky dot contacts of area $\sim 10^{-3} cm^2$ are deposited on the sample surface. In this method, the reverse breakdown voltage of the Schottky diode decides the maximum depth of profiling. For the materials with very high carrier concentrations ($>10^{18} cm^{-3}$), the depletion layer is narrow and this method is not useful. This limitation is overcome by using an electrochemical etching system, in which the semiconductor-electrolyte interface behaves as a Schottky diode. This apparatus combines electrochemical etching and capacitance measurement with bias which gives doping concentration [51]. By making use of a well-defined electrochemical dissolution reaction, the material can be profiled to any depth at a controlled and calculated rate. In this work, electrochemical C-V profiler (Bio-Rad PN4300) is used to measure the carrier profile in the device structures. Fig. 2.12 shows the schematic diagram of electro-chemical cell used for these measurements. The cell body is made of 'Teflon' to avoid corrosion due to the chemicals used. The sample is mounted on a 'O' shaped rubber ring and pressed using the plunger. For AlGaAs/GaAs materials, NaOH: EDTA (ethylene diamine tetra acetate) solution is used for etching.

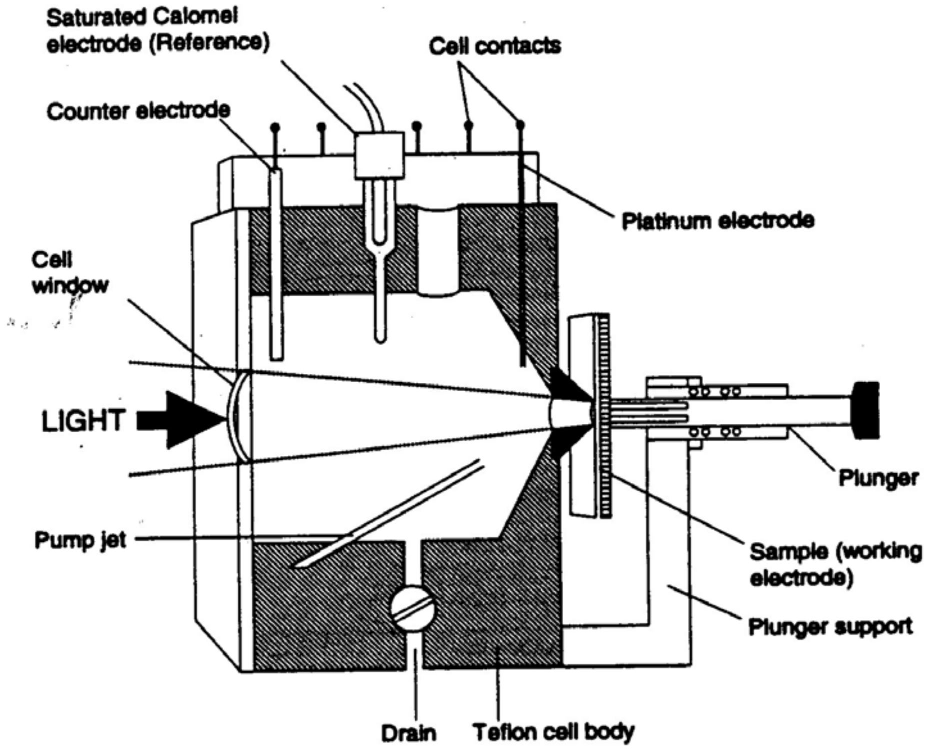

Fig. 2.12 The electrochemical cell

A platinum electrode is used for C-V measurements, a carbon electrode is used to complete the circuit for etching and a saturated calomel electrode is used as a reference. The sample is etched by passing a current through it. While p-type samples could be etched without light, n-type samples require shining light to pass appreciable current. C-V measurement at each etch step gives the carrier concentration using the relation, $n = [1/e\varepsilon_o\varepsilon_r A^2]\ [C^3/dC/dV]$. In this equation, e is the charge of electron, ε_o is the permittivity of free space, ε_r is the relative permittivity of the semiconductor, A is the effective contact area, and C is capacitance. dC/dV is obtained in the instrument by two measurements of capacitance at (i) zero bias and (ii) small reverse bias. The frequency of measurements is typically in 0.5-1.5 kH_z range. This measurement gives a plot of carrier concentration as a function of depth during the etching of the layer.

2.10.4] Photoluminescence measurements: Optical quality and composition of single layers and heterostructures are determined using room temperature / low temperature photoluminecsence (PL) spectroscopy [52-53]. The mechanism of PL emission with various recombination processes is shown in Fig. 2.13. Energy levels E_C, E_V, E_a and E_d denote the relative positions of the conduction band edge, valence band edge, acceptor level and donor level respectively. In PL spectroscopy, an intense laser beam of photon energy larger than the band gap of the semiconductor material under study is used to generate electrons and holes in the conduction and valence bands respectively (process1, in Fig.2.13). The electron hole pairs created in this manner are in a non-equilibrium state from which they rapidly relax into a quasi-equilibrium state and then get annihilated by radiative and non-radiative recombination transitions. The radiative transitions can occur by various processes as shown in Fig. 2.13. Apart from these processes, the emission may also occur by excitonic processes and

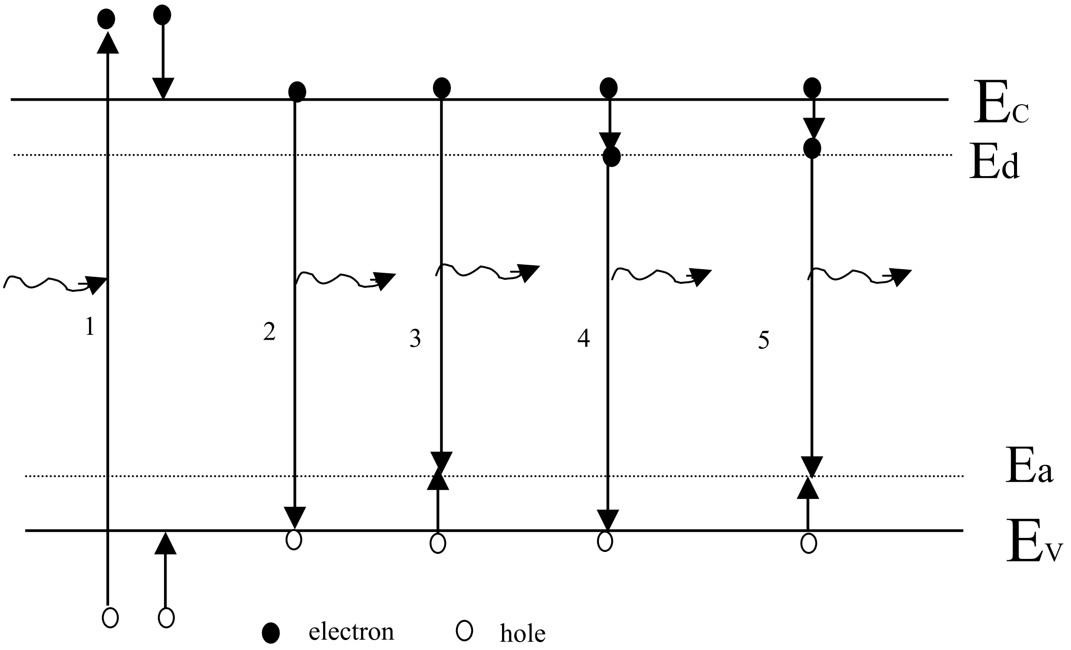

Fig. 2.13 Schematic of the radiative processes in photoluminescence spectroscopy (1) generation of electrons and holes (2) conduction band to valence band (BB) transition (3) conduction band to acceptor level (BA) (4) donor level to valence band (DB) and (5) donor level to acceptor level (DA).

recombinations involving a complex. PL spectroscopy involves the study of energy dependence of the number of photons emitted by a material by radiative transitions.

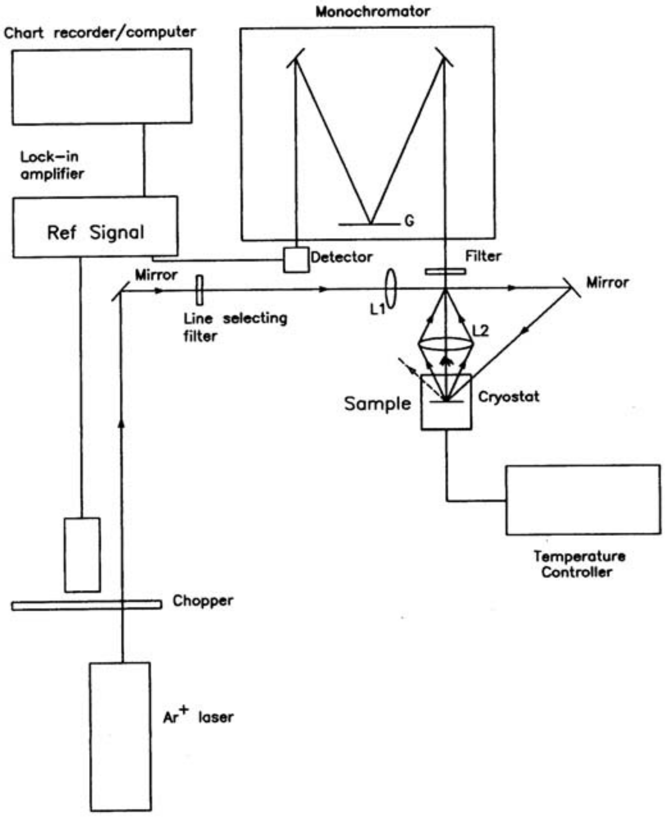

Fig. 2.14 PL measurements set up

The experimental set up used for PL measurements is shown in Fig. 2.14. The excitation source is air-cooled Argon ion laser whose 488nm line is selected by using a filter. Laser beam is chopped using a mechanical chopper for phase sensitive detection of the PL signal using a lock-in amplifier (SR-510, Standford Research Systems). For low temperature measurements, the sample is mounted on a cold finger of a closed cycle He cryostat (CTI Cryogenics) that is connected to a temperature controller. All the measurements have been done after ensuring the temperature stability. Using a lens, the luminescence signal from the sample is focussed on the entrance slits of a 0.67m monochromator (McPherson scanning monochromator). Long pass filters (OG 515 or 530nm) are used to cut off the stray laser light that might reach the monochromator after reflection from the sample. Luminescence signal at about 1μm, is detected and recorded using a silicon detector. PL plots of luminescence intensity versus wavelength have been recorded using this set up [54]. At low temperatures, various processes depicted in Fig. 2.13 give several spectral lines. In this case, band to band edge emission is generally not seen. However, high purity samples can provide free exciton emission. Compositions of $Al_xGa_{1-x}As$ can be obtained from low temperature PL plots using the relation, E_g (x) = 1.515 + 1.247x (eV), for $Al_xGa_{1-x}As$ materials provided the sample gives free exciton luminescence. At room temperature, band to band process is dominant in the direct bandgap materials. For these, the compositions can be obtained using the relation, E_g (x) = 1.424 + 1.247x (eV). In case of indirect bandgap materials, band to band PL may be too weak to be observed. In such cases PL emission is significant if an impurity/defect is involved. In these cases, composition is generally obtained by x-ray diffraction.

2.10.5] X-ray measurements: Measurement of lattice mismatch, strain and composition: In lattice matched materials such as GaAs/GaAs or nearly lattice matched AlGaAs/GaAs, several microns thick, smooth, dislocation free layers can be grown. Lattice parameter of GaAs is 5.6532Å, and that of AlAs is 5.6612Å. The lattice parameter of $Al_xGa_{1-x}As$ follows Vegard's law, given as $a_{AlxGa1-xAs}$ = 5.6532 + 0.008 x. Even though these compositions are closely lattice matched, one can get separate x-ray lines from different AlGaAs layers by using high-resolution x-ray diffraction. Measurement of the lattice mismatch is done using a high resolution X-ray diffractometer [Phillips X'PERT-MRD]. Fig. 2.15 shows the schematic of the set up. In this instrument, the beam emerging from the X-ray tube is passed through 4-reflection monochromator [Bartels type, four reflections, Ge (022)]. The monochromator provides Cu Kα_1 x-ray beam [λ = 1.54Å] of about 12-arcsec divergence in the scattering

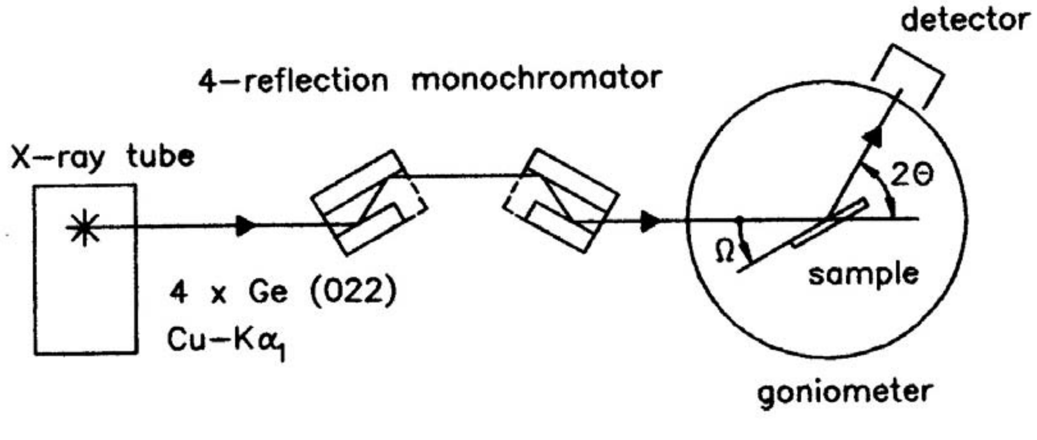

Fig. 2.15 HR-XRD measurement set up

plane. This beam is incident on the sample and the diffracted beam is detected using a detector. Most of the scans are recorded with 2^0 opening angle of the detector. HR-XRD plots are recorded using ω-2θ scans. Compositions of $Al_xGa_{1-x}As$ can be obtained by recording (004) diffraction scans (rocking curves) where separate peaks due to substrate (S) and layer (L) are recorded [Fig. 2.16].

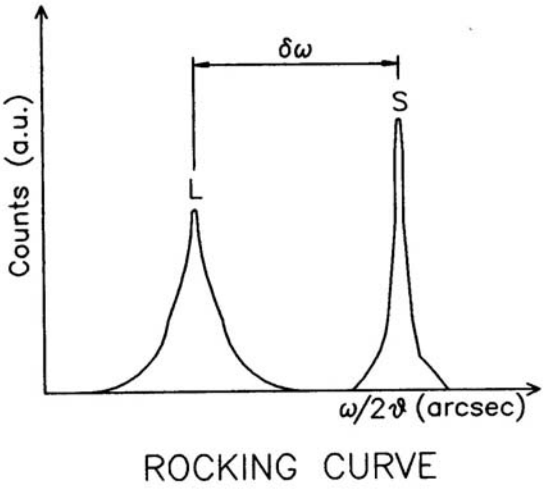

Fig. 2.16 Rocking curve recorded using HR-XRD

Using Bragg's law:

$\lambda = 2d \sin\theta$ for substrate and

$\lambda = 2(d + \delta d)\sin(\theta + \delta\theta)$ for the layer

where d is the spacing between layers and θ is Bragg angle. The peak separation between layer and the substrate $\delta\omega_{L,S}$ is related to strain parameter ($\varepsilon_\perp$)

$\varepsilon_\perp = |\delta d / d|_\perp = \delta\omega_{L,S} \cot\theta$.

Lattice mismatch (f) is defined through elastic coefficients [55] using,

$f = p\,\varepsilon_\perp$ where $p = C_{11} / (C_{11} + 2C_{12})$ for epi layer grown on (001) GaAs.

C_{11} and C_{12} are elastic coefficients for GaAs.

For $C_{11} = 11.9 \times 10^{11}$ (dyn.cm^{-2}), $C_{12} = 5.38 \times 10^{11}$ (dyn.cm^{-2}), p = 0.525. Lattice mismatch is defined as $f = \Delta a / a_s$. where $\Delta a = |a_l - a_s|$, a_l and a_s are lattice parameters of the layer and the substrate respectively. From experiment we obtain $\Delta a = f\,a_s$ such that composition [x] in $Al_xGa_{1-x}As$ is calculated using, $x = \Delta a / (a_{AlAs} - a_{GaAs})$, where a_{AlAs} and a_{GaAs} are lattice parameters of GaAs and AlAs respectively.

Next, we discuss briefly the heterostructures where the lattice parameter difference between the layer and the substrate (GaAs) is much larger than the case of GaAs and AlAs, as for example $a_{GaAs} = 5.6532Å$, $a_{GaP} = 5.4505Å$, and $a_{GaSb} = 6.0959Å$. Fig.2.17 shows schematic of lattice mismatched layers in which lattice constant of the layers (a_L) is either (a) larger or

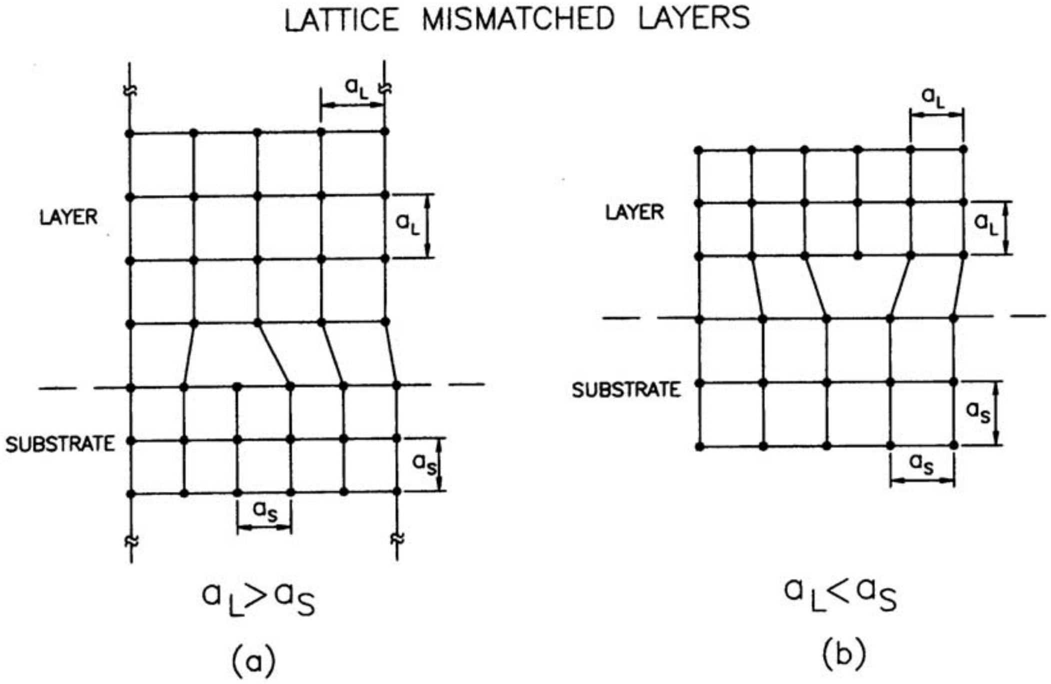

Fig. 2.17 Schematic of lattice mismatched layers

(b) smaller than that of the substrate (a_S). As seen, at the interface, two materials try to accommodate each other by adjusting the in plane lattice spacing, but if the mismatch is too large, then the defects called misfit dislocations are generated. The dislocations generated at the interface do not remain confined to the interface. They climb along the glide planes and move from one plane to another and thus generate a network spread throughout the thickness of the mismatched epi layer. In this case, the surface morphology is no longer smooth and appears as a crosshatch of dislocation lines. For thick epi layers with mismatch, the misfit dislocation network in the sample relieves strain. However, the strain can be fully accommodated if the thickness of the layer is kept below a critical value (h_c) given by Matthews and Blakeslee relation [56],

$(h_c) = a_0 (1-\sigma/4) [\ln (h_c\sqrt{2}/a_0) + 1] / (2\sqrt{2}) \pi f (1+\sigma)$,

where h_c is the critical thickness, a_0 is the lattice constant of the substrate, σ is the Poisson ratio, and [$f = \Delta a / a_s$] is the lattice mismatch between the epi layer and the substrate. If the strain is accommodated then no dislocations are generated. In this case, the lattice parameter of the epitaxial layer in the direction parallel to the interface is forced to be equal to the lattice parameter of the substrate, but the lattice parameter perpendicular to the interface undergoes substantial change and depends on the strain. These aspects are considered in some detail next.

Compressive strain: For epitaxial layer thinner than h_c, if the lattice parameter of the layer material is larger than the substrate material as shown in Fig. 2.18 (a), then during growth, in plane (parallel) lattice parameter ($a_{||}$) gets adjusted with the substrate lattice parameter (a_S) by compression. Correspondingly, the out-of plane (perpendicular) lattice parameter ($a_\perp$) gets elongated as seen in Fig. 2.18 (b).

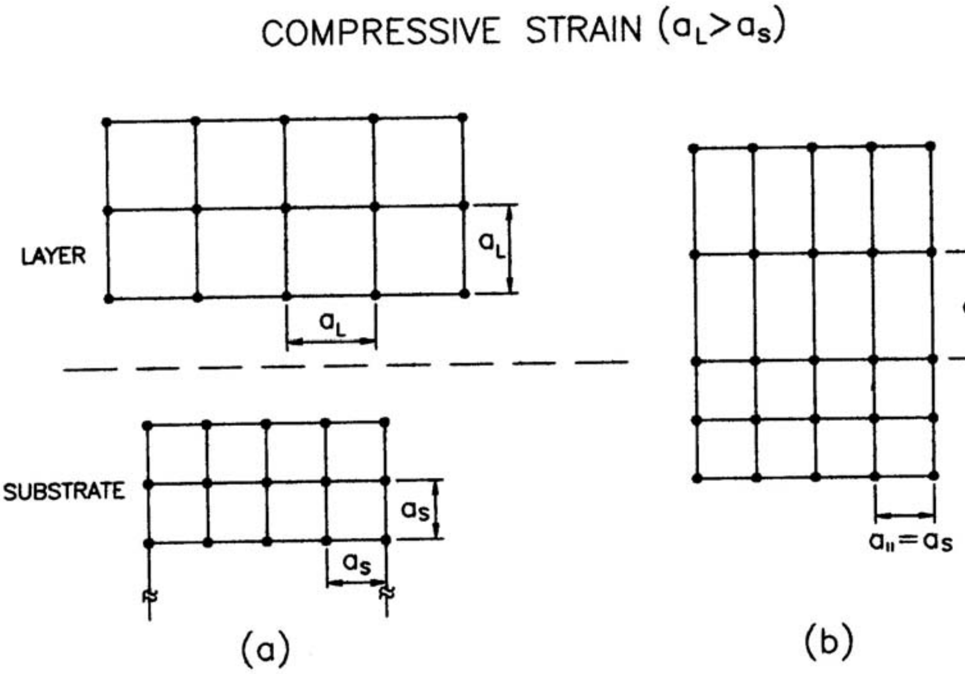

Fig. 2.18 Schematic of a compressive strain (a) Lattice parameters of substrate and layer materials (b) Lattice structure of fully strained heterostructure.

Tensile strain: Fig. 2.19 shows schematic of the case of a tensile strain for epi layer thinner than h_c. In this case, the lattice parameter of the layer material is smaller than that of the substrate material. During growth, the parallel lattice parameter of the layer is forced to expand under a tensile strain and perpendicular lattice parameter shrinks.

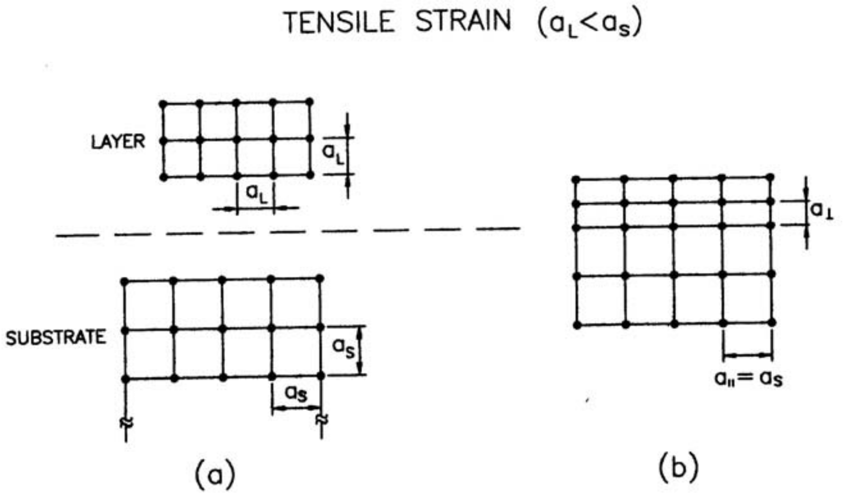

Fig. 2.19 Schematic of a tensile strain (a) Lattice parameters of substrate and layer materials (b) Lattice structure of fully strained heterostructure.

Such coherently strained layers discussed above are called pseudomorphic, since they take the morphology or form (in this case the lattice constant) of the substrate. The perpendicular ($\varepsilon_\perp$) and parallel ($\varepsilon_{||}$) strain parameters are defined with respect to the substrate as [57],

$\varepsilon_\perp = (a_\perp - a_{sub}) / a_{sub}$ and $\varepsilon_{||} = (a_{||} - a_{sub}) / a_{sub}$

where a_{sub} is the substrate lattice parameter, $a_\perp$ and $a_{||}$ are the out of plane and in plane lattice parameters for the strained layer, respectively. Thus, in fully strained case $a_{||} = a_{sub}$ and $\varepsilon_{||} = 0$.

For heterostructures in which layer thickness is larger than (h_c), strain is partially relaxed by producing dislocations. In this case $a_{||} \neq a_{sub}$ and $\varepsilon_{||} \neq 0$ and we need to determine both $\varepsilon_{||}$ and $\varepsilon_\perp$ for the layer to characterize it fully. The mismatch 'f 'of layer with respect to the substrate is defined through elastic coefficients [C_{ij}] as [55]

$f = p(\varepsilon_\perp - \varepsilon_{||}) + \varepsilon_{||}$ where for (001) GaAs substrate

$p = C_{11} / (C_{11} + 2C_{12})$.

In order to get $\varepsilon_\perp$ (out of plane) and $\varepsilon_{||}$ (in plane) strain parameters, it is necessary to measure several x-ray diffraction plots from symmetric reflections such as (004) and asymmetric reflections such as (115) and (026).

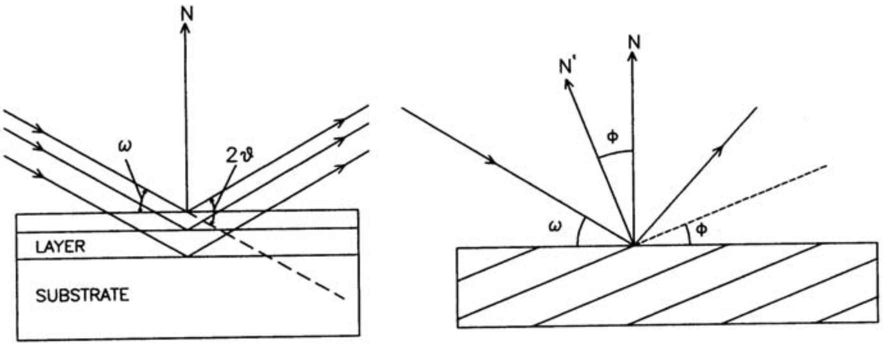

SYMMETRIC REFLECTIONS

ASYMMETRIC REFLECTIONS

Fig. 2.20 (a) and (b) schematic of the reflection geometry.

Figs. 2.20 (a) and (b) show schematic of the reflection geometries used in these measurements. As seen in Fig. 2.20 (a), in case of symmetric reflections such as (004), the reflecting planes of both the substrate and the layer are parallel to each other. In case of asymmetric reflections such as (115) and (026), the layer planes are inclined at an angle Φ, [Fig. 2.20 (b)], where Φ is the angle between reflecting plane and the surface. In both cases, the XRD measurements give a rocking curve similar to one shown schematically in Fig. 2.16 for $a_l > a_s$. The angular separation between the layer peak and substrate peak ($\delta\omega_{L,S}$) is now related to $\varepsilon_\perp$ and $\varepsilon_\parallel$ [58], as follows:

$\delta\omega_{L,S} = k_1 \varepsilon_\perp + k_2 \varepsilon_\parallel$, where

$k_1 = \cos^2 \Phi \tan \theta + (1/2) \sin 2\Phi$, and

$k_2 = \sin^2 \Phi \tan \theta - (1/2) \sin 2\Phi$

where θ is the Bragg angle of substrate reflection and Φ is the angle between the reflecting plane and the sample surface. The angle of incidence of the X-ray beam can be either $(\theta - \Phi)$ for low incidence or $(\theta + \Phi)$ for high incidence. It is clear from equations for k_1 and k_2 that only asymmetric reflections with $\Phi \neq 0$ can yield information on the in plane strain of the strained layer. Equation for $\Delta\omega_{L,S}$, linear in two strain parameters is used in a least square fit of the measured separations ($\Delta\omega_{L,S}$) for several reflections to obtain $\varepsilon_\perp$ and ε_{II} and their standard deviations. From the measured strain parameters, the lattice mismatch 'f' is computed. This is used to compute the critical thickness (h_c) and the composition of the active layer material using, $[X_P^S] = \Delta a / (a_{GaAs} - a_{GaP})$ and $[X_{Sb}^S] = \Delta a / (a_{GaAs} - a_{GaSb})$.

2.11 Fabrication of laser diodes

In the conventional broad-area device fabrication process, a stripe contact is first defined by chemical etching through the p+ GaAs cap/contact layer followed by deposition and patterning of an insulator like SiO_2 or Si_3N_4 before metallization. This process requires two photolithographic steps and deposition of insulator using sputtering or plasma-enhanced chemical vapor deposition. Furthermore, the devices have to be cut into individual chips for testing. This takes typically a week. There was a need for a quick turn around process to check the characteristics of the grown structures. For this a quick turn around process was developed in our laboratory and the devices could be fabricated in two/three days [59]. Fig. 2.21 shows the details of the fabrication steps.

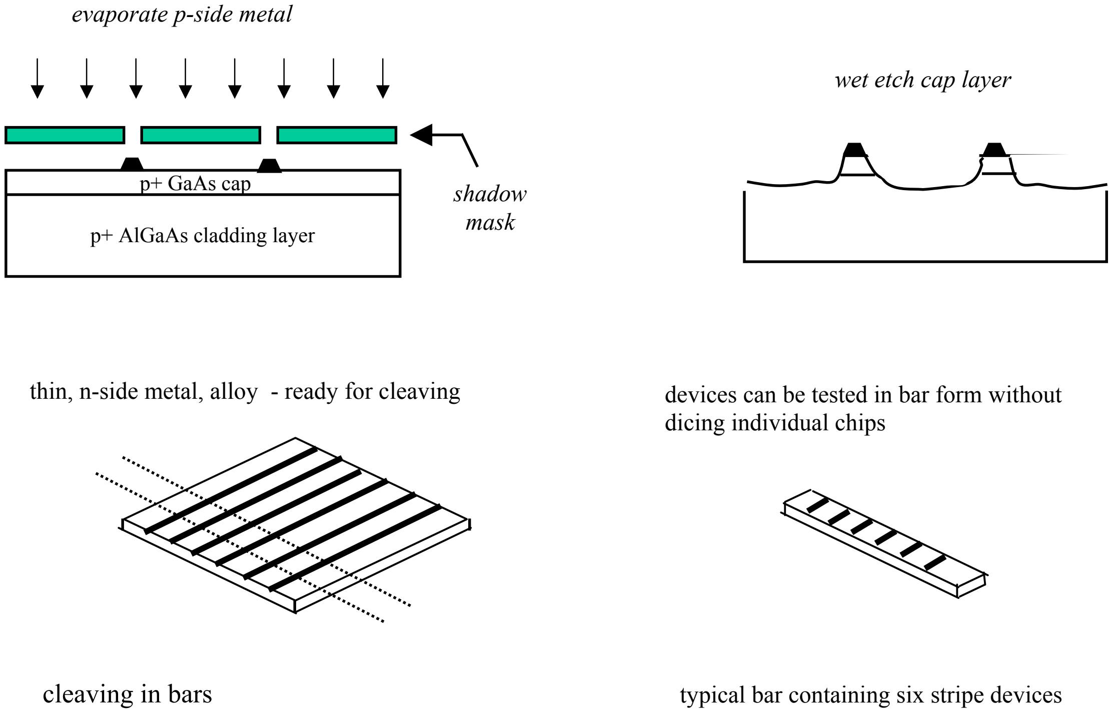
evaporate p-side metal
p+ GaAs cap
p+ AlGaAs cladding layer
shadow mask
wet etch cap layer
thin, n-side metal, alloy - ready for cleaving
devices can be tested in bar form without dicing individual chips
cleaving in bars
typical bar containing six stripe devices

Fig. 2.21 Schematic of the process steps for fabricating devices

This process begins with the deposition of 100μm wide stripes on the p-GaAs using Ti/Pd/Au metals through a shadow mask. These metal stripes themselves then serve as a mask to remove the p+ GaAs layer in between the stripes by wet chemical etch ($H_3PO_4:H_2O_2:H_2O_2$). This thus serves to electrically isolate the devices, enabling the device testing at bar level after subsequent processing. Wafer thinning and n-side metallization using Au-Ge-Ni alloy followed by rapid thermal annealing completes the fabrication process. As the devices are isolated there is no need for cutting the individual chips. The devices are cleaved perpendicular to the stripes into the bars of 250μm to 1mm resonator length containing several individual devices of 100μm aperture. This process was used to fabricate all the laser structures. Procedure used to measure characteristics of laser diodes is described in chapter 4.

REFERENCES

[1] H. Nelson, RCA Rev. 24 (1963) 603.

[2] L. R. Dawson, in progress in Solid State Chemistry, (1972), Vol. 7, Ed. H. Reiss and J. O. McCaldin (GaAs and AlGaAs)

[3] Special Edition of Journal of Crystal growth on liquid phase epitaxy vol. 27 (1974).

[4] K W. Benz and E. Bauser in Crystals-Growth, properties and applications (1980), vol.3, Ed. H. C. Freyhardt (Growth mechanisms)

[5] J. J. Hsieh in Handbook on Semiconductors, 3 (1980) 415. [General Review]

[6] J. C. Brice in Current Topics in Material Science (1980), vol.5, Ed. E. Kaldis (Theory, techniques, GaAs, AlGaAs)

[7] K. Nakajima in GaInAsP alloy Semiconductors, (1982), Ed. T. P. Pearsall (GaInAsP)

[8] P. D. Green in Advanced Crystal Growth, Ed. P. M. Dryburgh et al (1987).

[9] M. G. Astles in Liquid-Phase Epitaxial Growth of III-V Compound Semiconductor Materials and their Device Applications, Adams Hilger, Great Britain (1990).

[10] E. Kuphal, in Liquid Phase Epitaxy, Appl. Phys. A 52 (1991) 380.

[11] R. L. Moon, Journal of Crystal Growth, 170 (1997) 1.

[12] H. Rupprecht, Inst. Phys. Conf. Ser. No. 3, (1966) 57.

[13] M. B. Panish, I. Hayashi and S. Sumski, IEEE J. Quantum Electron. 5 (1969) 210.

[14] G. H. B. Thompson and P. A. Kirby, J. Crystal Growth 27, (1974) 70.

[15] Y. Horikoshi, Japn. J. Appl. Phys. 15, (1976) 887.

[16] Zh. I. Alferov, V. M. Andreev, S. G. Konnikov, V. R. Larionov and B. V. Pushny, Krist. Tech. 11 (1976) 1013.

[17] T. B. Reed, Solid State Research Report (1969:1) MIT Lincoln Laboratory, MA, USA

[18] J. J. Hsieh, J. Crystal Growth, 27 (1974) 49.

[19] R. Sankaran, G. A. Antypas, R. L. Moon, J. S. Escher and L. W. James, J. Vac. Sci. Technol. 13 (1976) 932.

[20] T. P. Pearsall and R. W. Hopson Jr. J. Appl. Phys. 48 (1977) 4407.

[21] K. Sakai, Y. Matsushima, S. Akiba and T. Yamamoto, Japn. J. Appl. Phys. 18 (1979) 1009.

[22] R. E. Nahory, M. A. Pollack, J. C. DeWinter and K. M. Williams, J. Appl. Phys. 48 (1977) 1607.

[23] H. Kano and K. Sugiyama, Electron. Lett. 16 (1980) 146.

[24] N. Kobayashi, Y. Horikoshi and C. Uemara, Japn. J. Appl. Phys. 18 (1979) 2169.

[25] S. D. Hersee, A. C. Carter, R. C. Goodfellow, G. Hawkins and I. Griffith, Solid state Electron Devices, 3 (1979) 179.

[26] J. J. Hsieh, M. C. Finn and J. A. Rossi, 6th Intl. Symp. on GaAs and related compounds, St. Louise (Inst. Phys. Conf. Ser.) 33a (1976) 37.

[27] Zh. I. Alferov, V. M. Andreev, D. Z. Garbuzov, Yu. V. Zhilyaev, E. P. Morozov, E. L. Portnoi and V. G. Trofim, Sov. Phys. Semicond. 4, (1971) 1573.

[28] I. Hayashi, M. B. Panish, P. W. Foy and S. Sumski, Appl. Phys. Lett. 17, (1970) 109.

[29] I. Hayashi, U. S. Patent No. 3,691,476 (1972)

[30] G. H. B. Thompson and P. A. Kirby, IEEE J. Quantum Electron. QE-9, (1973) 311.

[31] L. Schultheiss and K. Ploog, Phys. Rev. B 30 (1984) 1090.

[32] H. Kawai, K. Kaneko and N. Watanabe, J. Appl. Phys. 56 (1984) 463.

[33] C. F. J. Schanen, S. Illek, H. Lang, W. Thulke and M. C. Amann, IEEE Proc. Part J, 137 (1990) 69.

[34] Mu-Kuen-Chen, Tien-Chin Chang, and Hao-Hsiung Lin, J. Appl. Phys. 74 (1993) 3464.

[35] K. Ketling, K. Koehler and P. Zwicknagl, Appl. Phys. Lett. 48 (1986) 157.

[36] Zh. I. Alferov, A. A. Vodnev, O. O. Ivent'eva, V. R. Laroinov and V. D. Rumyantsev, Sov. Phys. Semicond, 20 (1986) 239.

[37] S. Subramanian and B. M. Arora, J. Appl. Phys. 49 (1978) 257.

[38] S. Chakravarty, B. M. Arora, A. K. Srivastava, S. Subramanian, and S. Anand, Thin Solid Films 163 (1988) 443.

[39] S. S. Chandvankar, R. Rajalakshmi, A. K. Srivastava, and B. M. Arora, J. Cryst. Growth 88 (1988) 303.

[40] S. S. Chandvankar, and B. M. Arora, J. Cryst. Growth 94 (1989) 270.

[41] B. M. Arora, S. S. Chandvankar, R. Rajalakshmi, A. K. Srivastava, and S Chakravarty, Thin Solid Films 163 (1988) 421.

[42] S. S. Chandvankar, T. K. Sharma, A. P. Shah, K. S. Chandrasekaran, B. M. Arora, A. K. Kapoor, Devendra Verma, B. B. Sharma, J. Cryst. Growth 213 (2000) 250.

[43] V. M. Andreev and V. P. Khovstikov, Private communication.

[44] G. B. Stringfellow and P. E. Greene, J. Phys. Chem. Solids, 30 (1969) 1779.

[45] G. A. Antypas, J. Elec. Chem. Soc., 117 (1970) 700.

[46] M. Quillec, C. G. Fonstad, and S. Garone, J. Appl. Phys., 49 (1978) 5920.

[47] R. E. Nahory, M. A. Pollack, J. C. Dewinter and K. M. Williams, J. Appl. Phys. 48 (1977) 1607.

[48] G. H. Olsen and M. Ettenberg, J. Appl. Phys. 45 (1974) 5112.

[49] L. J. van der Pauw, Phillips Research reports 13 (1958) 1.

[50] S. M. Sze in Physics of Semiconductor Devices, Wiley Eastern Ltd. (1981).

[51] I. C. Mayes in Bio-Rad Semiconductor notes, Note N0. 201 (1985).

[52] E. W. Williams and H. Bebb, Semiconductor and Semimetals, edited by R. K. Willardson and A. C. Beer Vol.8 (1972) P. 181. (Academic, New York, 1972)

[53] L. Pavesi and M. Guzzi, J. Appl. Phys. 75 (1994) 4779.

[54] A. K. Srivastava, Ind. J. of Pure and Applied Physics, 27 (1989) 386.

[55] W. J. Bartels, W. Nijman, J. Cryst. Growth 44 (1978) 518.

[56] J. W. Matthews and A. E. Blakeslee, J. Cryst. Growth 27 (1974) 118.

[57] S. T. Picraux, B. L. Doyle, and J.Y. Tsao, in: T. P. Pearsall (Ed.) Semiconductors and Semimetals, vol. 33 (1991) 174.

[58] R. Zaus, J. Appl. Cryst. 26 (1993) 801.

[59] S. S. Chandvankar, A. P. Shah, A. Bhattacharya, K. S. Chandrasekaran, and B. M. Arora Proceedings: Photonics-2000, International Conference on Fiber Optics and Photonics, Calcutta, Vol. 1, (2000) 203.

Chapter 3

Growth experiments and materials characterization.

3.1 Growth experiments:

The main objective of our growth experiments was to synthesize separately confined heterostructures (SCH) for laser diodes based on AlGaAs/GaAs material system, using our apparatus. We wanted to grow thinnest possible layer reproducibly that can be used as the active layer of laser diodes. Further, we wanted to grow thin lattice mismatched active layers for varying wavelength of laser emission. In our design, a typical laser diode structure consists of eight layers on n^+-GaAs substrate. Fig. 3.1 shows schematic of the complete laser heterostructure consisting of line drawing of the undulations of the conduction band edge.

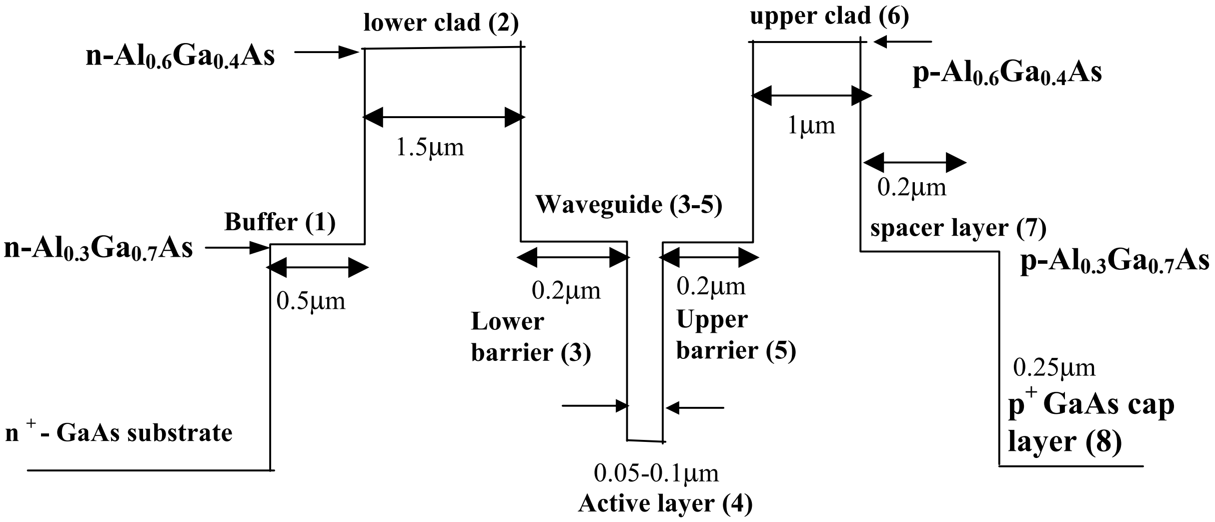

Fig. 3.1 Schematic of the layers in AlGaAs/GaAs heterostructures

Beginning with the substrate on the left, the structure is complete with a GaAs cap layer shown on the right. It is about 4μm thick and consists of layers of AlGaAs and GaAs deposited sequentially. Each layer is designed for a specific composition, doping and thickness. The layers are:

1] n-doped **buffer** layer: n-$Al_{0.3}Ga_{0.7}As$: Te
2] n-doped **lower cladding** layer: n-$Al_{0.6}Ga_{0.4}As$: Te
3] undoped **lower barrier** layer: $Al_{0.3}Ga_{0.7}As$
4] **active** layer: GaAs, or AlGaAs (lattice matched)
and GaAsP or GaAsSb (srained)
5] undoped **upper barrier** layer: $Al_{0.3}Ga_{0.7}As$
6] p-doped **upper cladding** layer: p-$Al_{0.6}Ga_{0.4}As$: Mg
7] p-doped **spacer** layer: p-$Al_{0.3}Ga_{0.7}As$: Mg
8] p-doped **cap layer**: p-GaAs: Mg

The main problems to be solved in synthesizing this structure are

We need to establish the temperature cycle i.e. the temperatures at which each layer will be grown. Since some layers such as the cladding layers, are quite thick (~1μm) whereas the active layer is thin (50-100nm), we need to determine the temperature interval and the growth duration of each layer separately before attempting multilayers. Corresponding to the growth cycle, we need to establish the amounts of aluminum and arsenic to be added to liquid gallium solvent to saturate each solution at a specific temperature, so as to achieve the desired aluminum content in each of the above layers. Additionally, some layers are doped n-type, some are doped p-type, while some others are undoped. Hence, we also need to establish the background doping of undoped layers and the amount of particular dopant to be added to the solution to achieve a desired doping level in the epi layer. Growth of multilayer structures is done over a wide range of temperatures between 700-500^{0}C.

Observations of surface morphology, measurements of layer thickness, Hall mobility and carrier concentration was useful in determining structural and electrical properties of the layers/structures. Electrochemical profiling technique was used to measure the doping profiles. Photoluminescence and x-ray diffraction plots were used for evaluating optical quality and lattice matching of various layers in the heterostructures.

3.2 Growth experiments using graphite boat made at TIFR:

3.2.1] Growth of single layers of undoped GaAs at various temperatures

In these growth experiments, a semi-insulating GaAs substrate was used for the deposition of a single epitaxial layer. The substrate was first cleaned in organic solvents like methanol, acetone and trichloroethylene, rinsed in water and then etched in 5 H_2O + 1 H_2O_2 + 1 H_2SO_4 solution for five minutes. This removed about 5μm GaAs from surface. Etched substrate was dried under nitrogen jet and quickly loaded in the recess in the graphite boat and covered with top graphite housing. Solution containing 1gm gallium and undoped GaAs pieces was placed in the first solution well. Amount of GaAs added to the solution varied with the saturation temperature (T_S) and it was calculated using the liquidus data available for GaAs [1]. Table 3.1 shows details of the growth experiments done.

Table 3.1 – Single layers of undoped GaAs

Sample Number	Saturation temp. (^{0}C)[T_S]	Growth temp. range (^{0}C)[T_G]	GaAs (mg)	Growth duration [minutes]
94 HS 01	760	750-690	35.7	030
95 HS 01	710	700-415	19.7	150
94 HS 27	700	695-420	14.7	135
95 HS 03	610	600-390	04.1	150

After loading the substrate and the solution, the boat was placed in the furnace and purged overnight in pure hydrogen ambient. During the growth experiment, the furnace was heated rapidly above saturation temperature and held for 60minutes to ensure the homogenous mixing of GaAs pieces in the solution. Then the cooling program was commenced and the furnace was cooled at the rate ~2^{0}C/minute. The growth solution was dropped in the empty space next to the piston at the starting growth temperature (T_G) which was typically 5-10^{0}C below the saturation temperature. Using piston the solution was pushed onto the substrate to begin the growth. Solution cooling was continued and then the furnace was switched off at the end of the growth duration. The solution stayed on the substrate and cooled to room temperature. Apart from the first growth 94 HS 01 (Table 3.1), in which the cooling was done for 750^{0}C to 690^{0}C, the limit of ramp cooling in other cases was sufficiently low so that very little excess growth was expected during further cool down to room temperature.

3.2.2] Growth of single layers of p-doped GaAs [cap layer]

P-doped GaAs layer is required on top of the structure. Single p-GaAs layers were grown at different temperatures using the same procedure described above. For doping, small pieces of Ge, Zn or Mg were added to the growth solution. These pieces were degreased in hot organic solvents, rinsed in water, dried and weighed before adding to the growth solution. Zn was added in the form of $ZnAs_2$ without etching, whereas Ge and Mg pieces were etched in concentrated HCl. Table 3.2 shows details of the growth experiments and solution compositions used for one gm gallium solvent.

Table 3.2 – P-doping in GaAs using Ge, Zn or Mg

Sample Number	Saturation temp.(^{0}C)	Growth temp. range (^{0}C)	GaAs (mg)	Dopant (mg)	Growth duration [minutes]
94 HS 14	700	690-430	15.3	1.0 (Ge)	135
94 HS 16	690	680-410	14.8	0.24 (Ge)	135
96 HS 07	630	620-410	05.5	0.17 (Mg)	120
95 HS 05	610	600-400	04.7	0.53 (Zn)	150

3.2.3] Growth of single layers of n and p-doped $Al_xGa_{1-x}As$ [x = 0.1-0.35]

Materials with Al atom fraction of ~0.3 are required as waveguide barrier layers. Amount of aluminum added to the growth solution was estimated using the known phase diagram as given in Chapter 2 for low growth temperatures (700-500^{0}C) [2]. Several single layers were grown using Sn, Te, Ge, Mg, and Zn dopants. Table 3.3 gives details of some of the growth experiments and the solution compositions used for 1gm gallium. The saturation temperature of each solution (T_S) was about 10^{0}C higher than the corresponding growth temperature (T_G).

Table 3.3 – Doping in $Al_xGa_{1-x}As$ [for $x \cong 0.3$]

Sample Number	Growth temp. range(^{0}C)[T_G]	GaAs (mg)	Aluminum (mg)	Dopant (mg)	Growth duration (minutes)
95 HS 01	700-415	14.8	-	none	150
94 HS 18	650-620	08.9	0.3	none	015
94 HS 04	690-490	12.6	0.62	083 (Sn)	100
94 HS 08	695-480	11.2	0.45	300 (Sn)	120
93 HS 24	670-460	10.0	0.39	0.48 (Te)	110
93 HS 25	670-390	11.5	0.35	0.34 (Te)	120
94 HS 09	680-450	10.5	0.45	4.38 (Ge)	120
94 HS 17	650-425	10.1	0.32	0.12 (Ge)	120
93 HS 26	620-460	05.7	0.25	0.54 (Mg)	100
95 HS 04	620-410	06.7	0.60	-	135
95 HS 06	610-365	06.0	0.55	2.0 (Zn)	150

3.2.4] Attempts to synthesize multilayered structures: Before synthesizing the multilayered structure containing eight layers, we synthesized number of double heterostructures (DH) containing three layers viz.

1] n-doped layer [n-$Al_{0.3}Ga_{0.7}As$: Te]
2] undoped **active** layer [GaAs]
3] p-doped layer [p-$Al_{0.3}Ga_{0.7}As$: Mg]

Small pieces of Te doped GaAs were added in the solution for the growth of n-type layers, whereas tiny pieces of Mg were used for p-type layers. Table 3.4 gives solution compositions used for a typical DH structure.

Table 3.4 – Solution compositions and growth schedule for synthesis of DH structure. [Solution: 1gm gallium + GaAs + Al + dopant]

Layer grown	**Growth temp. range (^0C) [T_G]**	**GaAs (mg)**	**Al (mg)**	**Dopant (mg)**	**Growth duration [minutes]**
n-$Al_{0.3}Ga_{0.7}As$: Te	700-600	11.3	0.3	0.16	52
active layer: GaAs	600	03.8	-	-	30 seconds
p-$Al_{0.3}Ga_{0.7}As$: Mg	598-400	15.5	0.3	0.63	100

In this growth experiment, n^+-GaAs substrate was placed in the recess in the boat and the solutions were put in the three wells of the graphite boat. After purging the reactor for several hours with hydrogen, it was then heated rapidly to ~725^{0}C. This temperature was maintained for about one hour to allow complete dissolution of GaAs pieces, aluminum and dopant in the solutions. Then the cooling was commenced at the rate of ~2^{0}C/minute and it continued till the growth of the last layer. At about 700^{0}C, first solution was moved and allowed to drop in the empty space next to piston. This solution was then forced into the narrow tunnel over the substrate surface. After fifty-two minutes of growth, the piston was pulled back and the second solution was dropped and forced over the substrate. This second solution displaced the first one that deposited n-AlGaAs layer. It was used to deposit active GaAs layer for thirty seconds and then displaced by the third solution prepared for the growth of p-AlGaAs. After the growth period of one hundred minutes, the furnace was switched off. Thus, three-layer structure was synthesized. We synthesized number of DH structures to check the reproducibility and repeatability of growth experiments.

3.3 Growth experiments using graphite boat made at Ioffe Institute, Russia.

The graphite boat fabricated in Russia had a facility of using ten melts and each solution well had a capacity to hold maximum of 3.0gm solution. We decided to use 2.5gm gallium for each solution. The substrate recess could hold 15mm x 15mm x 0.4mm GaAs wafer and the graphite slider holding it could be pulled out of the last solution at the end of the growth experiment. With this, we could avoid the excess growth from last solution. We continued the work of multilayer structures using this boat and the following layers/structures were grown:

3.3.1] Growths of single layers of undoped, Te and Mg doped GaAs, $Al_xGa_{1-x}As$, ($x = 0.3$, 0.6) were done as above, for assessing the growth rate, composition, optical and electrical quality and the reproducibility of the layers.

3.3.2] Growth of DH structures with active layer grown at 580^{0}C for different growth durations. In this experiment, we synthesized a set of three structures containing five layers, [sample numbers 98hs12-14 as listed in Table 3.5]. Except the first n-type (AlGaAs: Te) layer, all the other layers were undoped. The active layer in these structures was grown for ~3, 10 and 20 seconds. Solution compositions used and the growth schedule followed were identical in all the three experiments. Typical compositions of the solutions using 2.5gm gallium are given in Table 3.5. This experiment was necessary to study the effect and extent of solution mixing, particularly in the active layers.

Table 3.5 – Typical solution compositions and growth schedule for samples 98hs12-14.

Layer grown	**Saturation temp. (^{0}C)**	**Growth temp. range (^{0}C)**	**GaAs (mg)**	**Aluminum (mg)**	**Growth duration (minutes)**
n-$Al_{0.6}Ga_{0.4}As$: Te	700	680-605	14.3	3.6	45
ud-$Al_{0.3}Ga_{0.7}As$	630	605-580	8.8	0.6	20
undoped-GaAs	600	580	7.3	-	3,10,20 sec. (*)
ud-$Al_{0.3}Ga_{0.7}As$	630	580-540	8.5	0.6	20
ud-$Al_{0.6}Ga_{0.4}As$	600	540-480	3.5	0.7	60

(*) Growth duration: 98Hs12 - **20 sec**, 98HS13 - **10sec**, 98HS14 - **03 sec.**

3.3.3] Growth of SCH laser structures. Several SCH structures with the active layer grown at 650, 600 and 550^{0}C were synthesized using this boat. For laser structure, the optimum temperature for the growth of active layer was found to be ~645^{0}C. At this temperature, we could grow 0.04-0.1μm thick layers in 5-20 seconds. We could complete the growth of the remaining laser structure between 645-450^{0}C. Hence we decided to follow the same scheme in all the growth experiments for SCH lasers.

Table 3.6 (a) gives a typical temperature/time schedule used for synthesizing SCH laser structure. Table 3.6 (b) gives the corresponding solution compositions used for growing the layers in the heterostructure. Each solution consists of - 2.5gm gallium + GaAs + Al + dopant as required. Using this scheme, we synthesized number of SCH laser diode structures.

Table 3.6 (a) Growth schedule for laser structure of eight layers.

Layer grown	**Composition of the layer**	**Growth temp. interval [^{0}C]**	**Growth duration [minutes]**	**Thickness [μm]**
1] Buffer	n-$Al_{0.3}Ga_{0.7}As$: Te	685-682	03	0.5
2] Lower clad	n-$Al_{0.6}Ga_{0.4}As$: Te	682-645	55	1.5
3] Lower barrier	undoped $Al_{0.3}Ga_{0.7}As$	645-643	05	0.25
4] Active	undoped GaAs	643	0.05-0.50	0.05-0.16
5] Upper barrier	undoped $Al_{0.3}Ga_{0.7}As$	643-641	05	0.25
6] Upper clad	p-$Al_{0.6}Ga_{0.4}As$: Mg	641-560	80	1.1
7] Spacer	p-$Al_{0.3}Ga_{0.7}As$: Mg	560-540	20	0.2
8] Cap	p-GaAs: Mg	540-480	60	0.45

Table 3.6 (b) Typical solution compositions used for laser structure (each solution consists of - 2.5gm gallium + GaAs + Al + dopant)

Layer type/(composition)	**Solution composition**		
	GaAs (mg)	**Al (mg)**	**Dopant (mg)**
1] Buffer (n-$Al_{0.3}Ga_{0.7}As$: Te)	24.6 *	1.0	Te (GaAs:Te)
2] Lower clad (n-$Al_{0.6}Ga_{0.4}As$: Te)	12.0 *	3.3	Te (GaAs:Te)
3] Lower barrier (undoped $Al_{0.3}Ga_{0.7}As$)	16.0	0.9	-
4] Active (undoped GaAs)	16.7	-	-
5] Upper barrier (undoped $Al_{0.3}Ga_{0.7}As$)	16.0	0.9	-
6] Upper clad (p-$Al_{0.6}Ga_{0.4}As$: Mg)	8.0	2.6	1.6 (Mg)
7] Spacer (p-$Al_{0.3}Ga_{0.7}As$: Mg)	2.1	0.3	1.0 (Mg)
8] Cap (p-GaAs: Mg)	3.1	-	0.8 (Mg)

* Te doped GaAs was used for saturating these solutions. In all other cases undoped GaAs was used for saturating growth solutions.

In a typical run, after one hour of homogenization at about 720^{0}C, cooling program was initiated to cool the reactor at about 0.5^{0}C per minute. Solutions 1-8 were then brought in contact with the substrate sequentially at the respective growth temperatures. The slider carrying the substrate was pulled out at the end of the growth of the last layer. The substrate was free from the growth solution with the deposition of the desired layers / structure.

3.3.4] Growth of strained SCH laser structures. Lattice mismatch introduces strain in the active layer of a laser structure. This is achieved by changing the active layer material from GaAs or AlGaAs (no strain) to $GaAs_xP_{1-x}$ (tensile strain) or $GaAs_xSb_{1-x}$ (compressive strain). For growing these layers, in addition to GaAs, we added GaP or GaSb in the solution used for the growth of active layer. For the synthesis of laser structures with phosphorus in the active layer, five structures were grown using the solutions with compositions given in Table 3.7(a). The active layer was grown at ~650^0C for 20 seconds in each case. The amount of GaP added to the solution in our growth experiments is much more than required to incorporate a particular amount in the active layer. This was necessary to make up for the loss of phosphorus due to evaporation.

Table 3.7(a). Solution compositions used for growth of active layer containing phosphorus in solution.

Sample Number	GaP (mg)	Atom fractions of Ga, As and P in growth solution		
		X_{Ga}^1	X_{As}^1	X_P^1
00hs14	-	0.9963	0.0037	-
00hs04	0.3	0.9961	0.0038	8.1×10^{-5}
00hs11	0.9	0.9959	0.0037	2.5×10^{-4}
00hs12	1.7	0.9957	0.0037	4.7×10^{-4}
00hs17	2.9	0.9954	0.0037	7.7×10^{-4}
00hs19	4.0	0.9952	0.0037	1.1×10^{-3}

For the synthesis of laser structures with GaSb in the active layer, we followed the same scheme as described above, using solution compositions for the active layer deposition given in Table 3.7(b). In the initial experiments, the active layer was grown for 20seconds. However such structures gave very poor electroluminescence and the devices did not lase. Hence we decided to reduce the growth duration to 3-5seconds. We note that the amount of GaSb added to the solution in these experiments is about 100times more than the amount of GaP. This is because the incorporation of antimony from the solution into the active layer is much smaller as compared to the incorporation of phosphorus. The calculated amounts are given in chapter 2.

Table 3.7(b). Solution compositions used for growth of active layer containing antimony.

Sample Number	GaSb (mg)	Atom fractions of Ga, As and Sb in the solution		
		X_{Ga}^{l}	X_{As}^{l}	X_{Sb}^{l}
01hs25	-	0.9968	0.0032	-
01hs26	30	0.9925	0.0032	0.44×10^{-2}
01hs27	95	0.9832	0.0032	1.36×10^{-2}
01hs39	250	0.9620	0.0031	3.49×10^{-2}
01hs40	400	0.9266	0.0029	6.75×10^{-2}

3.4 Results of characterization of the materials/heterostructures

3.4.1] Surface morphology: The surface morphology of the as-grown single layers was observed and recorded using optical microscope. Fig. 3.2 shows the optical micrograph of the surface of undoped GaAs layer grown from the starting temperature of 650^0C.

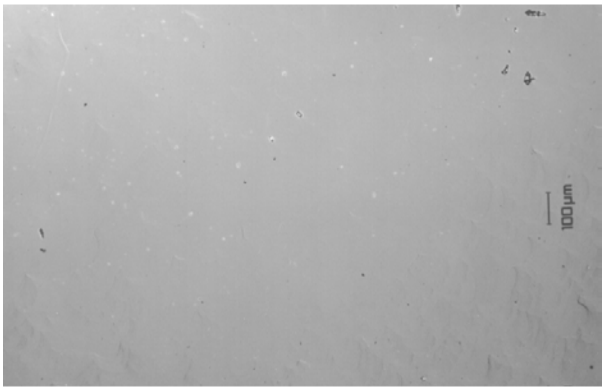

Fig. 3.2 Surface morphology of GaAs layer

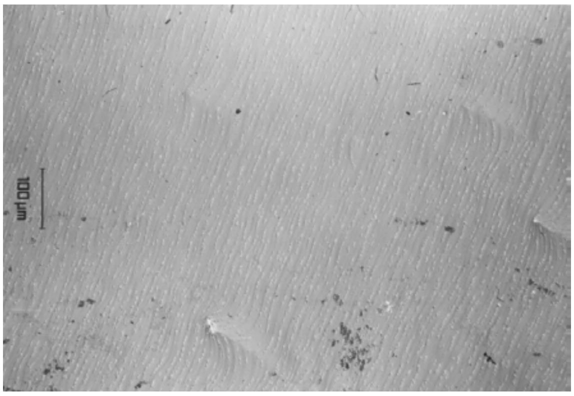

Fig. 3.3 Layer with rippled surface

The surface is smooth, shiny, and mirror like. In some layers, the appearance is shiny to the naked eye, but a rippled morphology typical of LPE growth is seen under the optical microscope. Fig. 3.3 shows a photograph of one such layer. Similar results are also obtained for AlGaAs epitaxial layers. However, we have observed unexpected morphological features when the dopants Ge, Te or Mg are added to the growth solution for growing GaAs or $Al_{0.2}Ga_{0.8}As$ layers. Typical features observed on the surfaces of these layers are shown in Fig.3.4-3.6. Ge doping produces rectangular pyramidal defects [Fig. 3.4], Te doping in $Al_{0.2}Ga_{0.8}As$ [Fig. 3.5] causes oblong elliptical patterns, while with Mg doping in $Al_{0.2}Ga_{0.8}As$ [Fig. 3.6], rectangular defects with cross-web like patterns are seen. In the case of Ge doping, we find from EDX (Energy Dispersive X-ray) measurements, the pyramid sites have excess Ge (nearly 80 atomic %). Some attempts were made to improve the surface morphology by reducing the Ge content in the solution. However, the improvement was not sufficient even with the lowest Ge content of ~0.05mg [$X_{Ge}^{l} = 10^{-5}$] used in our experiments. In the case of Te or Mg related defects, we could not ascertain the presence of excess Te or Mg from the EDX measurements. Surface profiling measurements showed Ge rich pyramids

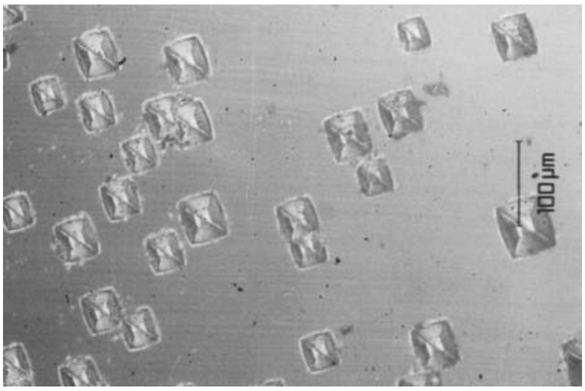

Fig. 3.4 surface of Ge doped GaAs

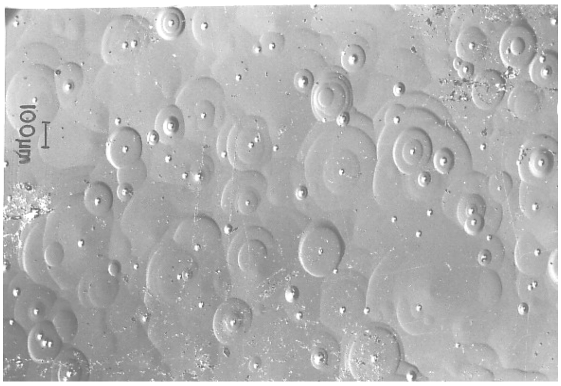

Fig. 3.5 Te doped AlGaAs

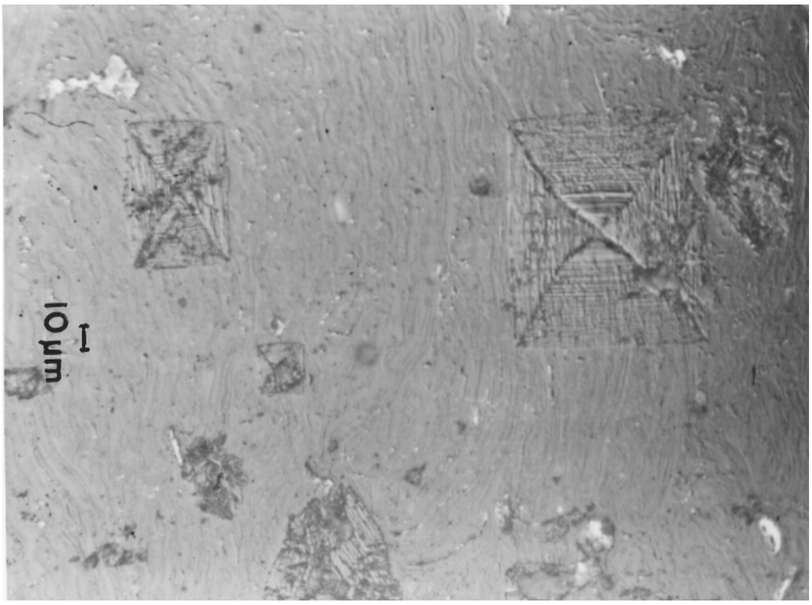

Fig. 3.6 Mg doped AlGaAs

to be raised 8-9 µm above the surface. On the other hand, Mg related defect turned out to be a pit with depth of about 1µm. Thickness of the epi layers in all these experiments is more than 2µm. From the orientations of the rectangular defects, we find that their edges are aligned along [110] directions and the tilted planes bounding the defects on the sides are [111]. While above dopants have been used by other groups for growing similar materials and structures at high temperatures [3-6], the defects seem to be enhanced in number and magnitude in the lower temperature range used by us in our growth experiments.

3.4.2] Thickness of epi layers in the heterostructures:

All the heterostructures were delineated for thickness measurements and stained using A-B etchant consisting of solution A–0.3gm $AgNO_3$ + 40ml HF + 40ml H_2O and solution B-40gm CrO_3 + 40ml H_2O. The layers in the heterostructure were observed using optical or scanning electron microscope (SEM). Fig. 3.7 shows two examples of cross-sections of DH structures recorded using an optical microscope. Junction line between the substrate and the layers is clearly seen in the photographs. The junction line is straight in the picture on left whereas the line is wavy in the picture on right due to uneven starting surface on which layers are grown. In both pictures, lines of various epilayers above the junction line are rather faint and not seen clearly. Hence we need to use a scanning electron microscope (SEM) for recording thickness of various layers. Fig. 3.8 shows SEM photomicrograph of the cross-section of a heterostructure consisting of eight layers of AlGaAs/GaAs. The substrate and the buffer layer are on the right and the arrow at the center shows an active layer ~50nm. It is sandwiched between two barrier layers ($Al_{0.3}Ga_{0.7}As$) that form a waveguide. Two thick n and p-clad layers of $Al_{0.6}Ga_{0.4}As$ are seen on either side of waveguide, a spacer layer (p-$Al_{0.3}Ga_{0.7}As$) is seen next to p-clad layer and a cap p-GaAs layer is at the extreme left.

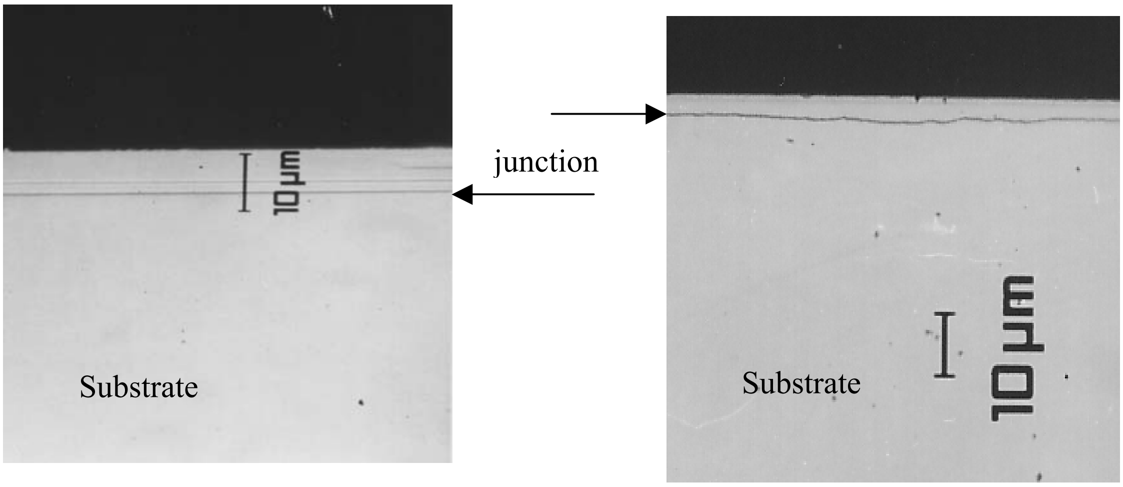

Fig. 3.7 Photographs of cross-section of two heterostructures

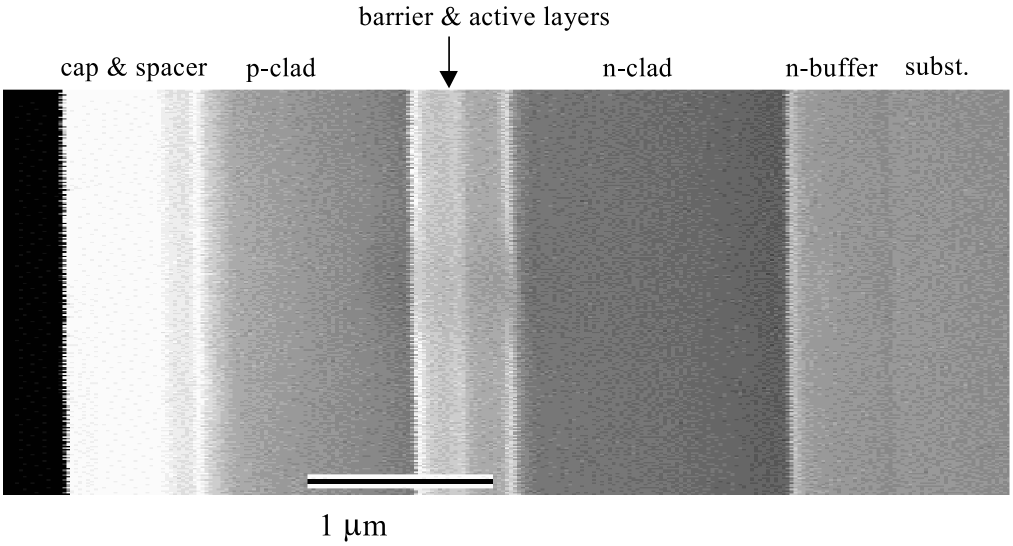

Fig. 3.8 Photomicrograph of the cross-section of a heterostructure.

3.4.3] Electrical measurements:

(a) Undoped GaAs layers: Results of Hall measurements (viz. mobility and carrier density), layer thickness (t) of the samples and the solution compositions used for the growth of undoped layer are given in Table 3.8. These layers are grown from the solutions cooled to room temperature. The layers are n-type with carrier densities in the range of 1-5 x 10^{16}cm^{-3} with mobility ~ 5000cm^2/v.s.

Table 3.8 – Results of undoped GaAs

Sample Number	**T_S (^{0}C)**	**T_G (^{0}C)**	**Atom fractions**		**(t) (μm)**	**Carrier density (cm^{-3})**	**Mobility cm^2/v.s**
			[X_{Ga}^l]	**[X_{As}^l]**			
94 HS 01	760	750	0.9834	0.0166	12.0	1.8 x 10^{16}	4116
95 HS 01	710	700	0.9909	0.0091	6.4	1.7 x 10^{16}	5412
94 HS 27	700	690	0.9930	0.0069	5.1	4.8 x 10^{16}	5280
95 HS 03	610	600	0.9981	0.0021	1.5	2.0 x 10^{16}	5432

Fig. 3.9 shows a semi-logarithmic graph between the thickness of the undoped GaAs layers listed in Table 3.8 versus 1000/T_s where T_s is the saturation temperature of each solution. We find that the growth thickness fits the relationship in the form $S(T_s) = S_0 e^{-\Delta / kT}$. In Fig. 3.9, we have also plotted the As atom fraction x^l_{As} used to saturate the solution at the temperature T_s. It is seen that the plots of x^l_{As} and $S(T_s)$ follow each other very closely with $\Delta \sim 1$ eV.

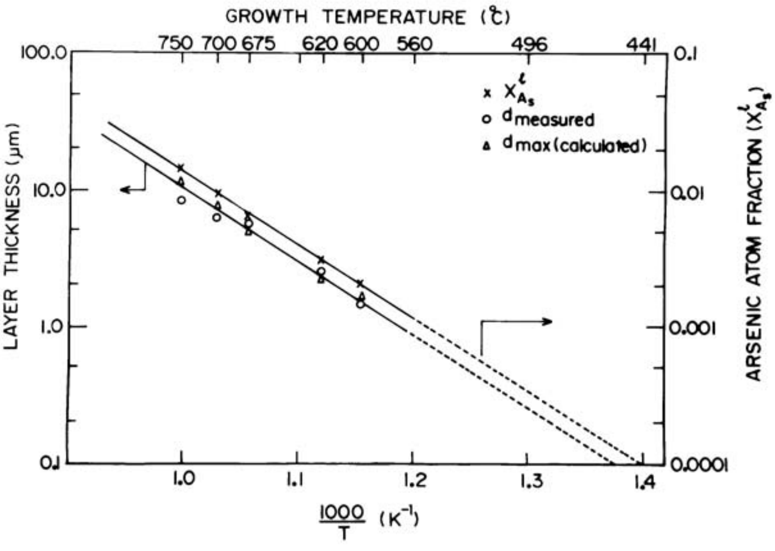

Fig. 3.9 Thickness of GaAs

This behavior of the total thickness grown may be expected since the growth is controlled mainly by the diffusion of As in the solution to the growth front. The total amount of deposited As is therefore, proportional to the atom fraction of As in the solution. To get an estimate of the layer thickness, it is useful to calculate its upper limit d_{max} which is deposited after a very long growth time. It depends only on solution height and the phase diagram if we assume that the solution area is equal to the substrate area. This situation is realized by means of the 'thin solution' technique used in our experiments, where all the material is grown over sufficiently long time. Thickness d_{max} follows from the condition that the number of atoms in the solid is equal to the number of atoms precipitated from the liquid [7],

$d_{max} = C_l \, [\, x\,(T_s) / N_x\,(T_S) - x\,(T_E) / N_x\,(T_E)]$,

with $C_l = \rho_l \, M_s \, h / \rho_s \, A_l$,

where h is the height of the solution, ρ_s and M_s are the density and molecular weight of GaAs, and ρ_l and A_l are the density and molecular weight of gallium respectively. In the equation for d_{max}, $x\,(T_s) = x^l_{As}$ is the atom fraction of the solute viz. As, N_x is atom fraction of solvent and $N_x\,(T_s) = 1 - x^l_{As}$, T_S is the saturation temperature and T_E is the temperature at which the substrate is separated from the solution. For LPE, the condition of dilute solutions is fulfilled at low growth temperatures and with $x^l_{As} << 1$, maximum thickness is given by:

$d_{max} = C_l \, [x\,(T_s) / N_x\,(T_S)] = C_l \, [\, x^l_{As} / 1 - x^l_{As} \,] \approx C_l \, x^l_{As}$.

From the values of the total thickness obtained from our experiments, the height of the solution (h) which fits the experimental data is estimated to be about 0.35mm. Using this value of h and X^l_{As} used for saturating the solutions, the calculated d_{max} values are plotted in Fig. 3.9 to show the fit. By extrapolating this plot, we get an estimate of the thickness of GaAs layer grown at low temperatures. Thus, with saturation temperature of about 450^0C, 0.1μm thick GaAs layer could be grown from the solution cooled to room temperature. Although this information may be useful in certain growth schedules for thin layer growth, it does not fit into our scheme.

(b) Doped GaAs layers: Results of the doped GaAs single layers are given in Table 3.9.

Table 3.9 – Results of doping in GaAs using Ge, Zn or Mg

Sample Number	**Dopant**	**[T_G] range (^{0}C)**	**(t) [μm]**	**Carrier density (cm^{-3})**	**Mobility cm^2/v.s**	**surface features**
94 HS 14	Ge	690-430	6.9	2×10^{18}	52	Ge Pyramids
94 HS 16	Ge	680-410	6.1	3×10^{18}	32	partially smooth
96 HS 07	Mg	620-410	2.2	3×10^{18}	97	rectangular defects
95 HS 05	Zn	600-400	2.1	3×10^{16}	193	smooth

p-type GaAs layer is required at the top of the heterostructure and is grown at temperatures below 600^0C. Surface of Ge doped GaAs grown at about 690^0C is very rough with pyramidal defects, although the layer is p-type with high doping density. At temperatures below 600^0C, it is very difficult to obtain p-type material with smooth surface morphology. Hence we decided to avoid using Ge as a p-type dopant for GaAs cap layer. With Zn doping at low temperatures, we could obtain p-type material. However, we avoided using Zn, since the adjacent melts could get contaminated due to evaporation of Zn at elevated temperatures (700-750^0C) used for initial homogenization of the solution in our growth experiments. Mg was found to give p-GaAs with small number of defects and hence we decided to use Mg doped p-GaAs at the top of the structure.

(c) Undoped/doped AlGaAs layers: Table 3.10 shows typical results of our doping experiments in AlGaAs layers. We have used Sn and Te for n-doped layers and Ge, Zn and Mg for p-doped layers. The starting temperature at which the growth is initiated in each case is also shown. Mobility and carrier concentrations are found using Hall measurements and the Al mole fraction in the epi layer has been found by EDX measurements.

Table 3.10 – Doping in $Al_xGa_{1-x}As$

Sample Number	Growth Temp. (^{0}C)	Layer Thickness (t) (μm)	Carrier concn. and (type) (cm^{-3})	Mobility (μ) ($cm^2/v.s$)	Dopant atom fraction [X^l_D]	Al mole fraction(x) [by EDX]
95 HS1	700	6.4	1.8×10^{16} (n)	5492	Undoped	0.00
94 HS18	650	2.3	6.5×10^{15} (n)	2018	Undoped	0.24
94 HS8	695	5.0	2.6×10^{17} (n)	1721	0.149 (Sn)	0.11
93 HS24	670	3.8	1.5×10^{19} (n)	430	2.4×10^{-4}(Te)	0.20
94 HS9	690	5.7	4.5×10^{17} (p)	100	4.5×10^{-3}(Ge)	0.18
93 HS26	620	1.2	3.7×10^{18} (p)	55	1.5×10^{-3} (Mg)	0.19
95 HS6	610	1.0	1.5×10^{17} (p)	56	3.7×10^{-4} (Zn)	0.37

All the undoped layers are n type with somewhat high background carrier density ~$10^{16}cm^{-3}$ for GaAs as well as for AlGaAs. Among the dopants used, Te has the highest distribution coefficient giving about $10^{19}cm^{-3}$ electron concentration for very small (~0.1mg) amount of Te in the solution. On the other hand, Sn dopant gives smooth surfaces but the distribution coefficient is smaller by two orders of magnitude, requiring large amount of Sn (~0.3gm) in the growth solution. Te required is very small to handle and hence we used Te doped GaAs pieces to saturate the growth solution. This gave us a very smooth surface with electron concentration ~$10^{18}cm^{-3}$. These results were useful in preparing the solutions used in synthesizing heterostructures for lasers.

3.4.4] ECV profiles: Electro-chemical voltage (ECV) measurements were done to record the carrier profile as a function of depth. Fig. 3.10 (a) shows a profile of a 6.5μm thick GaAs

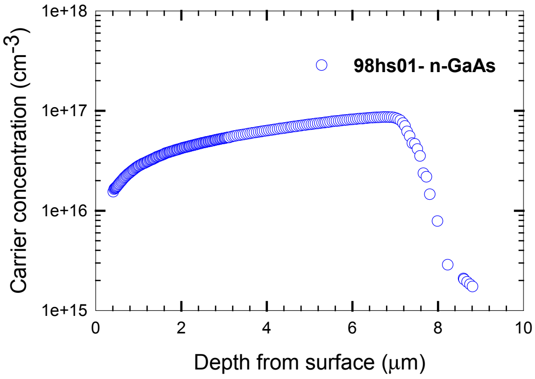

Fig. 3.10 (a) ECV profile of a GaAs layer

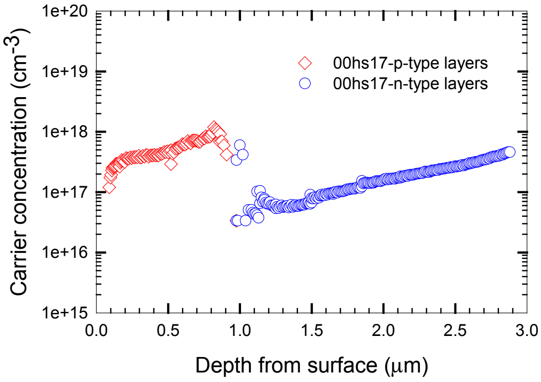

Fig. 3.10 (b) ECV profile of a multilayer structure

single layer grown on semi-insulating substrate. The material is n-type represented by blue circles and the carrier density is almost uniform over the entire thickness. Fig. 3.10 (b) shows the profile of a typical laser structure [sample 00hs17] in which total thickness of p type layers (top cap, spacer, upper clad) is about 1μm, waveguide is about 1μm and n type lower clad is 1.5μm thick. Red diamonds represent etching of p-layers and the carrier density is about 3-6 x 10^{17}cm^{-3}. Waveguide layers are n-type (blue circles) with background carrier density ~3-5 x 10^{16}cm^{-3}. Lower clad layer is n-type (Te doped) and the profile shows a steady rise in carrier density. This sample could be etched upto depth of 2.7μm only due to the oxidation of the Al containing surface.

3.4.5] Optical measurements: We have carried out low temperature photoluminescence measurements, to assess the optical quality of these materials, using the set up described in Chapter 2.

a) Single GaAs layers: We find very little PL signal from single layers of Te and Mg doped materials. Figs. 3.11(a)-(d) show PL spectra of number of GaAs and AlGaAs single layers. The PL spectral assignments are based on the similarities with the features found in the published literature [8-11]. Fig. 3.11(a) shows PL emission spectra of four GaAs samples

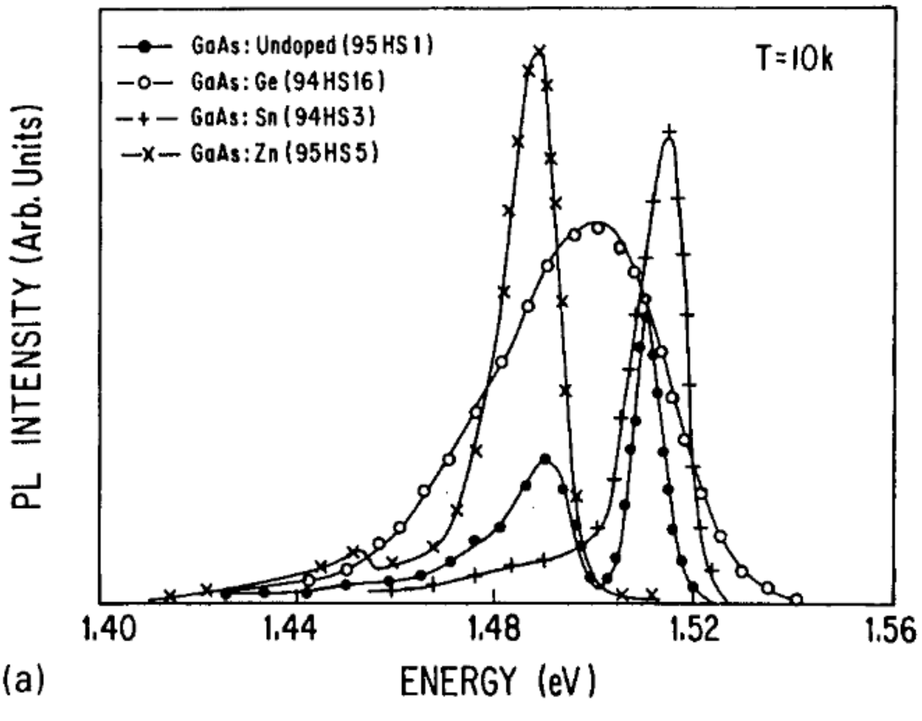

Fig. 3.11 (a) - PL spectra of four GaAs samples

with different dopants. The undoped sample [95 HS1: Table 3.8] shows a prominent 6meV wide peak at about 1.51eV and a broad band at about 1.49eV. Donor to valence band transition most likely causes the narrow peak, while the broad band appears to be donor-acceptor band. The background impurity responsible for these peaks appears to be predominantly silicon which gets incorporated in the solution to produce net electron concentration ~$10^{16}cm^{-3}$ under the conditions prevailing in our reactor ambient. Doping the epi-layer with Sn enhances the electron concentration [94 HS 03], to about 6 x $10^{17}cm^{-3}$. The corresponding PL peak shifts to higher energy ~1.515eV and broadening increases to ~11meV. This could be due to impurity banding and band filling effects. Doping with Zn to ~3 x $10^{16}cm^{-3}$ [95 HS 05: Table 3.9] produces a downward shift of the peak to 1.488eV, with a width of about 12.5meV. This peak results from the conduction band to Zn acceptor transition. Half width of this peak is considerably larger than expected at this acceptor doping concentration. As such, the PL peak could have contribution from donor to acceptor transition as well because the undoped material showed fairly large background donor concentration. A small peak is also seen at 1.454eV that could be LO phonon replica of the band (donor) to acceptor transition. Ge doping produces p-type material with rather heavy doping ~5 x $10^{18}cm^{-3}$ [94 HS 16: Table 3.9] and gives a very broad band with FWHM ~ 36meV. Donor-acceptor pairs, produced by Ge doping could cause this broad band.

b) Single AlGaAs layers: Undoped $Al_xGa_{1-x}As$ layer with background density ~6.5 x $10^{15}cm^{-3}$ [94 HS 18: Table 3.10], shows a peak at 1.746eV with FWHM ~5meV [Fig. 3.11(b)]. Aluminum composition value x obtained from PL peak is ~0.19, whereas the corresponding

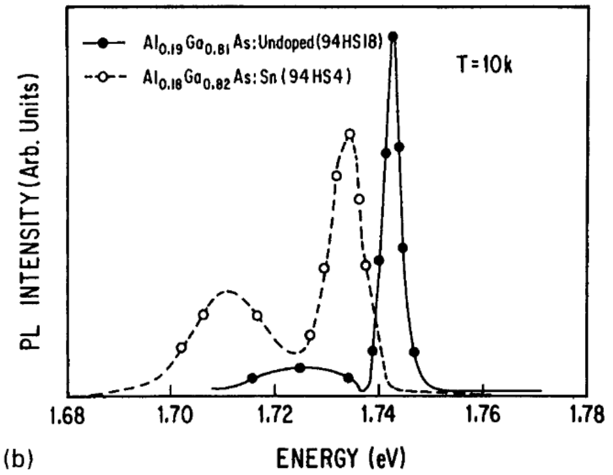

Fig. 3.11(b) PL spectra of undoped and Sn doped AlGaAs

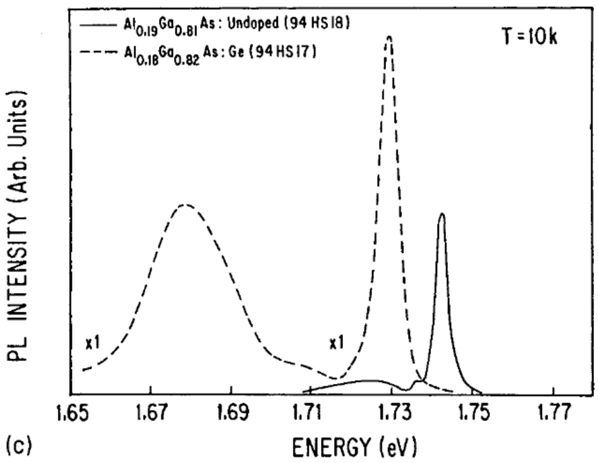

Fig. 3.11(c) PL spectra of undoped and Ge doped AlGaAs

nominal composition of this layer obtained from EDX is x~0.24, within the accuracy of our measurements. Since the peak is fairly sharp with small FWHM, it indicates grading is small in the material composition over the layer thickness of 2.3μm that is grown over a fairly wide temperature range starting from 650^0C. Strength of the PL emission of this sample is the strongest, implying good optical quality material useful for devices. The emission peak at 1.746eV is attributed to bound exciton transition involving Si impurity. There is also a weak and broad band at 1.73eV that could be a DA pair band. PL of two layers with similar Al content ≅ 0.19, but one containing Sn [94 HS 04: Table 3.3] and the other Ge [94 HS 17: Table 3.3] are shown in Fig. 3.11 (b) and Fig. 3.11 (c) respectively. Sn doping giving n-type material with the carrier density ≅ 5.6 x 10^{16}cm^{-3} broadens the PL emission to about 7.5meV with the peak at 1.734eV. There is also a donor-acceptor (DA) pair band at 1.708eV that has a substantially larger intensity. Ge doping giving p-type material with carrier density ≅ 2 x 10^{17}cm^{-3} also produces a peak at 1.73eV similar to the acceptor related bound exciton transition. In addition, we see a 24meV broad band peaking at 1.68eV that seems to be related to band to acceptor or donor-acceptor transition.

Fig. 3.11 (d) shows PL spectra of two layers containing nearly 36 % Al. The undoped layer with background carrier density ≅ 3 x 10^{15}cm^{-3} [95 HS 04: Table 3.3] has half width somewhat broader ~8meV. However, because of DX behavior of the donors of these alloy

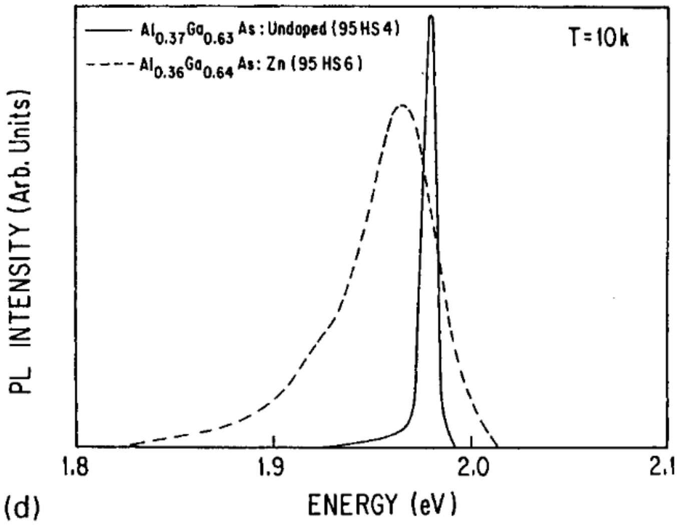

Fig. 3.11 (d) PL spectra of Zn doped AlGaAs

compositions, the measured electron density will be much smaller than the actual donor concentration [12]. Zn doping in $Al_{0.36}Ga_{0.64}As$ [95 HS 6: Table 3.10] produces p-type material with hole density ≅ 1.5 x $10^{17}cm^{-3}$ and a broad band at 1.962eV with half width ~46meV. This broad band seems to have structure that is characteristic of deep level vibronic band involving multiphonon emission.

c) Next, we present PL spectra of simple DH structures. Fig. 3.12 shows PL spectra of three samples that form the basic components of the complex heterostructure. These are:
1) n^+-GaAs substrate, 450μm thick, 2) undoped GaAs epi layer, 8μm thick [no. 92 HS 07] and 3) the DH structure [sample no. 93 HS 27, Table 3.4]. This DH structure is one of the trial structures grown to optimize solution compositions for desired Al content in $Al_xGa_{1-x}As$ layers. This structure is grown using boat fabricated in TIFR and it consists of three layers deposited sequentially on n^+-GaAs substrate in the following order:

Layer 1: n-$Al_{0.3}Ga_{0.7}As$: Te doped, 2 μm,
Layer 2: undoped GaAs: 0.2 μm and
Layer 3: p-$Al_{0.3}Ga_{0.7}As$: Ge, 2.5 μm.

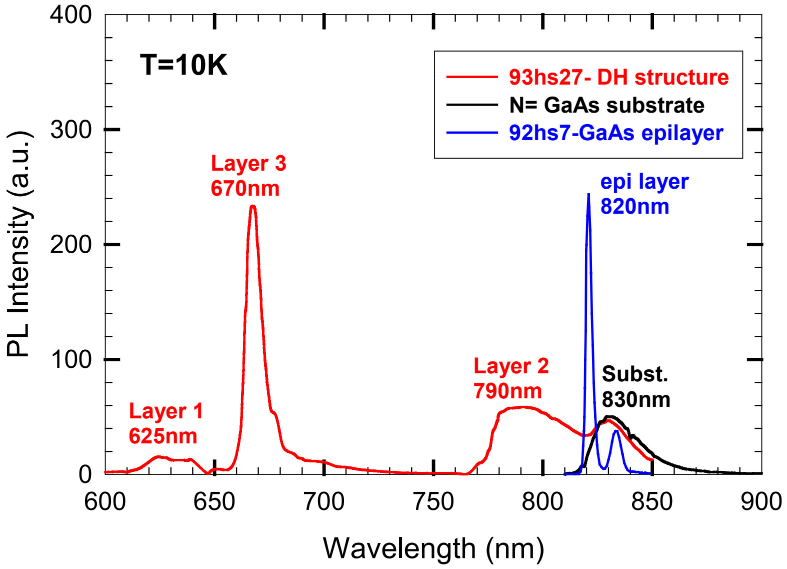

Fig. 3.12 PL spectra of substrate, epi layer and DH structure

PL signal from n^+-GaAs substrate shows low intensity broad peak centered at 830nm (1.493eV), whereas that from the epi layer shows two components: a high intensity sharp peak at ~820nm (1.5121eV) and a low intensity peak at ~835nm (1.485eV). PL signal from DH structure shows three well-resolved peaks from three layers: 1) A low intensity broad peak at ~625nm (1.984eV), from layer 1 deposited on n^+-GaAs substrate. Al content corresponding to this peak is x~0.375, 2) High intensity, sharp peak at 670nm (1.851eV), from layer 3 which gives Al content x~0.275 and 3) Low intensity broad peak at 790nm (1.571eV) from the middle layer number 2. In case of layer 2, the peak is shifted from the GaAs peak position by about 80meV. This shift is possible due to: a) material composition b) small size effect and c) strain due to mismatch in the layers. Thickness of the active layer is about 0.2 μm and hence the shift due to size is ruled out. AlGaAs/GaAs is a well lattice matched material system and hence shift due to strain is also not possible. Therefore, the shift is attributed to changed material composition. This is possible, since in our growth scheme, small amount of Al gets mixed during the action of solution number two displacing the solution number one for the growth of middle layer. From the PL peak position, the estimated layer composition is (x~0.04). Thus, the active layer in the DH structure is $Al_{0.04}Ga_{0.96}As$. This is a limitation of the piston boat and as we shall see, a small amount of Al is always incorporated in all the active layers of the DH structures reported in this thesis.

d) Structure consisting of five layers: This is a test structure synthesized using boat fabricated in Russia. It consists of five layers out of eight required for SCH laser diodes. The sequence of layers beginning from the substrate is [Table 3.5]:

Layer 1: n-$Al_{0.6}Ga_{0.4}As$: Te, 1.8 μm,
Layer 2: undoped- $Al_{0.3}Ga_{0.7}As$, ~0.25 μm.
Layer 3: undoped GaAs: 0.03-0.05 μm
Layer 4: undoped- $Al_{0.3}Ga_{0.7}As$, ~0.25 μm.
Layer 5: undoped- $Al_{0.6}Ga_{0.4}As$, 1.0 μm.

The active layer 3 is sandwiched between two barrier layers of $Al_{0.3}Ga_{0.7}As$ which forms a

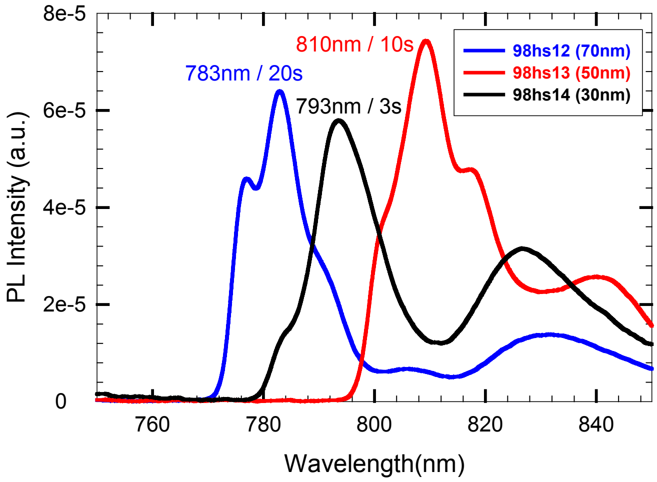

Fig. 3.13 PL from the active layer of three heterostructures

waveguide. Barrier layers are flanked on either side with $Al_{0.6}Ga_{0.4}As$ clad layers. Table 3.5 shows the details of the growth experiments in which three identical structures were grown and the growth duration of the layer number 3 was varied. Thickness of the active layer estimated from SEM images is < 0.03, 0.05 and 0.07μm for the growth duration of quick (<3seconds), 10 and 20 seconds respectively. Fig. 3.13 shows PL spectra from the active layer of these three samples recorded in 750-850nm range. It is seen that the spectra are broad and the peaks are spread over 780-810nm. This corresponds to the Al content of x~0.058, 0.042 and 0.015 in the three samples [98hs12, 98hs14 and 98hs13] respectively. Thus, the photoluminescence measurements on trial test structures give us an estimate of the extent of Al incorporated in the active layer, and it is in the range 1.5 to 5.8%. We do not see any systematic trend in the three results in Fig. 3.13 which suggests some randomness in the extent of mixing which may vary from one experiment to next.

3.4.6] X-ray measurements:

All the heterostructures described in Tables 7(a) and 7(b) were characterized using high resolution x-ray diffractometer (HR-XRD) Philips X'PERT. These measurements were useful in determining lattice matching between the layers and in estimating the strain in the active layer located at the center of the heterostructures. Fig 3.14 shows XRD plot (in blue) of sample number 00hs14 with GaAs active layer (apart from unintentional Al because of mixing). The profile in red is obtained using Philips software EPITAXY. As seen, the

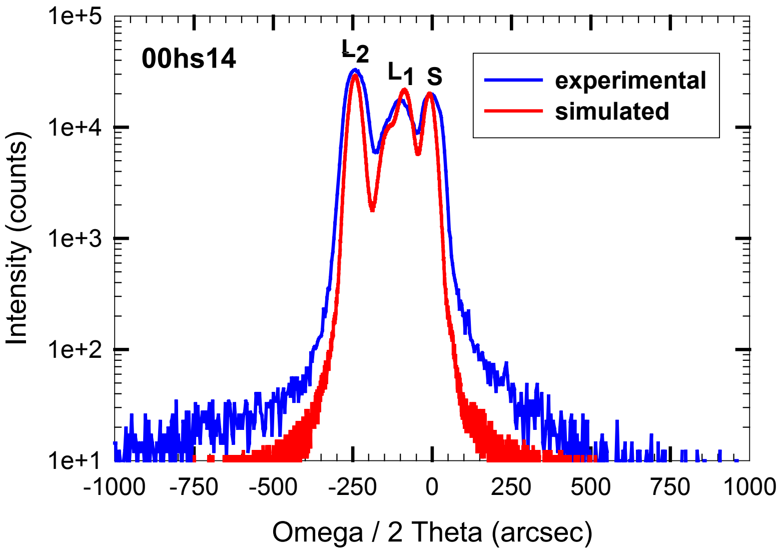

Fig. 3.14. XRD plots of AlGaAs/GaAs heterostructure

simulated profile is reasonably close to the measured one. These plots show three distinct peaks: a narrow, high intensity peak due to GaAs substrate (S), preceded by two peaks on left (L_1) due to the contribution from the buffer, barrier and spacer layers and (L_2) due to n and p-clad layers. Similar plots have been recorded for number of AlGaAs/GaAs heterostructures and they show similar features and three distinct peaks. Fig. 3.15 shows the plots obtained from the structures containing P in the active layer. As seen, three distinct peaks described above are seen clearly. In sample 00hs04, the peak on the right next to the substrate is not clearly resolved, but a shoulder is seen. However, in case of samples 00hs11, 00hs12 and 00hs17, low intensity broad peak (L_3) is seen on the right indicating the formation of a layer containing ternary alloy $GaAs_{1-x}P_x$. These samples also show a small peak on right next to and very close to the substrate peak indicating small amount of phosphorus present in the upper barrier layer. For 00hs17, a simulation program used to fit the experimental plot indicates the incorporation of about 6.9% P in the active layer and about 2% P in the upper barrier. Using simulation programs for other plots, we have estimated the P content in the active layers of other samples also.

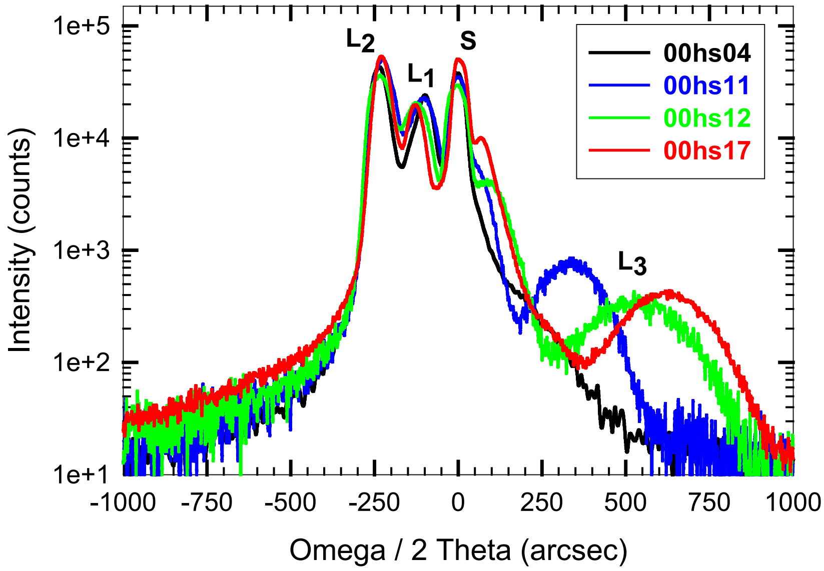

Fig. 3.15. XRD plots of P containing structures.

Fig. 3.16 shows plots obtained from the structures containing Sb in the active layer. In sample 01hs25 that does not contain any Sb, three peaks due to multilayers of AlGaAs and GaAs are

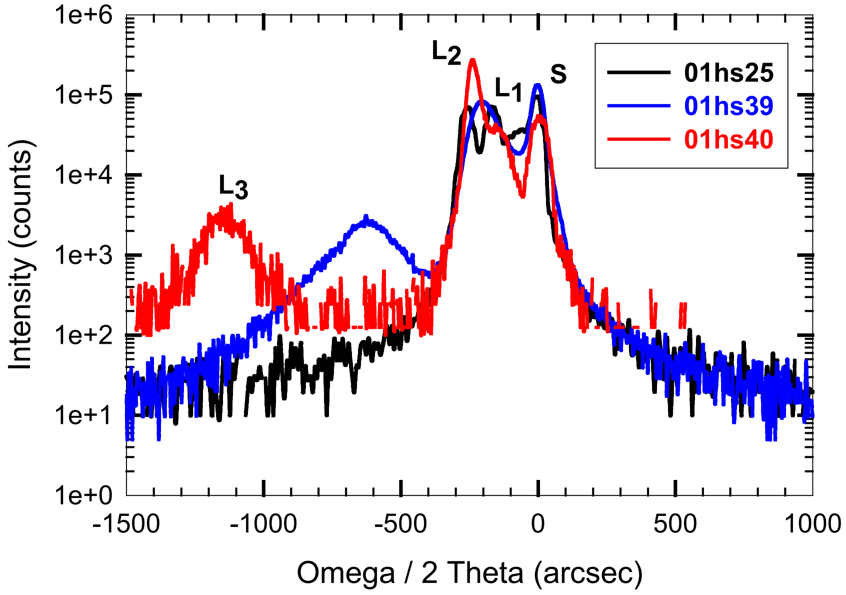

Fig. 3.16. XRD plots of Sb containing structures.

seen. For samples containing small amount of Sb in the melt, (samples 01hs26 & 27), neither a shoulder nor a separate peak is seen and the diffraction plots are similar to 01hs25 and

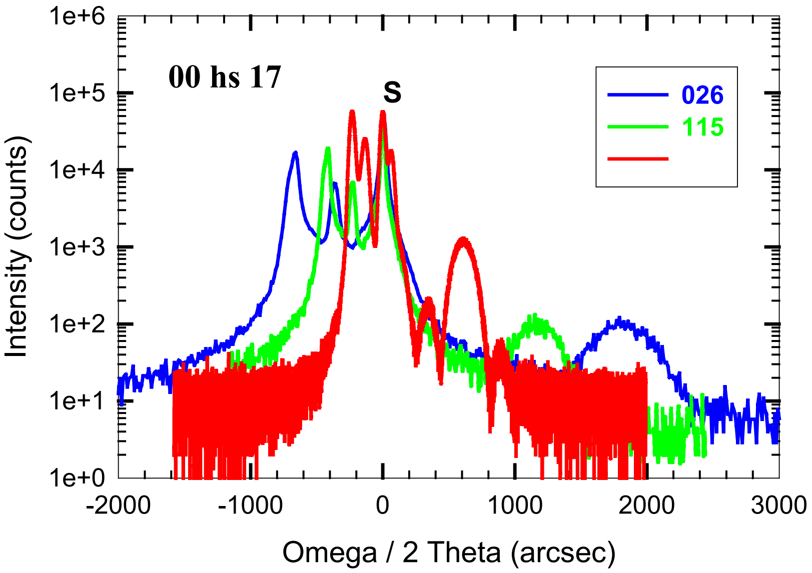

Fig. 3.17 XRD plots from symmetric and asymmetric reflections

hence not shown. However, in case of the sample containing rather large amount of Sb in the melt, (01hs39), we notice a low intensity peak (L_3) on the left, which corresponds to the incorporation of Sb in the active layer. X-ray plot of sample (01hs40) containing largest amount of GaSb in the melt shows similar broad peak shifted further to the left. Simulations fitting the experimental plots for these two samples give us an estimation of Sb content in the active layers of 3.4 and 5.8% respectively. In order to estimate the strain incorporated in these structures, x-ray diffraction plots from symmetric (004) and asymmetric (115) and (026) reflections were recorded. We have carried out two sets of analysis of x-ray measurements. First we estimated the in-plane ($\varepsilon_{\|}$) and out-of-plane ($\varepsilon_{\perp}$) strains in the active layer by measuring symmetric (004) and asymmetric (115) and (026) reflections. Fig. 3.17 shows one such plot for sample 00hs17 containing one symmetric (004) and two asymmetric (115 and 026) reflections. The separation between the substrate peak and the (L_3) peak [$\Delta\omega_{L,\ S}$] is analyzed to obtain the strain parameters. Table 3.11 lists the results of these measurements on four samples containing phosphorus and two samples containing antimony that gave peak (L_3) in x-ray measurements. We see that for all the samples, $\varepsilon_{\|}$ values are negligible within the error bars of the estimation, thus confirming that the active layers are fully strained with negligible in-plane strain. The critical thickness (h_c) for the estimated phosphorus and antimony content in these layers is also given in Table 3.11, as calculated using Matthews and Blakeslee relation [13]. The relation is: $h_c = a_s (1-\sigma/4) [\ln (h_c\sqrt{2}/a_s) + 1] / (2\sqrt{2}) \pi f (1+\sigma)$ where a_s is the lattice constant of GaAs substrate, σ is the Poisson ratio, and $f = \Delta a / a_s$ is lattice mismatch between the epi layer and the substrate. In all cases, the critical thickness is more than the measured layer thickness, consistent with the above observation of no measurable strain relaxation.

Table 3.11 – Results of XRD measurements

Sample number	**Strain** $\varepsilon_{\perp} \pm \Delta\varepsilon_{\perp}$ **(10^{-3})**	**Strain** $\varepsilon_{\|} \pm \Delta\varepsilon_{\|}$ **(10^{-3})**	$\Delta a/a$ **(10^{-3})**	**(%)** $X^S_{P/Sb}$ **cal/sim(♣)**	**thickness (nm)** **(d) SEM**	**[s](♦) x-ray**	h_c **Cal.**
* 00hs11	2.67 ± .02	0.15 ± .08	1.46	4.1 / 4.0	110	110	225 ± 8
* 00hs12	4.34 ± .04	-0.13 ± .18	2.19	6.1 / 6.1	100	100	140 ± 8
* 00hs17	4.77 ± .04	0.19 ± .25	2.57	7.2 / 7.2	100	125	117 ± 8
* 00hs19	4.66 ± .03	-0.18 ± .18	2.34	6.6 / 6.8	080	100	130 ± 6
# 01hs39	4.52 ± .03	0.05 ± .26	2.38	3.1 / 3.4	070	055	178 ± 9
# 01hs40	8.28 ± .01	0.30 ± .10	4.45	5.7 / 5.8	050	035	061 ± 1

- Samples containing P, # Samples containing Sb.
- (♣) Cal value of [$X^S_{P/Sb}$] obtained from $\Delta a/a$ listed above, simulated value of [$X^S_{P/Sb}$] obtained by simulation using PC-Epitaxy.
- (♦) active layer thickness used in simulations.

After obtaining the composition of the active layer as above and nominal thickness values of various layers from the SEM micrographs, we carried out simulations of x-ray profiles of various samples using dynamical diffraction calculation, with the active layer considered fully strained and pseudomorphic. Simulated profiles fairly close to the measured profiles were obtained, with small adjustments of nominal parameters by trial and error. The active layer compositions (in %) obtained in this manner are listed in Table 3.11 along with the values calculated from $\Delta a/a$ for comparison as outlined in Chapter 2. A close match is seen between the values obtained in two different ways of analyzing the x-ray data.

REFERENCES

[1] H. Nelson, RCA Rev. 24 (1963) 603.

[2] V. M. Andreev and V. P. Khovstikov, Private communication.

[3] Nuofu Chen, Xiulan Zhang, Yiwen Den, J. Crystal Growth, 148 (1995) 219.

[4] Zh. I. Alferov, V. M. Andreev, V, Yu, Aksenov, T. N. Nalet, Nguen Tkhan'Fyong, V. D. Rumyantsev and V. P. Khvostikov, Sov. Tech. Phys. Lett. 14 (1988) 893.

[5] A. J. Springthorpe, F. D. King, A. Becke, J. Electron. Mater. 4 (1975) 101.

[6] K. K. Shih, G. D. Pettit, J. Electronic Mater. 3 (1974) 391.

[7] E. Kuphal, Appl. Phys. A 52 (1991) 380

[8] E. W. Williams, H. B. Bebb, in: R. K. Willardson, A. C. Beer (Eds.), Photoluminescence II. Gallium Arsenide Semiconductors and Semimetals, vol. 8, Academic Press, New York, 1972.

[9] L. Pavesi, Properties of Aluminum Gallium Arsenide, EMIS date Review Series No. 7, S. Adachi (Ed.), INSPEC, The Institute of Electrical Engineers, London, 1993.

[10] D. W. Kisker, H. Tews, W. Rehm, J. Appl. Phys.54 (1983) 1332.

[11] L. Pavesi, M. Guzzi, J. Appl. Phys. 75 (1994) 4779.

[12] P. M. Mooney, J. Appl. Phys. 27 (1990) R1.

[13] J. W. Matthews and A. E. Blakeslee, J. Cryst. Growth, 27 (1974) 118.

Chapter 4.
Electro-optic characterization of heterostructures and laser diodes.

In this chapter, we describe and analyze the results of electro-optic characterization of the heterostructures containing unstrained and strained active layers. The characterization consists of measurements of L-I characteristics of the laser diodes fabricated and estimation of the lasing threshold. Results of measurements of electroluminescence (EL) spectra below and above lasing threshold current are presented. Also presented is the comparison of P and Sb content in the strained active layer as obtained from XRD, EL measurements and corresponding phase diagram calculations.

4.1 (L-I) - Light output-current characteristics of laser diodes:

The laser devices under test are in the form of rectangular bars, shown schematically in Fig. 4.1. As shown, top of the bar has three stripe contacts of 100-200μm width made on the epi-side. These are isolated from one another during the fabrication process. Each stripe along with the bottom contact at the substrate forms a diode.

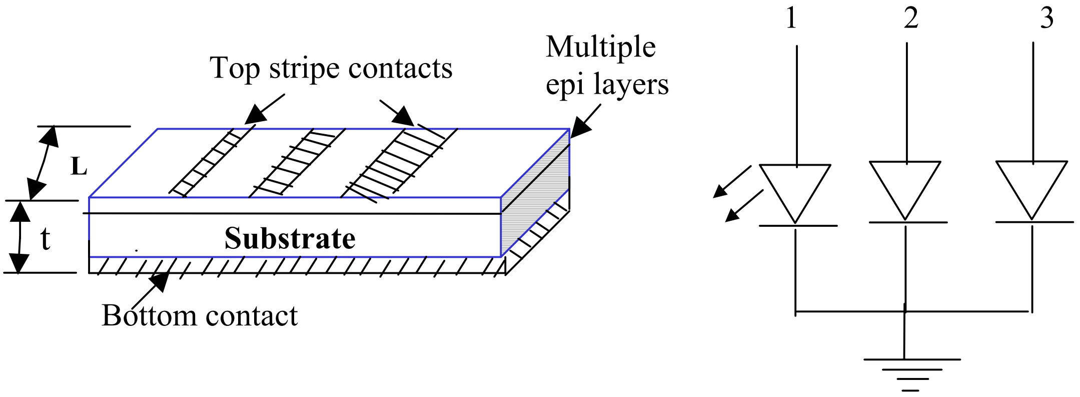

Fig. 4.1 Schematic of laser bar under test (left) and symbolic representation (right).

Typical cavity length L of the laser diode ranges between 0.2-1mm and thickness ‘t’ is about 0.1mm. Symbolic representation of these diodes is shown on the right. With this arrangement, all the devices on bar can be characterized without scribing them individually. The bar is mounted with substrate side in contact with a gold-coated stage. The contact to the top stripe is made using tiny gold probe mounted on a x-y-z movement. Light is emitted from the edge of the facet just below the stripe. In a typical measurement, a pulse generator [ILX-LDP 3840] is used to pass current pulses whose amplitude can be varied between 0-3A in small steps. Typical pulse duration is 1μs with pulse repetition interval (PRI) of 0.1msec. The emitted light is allowed to enter the integrating sphere (Labsphere IS-040) which is equipped with a calibrated Ge diode (GDA-050-V) for power measurement using controller (model no. SC-5500). Current in the diode is slowly increased and the power readings from the controller SC-5500 are recorded. Fig. 4.2 shows power output versus current characteristics of a typical laser structure sample 00hs17 that contains phosphorus in the active layer. The device consists of 170μm wide and 500μm long stripes.

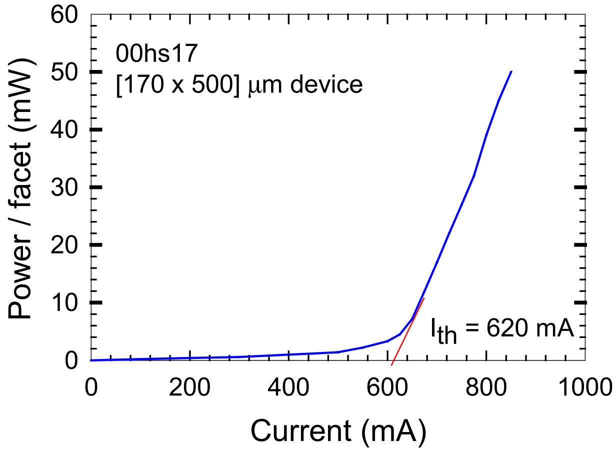

Fig. 4.2 Power output versus current characteristics of a laser diode.

It is operated at room temperature in pulsed mode. The light output is very low for low current values in the regime of spontaneous emission. At about 500mA the power begins to increase and beyond threshold value, it shoots up. This is the regime of stimulated emission and onset of laser emission. Beyond threshold current value the device operates as a laser diode. As seen, the threshold current is about 620mA and the corresponding current density (J_{th}) is ~730A/cm^2. We have carried out measurements on all the devices fabricated and selected those operating as lasers. Table 4.1 gives typical threshold current values for devices of different stripe width (W) and length (L) along with peak emission wavelengths recorded. Also listed is threshold current density, which seems to vary between 730-1350 A/cm^2. Sb containing samples are somewhat inferiors to those containing phosphorus. The exact reason for this is not clear to us at present. The results presented are not optimized from the point of view of device characteristics. The slope efficiency of better devices (Fig. 4.2) is within range of 0.22mW/mA. Other devices are somewhat poorer. These aspects require further investigation.

Table 4.1 Threshold current measured for typical laser devices

Sample Number	Device geometry [Width x Length] (µm x µm)	Threshold current I_{th} (mA)	Threshold density J_{th} (A/cm^2)	Peak emission wavelength (nm)
* 00hs04	170 x 500	650	765	833
* 00hs11	100 x 500	600	1200	830
* 00hs12	100 x 500	600	1200	818
00hs14	170 x 500	1000	1175	852
* 00hs17	170 x 250	325	765	795
00hs17	170 x 500	620	730	795
# 01hs26	100 x 500	500	1000	855
# 01hs40	150 x 500	1000	1330	900

* Active layer containing P, # Active layer containing Sb.

4.2 EL – Electroluminescence characteristics of laser diodes.

Fig. 4.3 shows the set up used for the spectral measurements, in which the current is passed through the diode using LDP-3840 pulse generator, and the emitted light is collected using an optical fiber and then fed to spectrometer [Ocean Optics, S-2000].

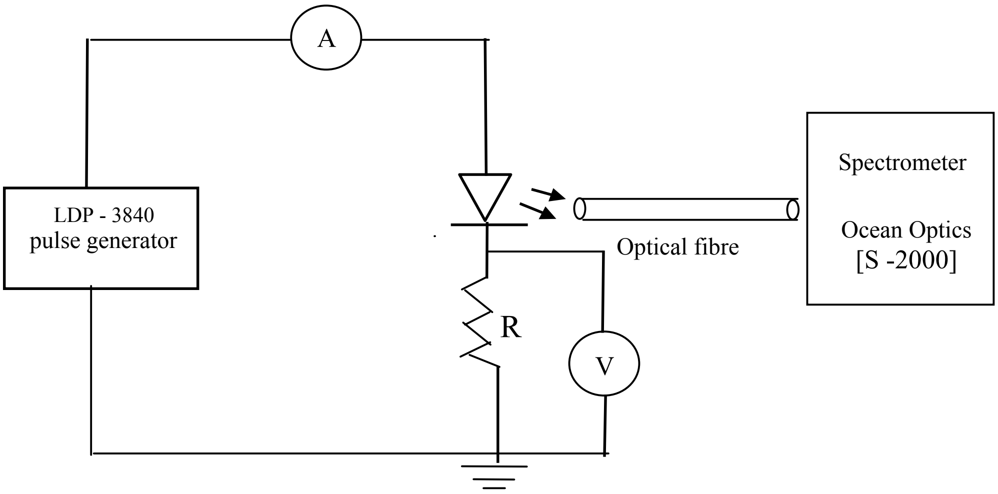

Fig. 4.3 Schematic of the set up used for spectral measurements.

Electroluminescence intensity for different wavelengths is recorded. Fig. 4.4 shows the emission spectra of sample 00hs17 at two current values for a device of length 250μm and the threshold current of about 400mA. At 50mA, a broad emission spectrum due to spontaneous emission is recorded. At about 325mA, this broad peak becomes more intense and narrow and centered around 798nm due to the onset of the stimulated emission.

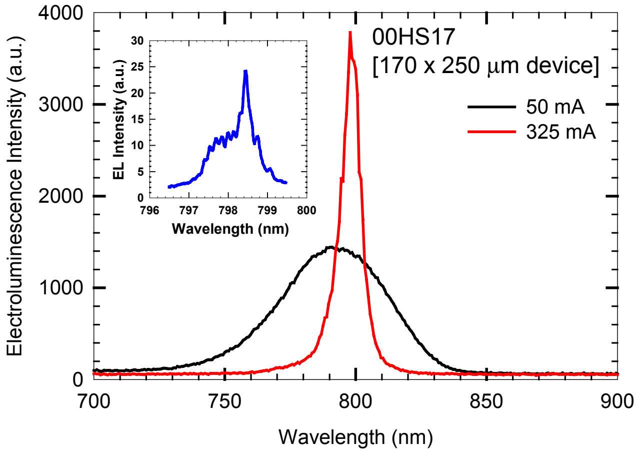

Fig. 4.4 Emission characteristics of a laser structure containing P in the active layer

These low-resolution spectra are recorded using fibre optic spectrometer [Ocean Optics S-2000]. Inset of Fig. 4.4 shows spectrum measured with a high-resolution spectrometer (Fig. 2.14) above 400mA excitation. Fig. 4.5 shows emission characteristics of a structure containing Sb in the active layer. In this case, the emission wavelength is around 900nm.

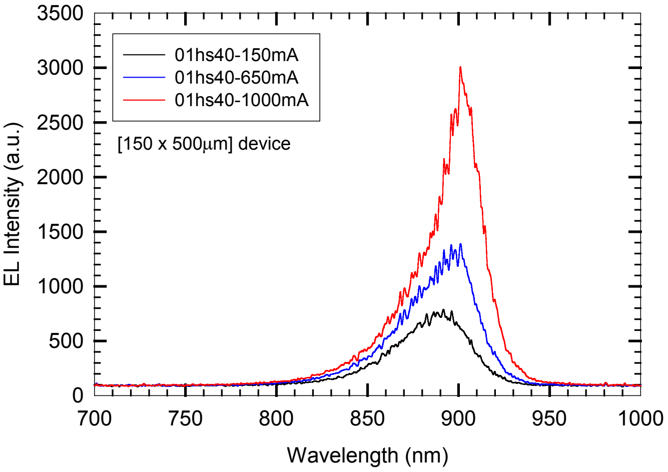

Fig. 4.5 Emission characteristics of a laser structure containing Sb in the active layer

4.3 Wavelength tuning by incorporating Sb or P in the active layer.

We have measured the peak emission wavelengths of the laser devices. As listed in Table 4.2, in case of samples containing P in the active layer, the emission wavelength varies from 795-833nm whereas in the case of Sb in the active layer, it varies from 855-900nm.

Table 4.2 Results of electroluminescence measurements

Sample Number	**λ_L (nm)**	**$E^S_{g(L)}$ (eV)**
00hs14	852	1.4554
* 00hs04	833	1.4886
* 00hs11	830	1.4941
* 00hs12	818	1.5159
* 00hs17	795	1.5598
* 00hs19	810	1.5308
01hs25	820	1.5122
# 01hs26	855	1.4502
# 01hs27	870	1.4252
# 01hs39	880	1.4091
# 01hs40	900	1.3777

* Active layer containing P, # Active layer containing Sb.

Table 4.2 also shows corresponding band gap energies, $E^S_{g\,(L)}(\text{eV}) = 1.24/\lambda$, where λ is the wavelength of laser emission in μm, superscript (S) denotes strain and the subscript (L) denotes band gap value obtained from laser emission wavelength. Variation of the band gap with composition for unstrained $GaAs_{1-y}P_y$ and $GaAs_{1-y}Sb_y$ is given respectively by [1-2]:

$$E_g^0\,[y] = 1.424 + 1.15\,y + 0.176\,y^2 \text{ for } GaAs_{1-y}P_y \qquad (1)$$

$$E_g^0\,[y] = 1.424 - 1.9\,y + 1.2\,y^2 \text{ for } GaAs_{1-y}Sb_y. \qquad (2)$$

Using these relations, it is possible to estimate the P or Sb content (y) in the active layer. However, in order to do so, we need to get E_g^0 [y]: unstrained band gap energies values from the measured $E^S_{g\,(L)}$ values by removing the contribution of strain incorporated in the active layers of these structures.

4.4 Change in band gap due to strain in the heterostructures.

Since the measured thickness of the active layers in the structures being analyzed lies in the 50-100nm range, we shall assume that the contribution of quantum size effect to the measured transition energies is negligible. Next, we estimate the strain energy. Change in the band gap energy due to strain (ΔE) is given by [3],

$$\Delta E = | f \; [2a\,(C_{11} - C_{12} / C_{11}) - b\,(C_{11} + 2C_{12} / C_{11})] \,|$$

where $f = (a^0_l - a^0_S) / a^0_S$ is the lattice mismatch estimated from x-ray measurements, C_{ij} are the elastic constants of the materials and a, b are the deformation potentials. Material parameters of GaAs, GaSb and GaP are listed in Table 4.3.

Table 4.3 Material parameters for GaAs, GaSb and GaP

Parameter	symbol (units)	GaAs	GaSb	GaP
Lattice constant	a^0(A°)	5.6532	6.0959	5.4505
Hydrostatic potential	$a_{(VB+CB)}$ (eV)	-9.22	-8.3	-9.5
Shear potential	$b_{(VB+CB)}$ (eV)	-2.0	-1.9	-1.5
Elastic constant	C_{11} (10^{11}) (dyn.cm^{-2})	11.9	8.83	10.22
Elastic constant	C_{12} (10^{11}) (dyn.cm^{-2})	5.38	4.02	5.76

We use linear interpolation for all the parameters a, b, C_{11} and C_{12}. As for example, the lattice parameter is $a^0\,[A_xB_{1-x}C] = x\,[a^0_{AB}] + (1-x)\,[a^0_{AC}]$, with A-Ga, B–As and C–P or Sb, a^0 is the lattice parameter and x is the mole fraction estimated from XRD measurements. Using these parameters, we have calculated ΔE for the samples in which separate peak due to P or Sb in the active layer was recorded and the results are listed in Table 4.4.

Table 4.4 Results of change in band gap energy due to strain (ΔE)

Sample Number	**x(%) (x-ray)**	**f (10^{-3})**	**a (eV)**	**b (eV)**	**C_{11} (10^{11})**	**C_{12} [dyn.cm^{-2}]**	**ΔE (meV)**
* 00hs11	4.0	1.4614	-9.23	-1.97	11.83	5.39	09.1
* 00hs12	6.1	2.1951	-9.23	-1.97	11.79	5.41	13.7
* 00hs17	7.2	2.5712	-9.24	-1.96	11.77	5.41	16.1
* 00hs19	6.8	2.3391	-9.24	-1.96	11.78	5.41	14.6
# 01hs39	3.4	2.3791	-9.19	-1.99	11.81	5.34	14.9
# 01hs40	5.8	4.4488	-9.16	-1.99	11.72	5.31	27.8

* Active layer containing P, # Active layer containing Sb.

Using these values of ΔE, we have calculated unstrained band gap energies $E_g^0 = E^S_{g(L)} + |\Delta E|$ for the tensile strained active layer containing phosphorus, and $E_g^0 = E^S_{g(L)} - |\Delta E|$ for the compressively strained active layer containing antimony. E_g^0 values obtained in this way are listed in Table 4.5.

Table 4.5 Results of laser emission wavelengths and band gap

Sample Number	λ_L (nm)	$E^S_{g\,(L)}$ (eV)	ΔE (meV)	E_g^0 (eV)
00hs14	852	1.4554	-	-
* 00hs04	833	1.4886	-	-
* 00hs11	830	1.4941	09.1	1.5032
* 00hs12	818	1.5159	13.7	1.5296
* 00hs17	795	1.5598	16.1	1.5758
* 00hs19	810	1.5308	14.6	1.5454
01hs25	820	1.5122	-	-
# 01hs26	855	1.4502	-	-
# 01hs27	870	1.4252	-	-
# 01hs39	880	1.4091	14.9	1.3942
# 01hs40	900	1.3777	27.8	1.3499

* Active layer containing P, # Active layer containing Sb.

4.5 Estimation of composition of active layers: problem of intermixing of solutions

We have used (E_g^0) – the unstrained band gap values obtained above for the estimation of the composition of the active layers in the heterostructures. However, a further correction has to be applied to the E_g^0 values listed in Table 4.5 to account for the Al incorporated in the active layer. This is due to the mixing between the active layer solution and the solution used to grow the lower barrier layer just prior to the growth of the active layer. This amount can be estimated from the emission wavelengths of the structures that do not have any P or Sb in the solution of the active layer. We have two such samples 00hs14 and 01hs25 grown at about 650^0C but for different growth duration. Considering E_g ($Al_xGa_{1-x}As$) = 1.424 + 1.247x [4], we get x = 0.025 in the active layer of sample 00hs14 which is grown for 20 seconds and x = 0.07 for sample 01hs25 which is grown for very short time (< 3-5 seconds). Thus, there is an uncertainty in the content of Al incorporated in the active layer. Corresponding to this uncertainty, there will be a spread in the estimated value of P/Sb atom fraction. With Al (x) in the active layer, equation (1) and (2) for band gap are modified as:

$E_g^0\ [x, y] = 1.424 + 1.247x + 1.15\ y + 0.176\ y^2$ for $Al_xGa_{1-x}As_{1-y}P_y$ (3)

$E_g^0\ [x, y] = 1.424 + 1.247\ x - 1.9\ y + 1.2\ y^2$ for $Al_xGa_{1-x}As_{1-y}Sb_y$. (4)

We have used these equations with x = 0.025 for the estimation of the compositions (y) in the active layer. The results are shown in Table 4.6.

Table 4.6 Results of P/Sb content of active layers

Sample Number	E_g^0 (eV)	$X^S_{P/Sb}$ (%) (laser)	$X^S_{P/Sb}$ (x-ray) [%] calculated/simulated
00hs14	-	-	-
* 00hs04	-	2.9 ($)	-
* 00hs11	1.5032	4.2 ($)	4.1 / 4.0
* 00hs12	1.5296	6.5 ($)	6.1 / 6.1
* 00hs17	1.5758	7.3 (&)	7.2 / 7.2
* 00hs19	1.5454	6.8 (@)	6.6 / 6.8
01hs25	- -	-	-
# 01hs26	- -	0.3 ($)	-
# 01hs27	-	1.6 ($)	-
# 01hs39	1.3942	3.3 ($)	3.1 / 3.4
# 01hs40	1.3499	5.7 ($)	5.7 / 5.8

* Active layer containing P, # Active layer containing Sb.
$ Calculated assuming Al content 2.5%.
(&) Calculated assuming Al content 5.5%.
(@) Calculated assuming Al content 3.5%.

Also listed are the P/Sb atom fractions in solid obtained from x-ray measurements and simulations. We see that there is general agreement between the compositions determined by different methods and the values lie within the spread envisaged in the Al content. Further, from comparison it is possible to state that the Al content in most of the active layers is about 2.5 %. For the samples 00hs17 and 00hs19, the agreement with the x-ray determined P content in the active layers is obtained if we assume the Al content to be 5.5 % and 3.5 % respectively. Thus, we have established a correspondence between P and Sb incorporated in strained layer as obtained from XRD and electroluminescence measurements. Next, we shall examine the correspondence with the values obtained using phase diagram calculations.

4.6 Comparison of experimental and calculated incorporation of P/Sb in the active layer

In Chapter 2, we have calculated the incorporation of P in $GaAs_xP_{1-x}$ layer and Sb in $GaAs_xSb_{1-x}$ layer from the corresponding solutions at 650^0C. To recapitulate, the P incorporation equations corresponding to a solution containing Ga, As and P are obtained as

$X \exp[0.55(1-X)^2] = 333\ (x_{Ga}{}^{l} x_{As}{}^{l})$ and

$(1-X) \exp[0.55(X)^2] = 5000\ (x_{Ga}{}^{l} x_{P}{}^{l})$

which gives x in $GaAs_xP_{1-x}$ with the restriction $x_{Ga}{}^{l} + x_{As}{}^{l} + x_{P}{}^{l} = 1$.

Similarly, the Sb incorporation equations corresponding to a solution containing Ga, As and Sb are obtained as

$X \exp[1.5047(1-X)^2] = 336\ (x_{Ga}{}^{l} x_{As}{}^{l})$ and

$(1-X) \exp[1.5047(X)^2] = 5.36\ (x_{Ga}{}^{l} x_{Sb}{}^{l})$

which again gives x in $GaAs_xSb_{1-x}$ with the restriction $x_{Ga}{}^{l} + x_{As}{}^{l} + x_{Sb}{}^{l} = 1$.

Results of these calculations are given in Figs. 4.6.and 4.7.

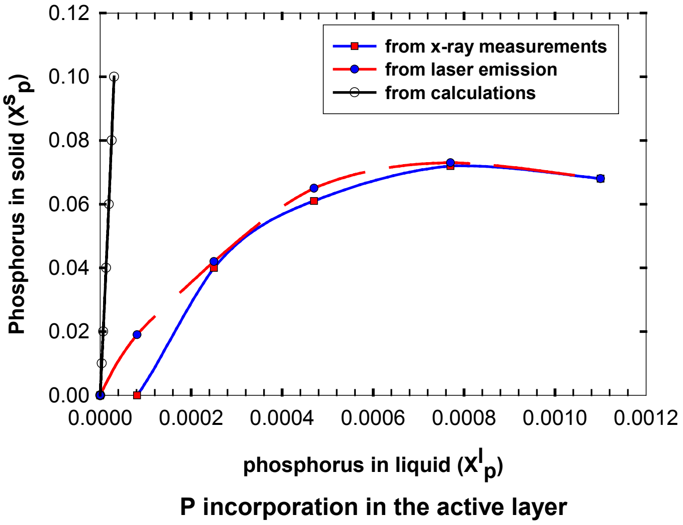

Fig. 4.6 Phosphorus incorporation in the active layer.

Also shown in these figures are the experimental values obtained from x-ray measurements as well as from lasing wavelength measurements. As seen, the experimental results show much less P incorporation as compared to the calculated values. This is expected since considerable phosphorus is lost during the solution homogenization at elevated temperatures above 720^{0}C. The agreement between the calculated Sb incorporation and the experimental values is close upto about $x^l_{Sb} = 0.02$. At higher Sb content, the experimental Sb content values are significantly less than expected from calculations. The Sb incorporation is about half as much as expected for $x^l_{Sb} = 0.06$. We consider the possible reason for this behavior in next section.

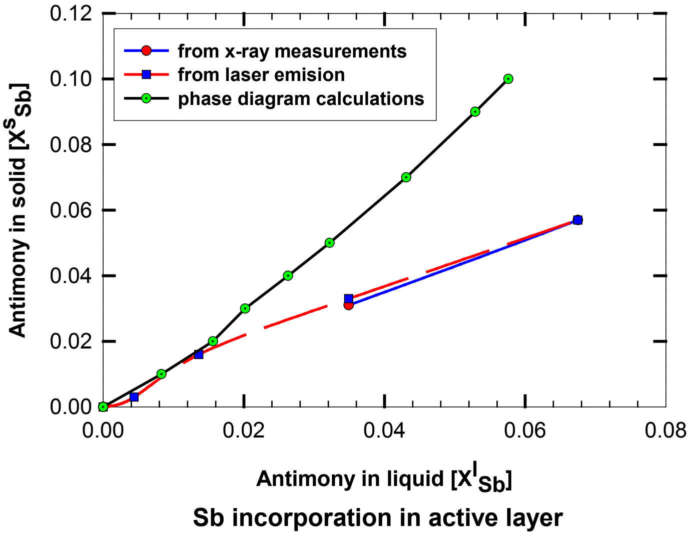

Fig. 4.7 Antimony incorporation in the active layer.

4.7 Effect of strain on growth process

Considering the causes for the lesser amount of Sb in the epi than expected from calculations, one possible reason could be strain in the epi layer. Strain is known to influence the fundamental growth process. Bugge and coworkers [5] showed that in the case of MOVPE growth of strained InGaAs/GaAs, the incorporation of indium in highly strained InGaAs layer is less than that in the relaxed InGaAs layer. Similar observation was reported regarding the incorporation of As in InAsP grown on InP by MBE [6] as well as MOVPE [7]. Thus we observe that reduced incorporation co-efficient is a fairly universal feature of strained epi-layer growth independent of the growth technique. Reduced incorporation is seen particularly for the component responsible for producing the strain, e.g. indium in InGaAs grown on GaAs, As in InAsP on InP and in the present case Sb in GaAsSb on GaAs, and is thus independent of the material system. There are reports in the LPE literature [8-9] incorporating the effect of strain on the phase diagram. This aspect thus has a broader significance and requires further investigation.

REFERENCES

[1] A. G. Thompson, M. Cardona, K. L. Shaklee, and J. C. Woolley, Phys. Rev. 146 (1966) 601.

[2] M. B. Thomas, W. M. Coderre and J. C. Woolley, Phys. Status Solidi (a) 2 (1970) K 141.

[3] F. H. Pollak, in: T. P. Pearsall (Ed.) Semiconductors and Semimetals, vol. 32 (1990) 17.

[4] H. C. Casey, Jr. And M. B. Panish, (Eds.) in: Heterostructure Lasers, (Academic Press) Part B (1978) 16.

[5] F. Bugge, U. Zeimer, M. Sato, M.Weyers and F. Trankle, J. Cryst. Growth, 183 (1998) 511.

[6] T. H. Kim, A. S. Brown, R. A. Metzger, J. Appl. Phys. 86 (1999) 2622.

[7] R. Venkataraghavan, M. R. Gokhale, A. P. Shah, A. Bhattacharya, K. S. Chandrasekaran and B. M. Arora, J. Cryst. Growth, 221 (2000) 535.

[8] R. E. Nahory, M. A. Pollack, E. D. Beebe, and J. C. Dewinter, J. Electrochem. Soc. 125 (1978) 1053.

[9] P. K. Bhattacharya and S. Srinivasa, J. Appl. Phys. 54 (1983) 5090.

Chapter 5

Summary and scope for further work

5.1 Summary

During the 'Investigations of multilayered III-V compound structures grown by liquid phase epitaxy', we have synthesized number of GaAs/AlGaAs based heterostructures on GaAs substrates. All the growth experiments were done at low temperatures in the 700^0C-500^0C range using piston boat. Attempts were made to grow ultrathin active layers. Compressive/tensile strain was incorporated in the active layer by using antimony/phosphorus respectively. Thickness of the active layer was adjusted to obtain pseudomorphic, dislocation free layers for lasers. Strained/non strained heterostructures have been characterized using HR-XRD measurements. Strained layer lasers emitting in 800-900nm wavelength range have been obtained. Salient features and achievements of this work are as follows:

(i) Piston boat is found suitable for low temperature [700^0C-500^0C] liquid phase epitaxy and useful for synthesizing device quality heterostructures with undoped, n type (Te), p type (Mg) AlGaAs and GaAs multilayered structures.

(ii) Thin epitaxial layers (about 50nm thick), for the active layer of laser diodes can be synthesized reproducibly using low temperature LPE.

(iii) Fully strained, defect-free, thin pesudomorphic layers such as GaAsP and GaAsSb can be synthesized on GaAs substrates using LPE. These layers are of device quality and can be used for the active region of strained-layer laser diodes.

(iv) A disadvantage of piston boat is an unavoidable mixing of successive solutions with the preceding ones. About 3-7% Al is incorporated in GaAs grown from a solution that displaces the solution used for growing $Al_{0.3}Ga_{0.7}As$ layer. This has to be taken into account in the design of a layer, particularly the active layer.

(v) Emission wavelength of laser diode fabricated from such heterostructure with GaAs active layer is in 820-850nm range. This variation is due to aluminium incorporation in the active layer because of solution mixing.

(vi) Incorporation of P produces tensile strain whereas compressive strain is produced by incorporation of Sb. The incorporation of P/Sb changes the active layer material band gap from that of GaAs and hence different emission wavelengths can be obtained. Thus, with P incorporation lasers emitting at 795, 818, 830 and 833nm are obtained whereas with Sb incorporation, lasers emitting at 855, 870, 880 and 900nm are obtained. It is shown by x-ray measurements that the layers are pseudomorphically strained.

5.2 Scope for further work

(i) LPE method is simple, relatively inexpensive and good for experimenting with new material systems. However, whether it is suitable for scaling up for industrial production of laser diodes emitting in 650-1600nm range remains to be established.

(ii) The thinnest layers grown reproducibly during this work are in 40-50nm range. It seems desirable to (a) automate the movements of the solutions and (b) improve the saturation/growth temperature control to establish growth of thinner layer (~10nm) reproducibly. Another aspect would be to incorporate such layers in devices and compare their performance with the devices synthesized using MBE and OMVPE.

(iii) We have demonstrated the growth of device quality pseudomorphic strained layers by LPE using anions such as P and Sb in the active layer. A straightforward extension of this work will be to incorporate cation such as indium by growing InGaAs as active layer. It will also be interesting to check out the effect of strain on the In incorporation in the epi layer grown by LPE.

(iv) This work can be extended using GaAs and other substrates, such as InP and GaSb, and with active layer of a variety of other alloys such as InGaP, InGaAs, InGaAsP, AlGaAsSb, and InGaAsSb to obtain lasers emitting in 650-1600nm range.

BIBLIOGRAPHY

Chapter 1

[1] Pallab Bhattacharya in Semiconductor Optoelectronic Devices, Prentice Hall (1995).

[2] R.N.Hall, G. E. Fenner, J. D. Kingsley, T.J. Soltys and R.O.Carlson, Phys. Rev. Lett.9, (1962) 366

[3] M. I. Nathan, W. P. Dumke, G. Burns, F. H. Dill Jr., and G. Lasher, Appl. Phys. Lett. 1, (1962) 63.

[4] T. M. Quist, R. H. Rediker, R. J. Keyes, W. E. Krag, B. Lax, A. L. McWhorter, and H. J. Ziegler, Appl. Phys. Lett. 1, (1962) 91.

[5] H. Kroemer, Proc. IEEE 51 (1963) 1782.

[6] Zh. I. Alferov and R. F. Kazarinov, USSR Patent 181737 (1963).

[7] Zh. I. Alferov, V. M. Andreev, D. Z. Garbuzov, Yu. V. Zhilyaev, E. P. Morozov, E. L. Portnoi and V. G. Trofim, Sov. Phys. Semicond. 4, (1971) 1573.

[8] I. Hayashi, M. B. Panish, P. W. Foy and S. Sumski, Appl. Phys. Lett. 17, (1970) 109.

[9] J. P. Van Der Ziel, R. Dingle, R. C. Miller, W. Wiegmann and W. A. Nordland Jr. Appl. Phys. Lett. 26, (1975) 463.

[10] R. D. Dupuis, P. D. Dapkus, N. Holonyak, Jr. E. A. Rezek and R. Chin, Appl. Phys. Lett. 32, (1978) 295.

[11] W. T. Tsang, C. Weibuch, R. C. Millar and R. Dingle, Appl. Phys. Lett. 35, (1979) 673.

[12] W. T. Tsang, Appl. Phys. Lett. 40, (1982) 217.

[13] A. R. Adams, Electron. Lett. 22 (1986) 249.

[14] E. Yablonovitch, and E. O. Kane J. Lightwave Technol. 4 (1986) 504.

[15] Y. Sasai, N. Hasae and T. Kajiwara, Japn. J. Appl. Phys. 24, (1981) L 137.

[16] E. A. Rezek, N. Holonyak Jr., B. A. Vojak, G. F. Stillman, J. A. Rossi, D. L. Keune, and J. D. Fairing, Appl. Phys. Lett. 31 (1977) 288.

[17] E. A. Rezek, B. A. Vojak, R. Chin, N. Holonyak Jr., and E. A. Samman, J. Electron. Mater. 10 (1981) 255.

[18] Zh. I. Alferov, I. N. Arsent'ev, L. S. Vavilova, D. Z. Garbuzov and V. V. Krasovskii, Sov. Phys. Semicond, 18 (1984) 1035.

[19] D. Z. Garbuzov, I. N. Arsent'ev, L. S. Vavilova, A. V. Tikunov and E. V. Tulashvili, Sov. Phys. Semicond, 19 (1985) 83.

[20] Mu-Kuen-Chen, Tien-Chin Chang, and Hao-Hsiung Lin, J. Appl. Phys. 74 (1993) 3464

[21] K. Ketling, K. Koehler and P. Zwicknagl, Appl. Phys. Lett. 48 (1986) 157.

[22] Zh. I. Alferov, A. A. Vodnev, O. O. Ivent'eva, V. R. Laroinov and V. D. Rumyantsev, Sov. Phys. Semicond, 20 (1986) 239.

[23] V. M. Andreev, A. B. Kazantsev, V. P. Khvostikov, E. V. Paleeva, V. D. Rumyantsev and S. V. Sorokina, Materials Chemistry and Physics, 45 (1996) 130.

[24] Strategies Unlimited, [an optoelectronic market research firm based in Mountain View, CA, USA], Laser Diode review, Forecast-1996, Report OM-6.

[25] R. L. Moon, J. Cryst. Growth 170 (1997) 1.

Chapter 2

[1] H. Nelson, RCA Rev. 24 (1963) 603.

[2] L. R. Dawson, in progress in Solid State Chemistry, (1972), Vol. 7, Ed. H. Reiss and J. O. McCaldin (GaAs and AlGaAs)

[3] Special Edition of Journal of Crystal growth on liquid phase epitaxy vol. 27 (1974).

[4] K W. Benz and E. Bauser in Crystals-Growth, properties and applications (1980), vol.3, Ed. H. C. Freyhardt (Growth mechanisms)

[5] J. J. Hsieh in Handbook on Semiconductors, 3 (1980) 415. [General Review]

[6] J. C. Brice in Current Topics in Material Science (1980), vol.5, Ed. E. Kaldis (Theory, techniques, GaAs, AlGaAs)

[7] K. Nakajima in GaInAsP alloy Semiconductors, (1982), Ed. T. P. Pearsall (GaInAsP)

[8] P. D. Green in Advanced Crystal Growth, Ed. P. M. Dryburgh et al (1987).

[9] M. G. Astles in Liquid-Phase Epitaxial Growth of III-V Compound Semiconductor Materials and their Device Applications, Adams Hilger, Great Britain (1990).

[10] E. Kuphal, in Liquid Phase Epitaxy, Appl. Phys. A 52 (1991) 380.

[11] R. L. Moon, Journal of Crystal Growth, 170 (1997) 1.

[12] H. Rupprecht, Inst. Phys. Conf. Ser. No. 3, (1966) 57.

[13] M. B. Panish, I. Hayashi and S. Sumski, IEEE J. Quantum Electron. 5 (1969) 210.

[14] G. H. B. Thompson and P. A. Kirby, J. Crystal Growth 27, (1974) 70.

[15] Y. Horikoshi, Japn. J. Appl. Phys. 15, (1976) 887.

[16] Zh. I. Alferov, V. M. Andreev, S. G. Konnikov, V. R. Larionov and B. V. Pushny, Krist. Tech. 11 (1976) 1013.

[17] T. B. Reed, Solid State Research Report (1969:1) MIT Lincoln Laboratory, MA, USA

[18] J. J. Hsieh, J. Crystal Growth, 27 (1974) 49.

[19] R. Sankaran, G. A. Antypas, R. L. Moon, J. S. Escher and L. W. James, J. Vac. Sci. Technol. 13 (1976) 932.

[20] T. P. Pearsall and R. W. Hopson Jr. J. Appl. Phys. 48 (1977) 4407.

[21] K. Sakai, Y. Matsushima, S. Akiba and T. Yamamoto, Japn. J. Appl. Phys. 18 (1979) 1009.

[22] R. E. Nahory, M. A. Pollack, J. C. DeWinter and K. M. Williams, J. Appl. Phys. 48 (1977) 1607.

[23] H. Kano and K. Sugiyama, Electron. Lett. 16 (1980) 146.

[24] N. Kobayashi, Y. Horikoshi and C. Uemara, Japn. J. Appl. Phys. 18 (1979) 2169.

[25] S. D. Hersee, A. C. Carter, R. C. Goodfellow, G. Hawkins and I. Griffith, Solid state Electron Devices, 3 (1979) 179.

[26] J. J. Hsieh, M. C. Finn and J. A. Rossi, 6th Intl. Symp. on GaAs and related compounds, St. Louise (Inst. Phys. Conf. Ser.) 33a (1976) 37.

[27] Zh. I. Alferov, V. M. Andreev, D. Z. Garbuzov, Yu. V. Zhilyaev, E. P. Morozov, E. L. Portnoi and V. G. Trofim, Sov. Phys. Semicond. 4, (1971) 1573.

[28] I. Hayashi, M. B. Panish, P. W. Foy and S. Sumski, Appl. Phys. Lett. 17, (1970) 109.

[29] I. Hayashi, U. S. Patent No. 3,691,476 (1972)

[30] G. H. B. Thompson and P. A. Kirby, IEEE J. Quantum Electron. QE-9, (1973) 311.

[31] L. Schultheiss and K. Ploog, Phys. Rev. B 30 (1984) 1090.

[32] H. Kawai, K. Kaneko and N. Watanabe, J. Appl. Phys. 56 (1984) 463.

[33] C. F. J. Schanen, S. Illek, H. Lang, W. Thulke and M. C. Amann, IEEE Proc. Part J, 137 (1990) 69.

[34] Mu-Kuen-Chen, Tien-Chin Chang, and Hao-Hsiung Lin, J. Appl. Phys. 74 (1993) 3464.

[35] K. Ketling, K. Koehler and P. Zwicknagl, Appl. Phys. Lett. 48 (1986) 157.

[36] Zh. I. Alferov, A. A. Vodnev, O. O. Ivent'eva, V. R. Laroinov and V. D. Rumyantsev, Sov. Phys. Semicond, 20 (1986) 239.

[37] S. Subramanian and B. M. Arora, J. Appl. Phys. 49 (1978) 257.

[38] S. Chakravarty, B. M. Arora, A. K. Srivastava, S. Subramanian, and S. Anand, Thin Solid Films 163 (1988) 443.

[39] S. S. Chandvankar, R. Rajalakshmi, A. K. Srivastava, and B. M. Arora, J. Cryst. Growth 88 (1988) 303.

[40] S. S. Chandvankar, and B. M. Arora, J. Cryst. Growth 94 (1989) 270.

[41] B. M. Arora, S. S. Chandvankar, R. Rajalakshmi, A. K. Srivastava, and S Chakravarty, Thin Solid Films 163 (1988) 421.

[42] S. S. Chandvankar, T. K. Sharma, A. P. Shah, K. S. Chandrasekaran, B. M. Arora, A. K. Kapoor, Devendra Verma, B. B. Sharma, J. Cryst. Growth 213 (2000) 250.

[43] V. M. Andreev and V. P. Khovstikov, Private communication.

[44] G. B. Stringfellow and P. E. Greene, J. Phys. Chem. Solids, 30 (1969) 1779.

[45] G. A. Antypas, J. Elec. Chem. Soc., 117 (1970) 700.

[46] M. Quillec, C. G. Fonstad, and S. Garone, J. Appl. Phys., 49 (1978) 5920.

[47] R. E. Nahory, M. A. Pollack, J. C. Dewinter and K. M. Williams, J. Appl. Phys. 48 (1977) 1607.

[48] G. H. Olsen and M. Ettenberg, J. Appl. Phys. 45 (1974) 5112.

[49] L. J. van der Pauw, Phillips Research reports 13 (1958) 1.

[50] S. M. Sze in Physics of Semiconductor Devices, Wiley Eastern Ltd. (1981).

[51] I. C. Mayes in Bio-Rad Semiconductor notes, Note N0. 201 (1985).

[52] E. W. Williams and H. Bebb, Semiconductor and Semimetals, edited by R. K. Willardson and A. C. Beer Vol.8 (1972) P. 181. (Academic, New York, 1972)

[53] L. Pavesi and M. Guzzi, J. Appl. Phys. 75 (1994) 4779.

[54] A. K. Srivastava, Ind. J. of Pure and Applied Physics, 27 (1989) 386.

[55] W. J. Bartels, W. Nijman, J. Cryst. Growth 44 (1978) 518.

[56] J. W. Matthews and A. E. Blakeslee, J. Cryst. Growth 27 (1974) 118.

[57] S. T. Picraux, B. L. Doyle, and J.Y. Tsao, in: T. P. Pearsall (Ed.) Semiconductors and Semimetals, vol. 33 (1991) 174.

[58] R. Zaus, J. Appl. Cryst. 26 (1993) 801.

[59] S. S. Chandvankar, A. P. Shah, A. Bhattacharya, K. S. Chandrasekaran, and B. M. Arora Proceedings: Photonics-2000, International Conference on Fiber Optics and Photonics, Calcutta, Vol. 1, (2000) 203.

Chapter 3

[1] H. Nelson, RCA Rev. 24 (1963) 603.

[2] V. M. Andreev and V. P. Khovstikov, Private communication.

[3] Nuofu Chen, Xiulan Zhang, Yiwen Den, J. Crystal Growth, 148 (1995) 219.

[4] Zh. I. Alferov, V. M. Andreev, V, Yu, Aksenov, T. N. Nalet, Nguen Tkhan'Fyong, V. D. Rumyantsev and V. P. Khvostikov, Sov. Tech. Phys. Lett. 14 (1988) 893.

[5] A. J. Springthorpe, F. D. King, A. Becke, J. Electron. Mater. 4 (1975) 101.

[6] K. K. Shih, G. D. Pettit, J. Electronic Mater. 3 (1974) 391.

[7] E. Kuphal, Appl. Phys. A 52 (1991) 380

[8] E. W. Williams, H. B. Bebb, in: R. K. Willardson, A. C. Beer (Eds.), Photoluminescence II. Gallium Arsenide Semiconductors and Semimetals, vol. 8, Academic Press, New York, 1972.

[9] L. Pavesi, Properties of Aluminum Gallium Arsenide, EMIS date Review Series No. 7, S. Adachi (Ed.), INSPEC, The Institute of Electrical Engineers, London, 1993.

[10] D. W. Kisker, H. Tews, W. Rehm, J. Appl. Phys.54 (1983) 1332.

[11] L. Pavesi, M. Guzzi, J. Appl. Phys. 75 (1994) 4779.

[12] P. M. Mooney, J. Appl. Phys. 27 (1990) R1.

[13] J. W. Matthews and A. E. Blakeslee, J. Cryst. Growth, 27 (1974) 118.

Chapter 4

[1] A. G. Thompson, M. Cardona, K. L. Shaklee, and J. C. Woolley, Phys. Rev. 146 (1966) 601.

[2] M. B. Thomas, W. M. Coderre and J. C. Woolley, Phys. Status Solidi (a) 2 (1970) K 141.

[3] F. H. Pollak, in: T. P. Pearsall (Ed.) Semiconductors and Semimetals, vol. 32 (1990) 17.

[4] H. C. Casey, Jr. And M. B. Panish, (Eds.) in: Heterostructure Lasers, (Academic Press) Part B (1978) 16.

[5] F. Bugge, U. Zeimer, M. Sato, M.Weyers and F. Trankle, J. Cryst. Growth, 183 (1998) 511.

[6] T. H. Kim, A. S. Brown, R. A. Metzger, J. Appl. Phys. 86 (1999) 2622.

[7] R. Venkataraghavan, M. R. Gokhale, A. P. Shah, A. Bhattacharya, K. S. Chandrasekaran and B. M. Arora, J. Cryst. Growth, 221 (2000) 535.

[8] R. E. Nahory, M. A. Pollack, E. D. Beebe, and J. C. Dewinter, J. Electrochem. Soc. 125 (1978) 1053.

[9] P. K. Bhattacharya and S. Srinivasa, J. Appl. Phys. 54 (1983) 5090.

Synopsis

Name of the student : S. S. Chandvankar

Name of the Guide : Professor B. M. Arora

Title of the thesis : Investigations of multilayered III-V compound structures grown by liquid phase epitaxy.

Degree : Ph. D. in Physics.

Registration Number : T.I.F.R.-17 Dated: 04.12.1992

Place of Research : Tata Institute of Fundamental Research,
Homi Bhabha Road, Mumbai – 400 005.

This thesis describes investigations of multilayered III-V compound semiconductor structures grown by liquid phase epitaxy, using aluminium gallium arsenide and gallium arsenide materials. The investigations include synthesis of strained / non-strained heterostructures for semiconductor lasers, characterization of the structures and fabrication of laser diodes in 800-900 nm wavelength range. Beginning with an introduction to the subject and experimental techniques, we describe the new findings of the present work and indicate further possibilities using these investigations.

A perfect crystalline inorganic bulk semiconductor has a band of electronic states completely filled at absolute zero temperature (termed as valence band), separated from another completely empty band of electronic states (termed as conduction band) by a region of forbidden energy. At absolute zero temperature, this ideal intrinsic semiconductor is a perfect insulator. At higher temperatures, a few electrons from the valence band acquire sufficient thermal energy and are excited across the forbidden energy gap to partially fill the electronic states in the conduction band and leave empty states in the valence band. Both the electrons in the partially filled conduction band and the positively charged empty states (termed as holes) in the valence band contribute to electrical conduction in semiconductors. The conductivity of an intrinsic semiconductor can be altered and enhanced by doping with appropriate impurities which are either electron donors making it n type or electron acceptors making it p type.

Depending on the nature of constituent atoms and the crystal structure, electronic energy depends on momentum in a complex way. There are maxima and minima in energy along specific directions in the momentum space. The energy separation between the lowest conduction band minimum and the highest valence band maximum is termed as the fundamental energy gap or simply the band gap of the material. Examples of the inorganic bulk semiconductors, with different energy gaps are: (i) elemental semiconductors in which only group IV elements are assembled in a diamond lattice structure, viz. Si: 1.12 eV, Ge: 0.67 eV, and (ii) compound semiconductors constituting group III and group V elements of the periodic table having zinc blende or hexagonal lattice structure, viz. GaN: 3.36 eV, GaP: 2.1 eV, GaAs: 1.42 eV, GaSb: 0.7 eV, InP: 1.35 eV. InAs: 0.36 eV, and InSb: 0.17 eV.

If the conduction band minimum (CBM) and the valence band maximum (VBM) occur at the same momentum, the semiconductor is called direct gap and if the CBM and VBM occur at different points in the momentum space, the semiconductor is called indirect. The fundamental band gap of elemental semiconductors such as Si and Ge is indirect. In these, the absorption coefficient near the band edge energy is relatively low and correspondingly they are poor light emitters. On the other hand, several compound semiconductors (although not all) such as GaAs, InP and GaSb have direct fundamental energy gap. They have high absorption coefficients near the band edge energy and are also efficient light emitters. These compounds can be combined or alloyed using one or more group III elements with one or more group V elements to form mixed crystals such as AlGaAs, AlGaAsP, InGaAs, InGaP, InGaAsP, GaAsSb, AlGaAsSb etc. Band gap of each alloy varies with the composition and hence these materials are useful for synthesizing light emitting diodes and lasers over an extended wavelength range 650-1600 nm. These ternary and quaternary compounds are typically used in the form of thin epitaxial films deposited on GaAs, InP or GaSb substrates.

Epitaxial deposition is carried out using techniques such as liquid phase epitaxy (LPE), organometallic vapour phase epitaxy (OMVPE) or molecular beam epitaxy (MBE). Highly perfect epitaxial growth, free from structural defects, is essential for device quality material. Growth of epitaxial layers of high perfection poses certain restrictions on the lattice parameters of the layer with respect to the lattice parameter of the substrate. The lattice parameter of the layer depends on the composition. For thick epitaxial layer growth, it is essential that the lattice parameter of the layer is identical to that of the substrate. If the lattice matching is not perfect, defects such as misfit dislocations are produced which deteriorate the material properties. So, for a required band gap, composition has to be generally chosen with the lattice parameter same as the substrate. This rigid restriction of lattice matching however can be violated in very thin epi-layers for which the strain-thickness product is less than a critical value. Such layers are known as pseudomorphic strained epi-layers and contain no defects. These epi-layers have proved beneficial in optoelectronic and high frequency devices since the built-in strain alters the bandgap and the bandstructure of the material.

Semiconductor laser diodes have evolved from the original homojunction p-n diodes to double heterostructure (DH) lasers to quantum well (QW) lasers. A present day laser diode has typically five functional layers: two cladding layers each about one micrometer thick, one of which is n-type and the other p-type and have the largest band gap in the laser structure. The cladding layers flank two 0.1-0.2 micrometer thick, undoped barrier layers of smaller band gap. The relatively low refractive index cladding layers with the higher refractive index barrier layers together form a waveguide in which the generated light is confined and guided. A very thin active layer of smallest band gap is embedded between the barrier layers and is located at the center of the structure. Light is generated by the recombination of the injected electrons and holes in the active layer. Apart from these layers there will be a heavily doped n type buffer layer right above the (n+ type) conducting substrate and a contact layer of p type conductivity at the top. Thus, a semiconductor laser requires a sequential deposition of several thin layers of III-V compound semiconductors and their alloys with well controlled thickness, composition and doping.

Historically, AlGaAs/GaAs lasers were the earliest to be synthesized and studied extensively due to excellent lattice matching between AlAs and GaAs. The active GaAs layer in these lasers was usually 100-200 nm thick, and the emission wavelength was centered at about 870 nm. Emission wavelength can be altered by varying composition of the active layer, say by introducing aluminum. In the next series of developments, the thickness of GaAs active layer was reduced to < 10 nm. Such thin active layer together with adjacent barrier layers forms a quantum well (QW) in which electrons and holes are confined and energy levels are quantized. As a result, the effective band gap of the active layer (and the emission wavelength of QW laser) changes with the width of the quantum well. Laser wavelength changes if there is a strain in the active layer. Strain can be introduced by using a ternary/quaternary alloy as the active layer with lattice parameter different from the substrate. As expected, the band gap of the active layer depends on the alloy composition. Additionally, strain further alters the band gap. As remarked earlier, the strain can be accommodated without producing defects if the layer thickness is kept below a critical value. Quantum well lasers and strained layer lasers generally employ extremely thin active layers (~10 nm) grown by OMVPE and MBE. It is very difficult to grow very thin strained layers using liquid phase epitaxy. This thesis describes our efforts in synthesizing pseudomorphic strained layers (~50 nm thick) of GaAsP and GaAsSb in AlGaAs/GaAs heterostructures to yield lasers emitting in 800-900 nm range.

This thesis consists of five chapters. We shall describe briefly the salient features of the topics covered in each chapter below.

Chapter 1 is an introduction to semiconductor heterostructures describing briefly:

(i) materials used and their characteristics, (ii) historical aspects and development of homojunction and heterojunction lasers, improvements due to double heterostructure, (iii) use of lattice matched / strained heterostructures in light emitters and detectors and (iv) motivation for this work, viz. 'Investigation of multilayer AlGaAs/GaAs laser diode structures containing extremely thin strained / non-strained active layers.'

In ***Chapter 2,*** we shall describe the experimental techniques used in the course of this work: (i) synthesis of single layers and multilayer heterostructures (ii) characterization of heterostructures (iii) fabrication of laser diodes and characterization of devices. A brief outline of these topics follows.

(i) In this work, synthesis has been done using low-temperature liquid phase epitaxy over a temperature range 700^0-400^0C. Since long time, LPE has been used for synthesis of structures used for fabrication of laser diodes. Most of the early LPE growth experiments of AlGaAs/GaAs materials using multibin slider graphite boats were done at temperatures above 800^0C. At these temperatures, growth rates are typically 1-1.5 μm/minute for GaAs and it is difficult to grow very thin layers controllably. Hence it is necessary to reduce the growth temperature considerably in the 600-700^0C range. However at low temperatures, non-wetting of the substrate surface with the solution becomes a serious problem, particularly with the solutions containing aluminium because of the formation of an oxide film over the solution. Zh. I. Alferov and his colleagues at A. F. Ioffe Physico-Technical Institute, Russia solved this problem by using a novel ‘piston’ type boat in which the growth solution is pushed over the substrate through a narrow channel, thereby removing any oxide film present on the surface of the solution. We use this scheme in the experiments described in this thesis. The solutions are displaced sequentially during the growth of the designed heterostructure. Details of a piston type graphite boat fabricated at TIFR and another at A. F. Ioffe Physico-Technical Institute, Russia will be given in this section. Phase diagram data for AlAs-GaAs materials is well known over temperature range 1100^0C-400^0C and the solution compositions can be computed using known formulae from the literature. Low temperature phase diagram data for growing the active layers $GaAs_xP_{1-x}$ and $GaAs_xSb_{1-x}$, (T_g~650^0C) is not readily available. Hence, we have calculated solution compositions required to grow these alloys in the range [1-x = 0-0.1]. Calculations are based on regular solution model and details are given in this section.

(ii) In this section we provide description of the methods used for characterizing the grown materials listed below.

(a) Surface morphology of undoped and (Te, Ge, Mg) doped GaAs and AlGaAs single layers is studied using Nomarski interference contrast microscopy. Thickness of various layers is evaluated using cross-section of heterostructures recorded using scanning electron microscopy.

(b) Electrical measurements: i) Mobility and carrier concentration in single GaAs and $Al_xGa_{1-x}As$ ($x=0.3$) layers are obtained using Hall measurements. ii) Doping profile of heterostructures is obtained using electrochemical C-V profiling in which carrier density and conductivity (n/p) type is recorded while etching the structure electro-chemically.

(c) XRD measurements: i) Double crystal x-ray diffraction plots are obtained from samples with and without P or Sb. ii) Simulated profiles with model sample structures are compared with experimental plots to estimate thickness, aluminium content of each layer and P/Sb content of active layer.

(d) Optical measurements: i) Photoluminescence spectroscopy is used to determine optical quality of single layers and heterostructures, from the luminescence signal strength and full width at half maximum (FWHM) of the spectrum. ii) Composition of each AlGaAs layer is obtained from position of the peak in the spectrum for single layer as well as for number of layers in a multilayer heterostructure.

(iii) We have developed a quick turn around process of fabricating laser diodes from the heterostructures synthesized in our laboratory. The process gives electrically isolated devices on bars of 0.25 to 1mm resonator length containing individual devices of 100-200 μm aperture. Light-output versus current characteristics of laser diodes are measured to check the lasing and to determine the threshold current. The emission spectrum is also measured to obtain lasing wavelength and confirm laser operation.

In ***Chapter 3,*** we shall describe the growth experiments leading to the synthesis of variety of multilayered structures using AlGaAs/GaAs materials in the temperature range 700^0-400^0C. These experiments are: (i) growth of single layers of undoped GaAs. (ii) growth of undoped and doped $Al_xGa_{1-x}As$, [x = 0-0.3] layers using Sn, Te (n type dopants) and Ge, Mg (p type dopants). (iii) synthesis of five-layer structures to understand the problem of solution mixing and to test the feasibility of growing 5-10 nm thick layers, and eight layer structures for laser diodes. Layers in typical test structures are as follows:

(a) synthesis of five layer heterostructure consisting of -
1] n-doped lower cladding layer: n-$Al_{0.6}Ga_{0.4}As$: Te
2] undoped lower barrier layer: $Al_{0.3}Ga_{0.7}As$
3] active layer: undoped GaAs
4] undoped upper barrier layer: $Al_{0.3}Ga_{0.7}As$
5] undoped/doped upper cladding layer: $Al_{0.6}Ga_{0.4}As$ / p-$Al_{0.6}Ga_{0.4}As$: Mg

(b) synthesis of eight layer heterostructure for laser diodes consisting of -
1] n-doped buffer layer: n-$Al_{0.3}Ga_{0.7}As$: Te
2] n-doped lower cladding layer: n-$Al_{0.6}Ga_{0.4}As$: Te
3] undoped lower barrier layer: $Al_{0.3}Ga_{0.7}As$
4] active layer: GaAs, or GaAsP or GaAsSb (*)
5] undoped upper barrier layer: $Al_{0.3}Ga_{0.7}As$
6] p-doped upper cladding layer: p-$Al_{0.6}Ga_{0.4}As$: Mg
7] p-doped spacer layer: p-$Al_{0.3}Ga_{0.7}As$: Mg
8] p-doped cap layer: p-GaAs: Mg

[(*) Thin active layer consists of either GaAs or GaAsP or GaAsSb]. A number of heterostructures with different amounts of P and Sb in the active layer have been grown.

The main problems to be solved in synthesizing the structures listed above are:

We need to establish the amounts of aluminum and arsenic to be added to liquid gallium solvent to saturate each solution at a specific temperature, and to achieve the desired aluminum content in each of the above layers. Some layers such as the cladding layers, are quite thick (~1 µm) whereas the active layers are quite thin (50-100nm), and hence we need to establish the temperature interval and the growth duration of each growth separately before attempting multilayers. Since the growth in the LPE process occurs by supercooling, growth of multilayer structures is done over a wide range of temperatures between 700^0-400^0C. Observations of surface morphology, measurements of cleaved cross sections, photoluminescence and x-ray diffraction were useful for evaluating various parameters of the grown layers. Additionally, some layers are doped n type and some are doped p type, while some others are undoped. We need to establish the background doping of undoped layers and the amount of particular dopant to be added to the solution to achieve a desired doping level. We have conducted extensive single-layer growth experiments to establish these aspects. We have found some specific morphological features obtained with different dopants. Smooth surface morphology is of course necessary for device-quality materials and hence we optimized our growth experiments to deposit layers reproducibly with required doping level and having a smooth morphology. Hall measurements were used for evaluating doping experiments. For multilayer structures, electrochemical C-V profiling technique was used to record doping levels in various layers.

In going from the single layer to multilayer growth using several solutions, we encountered the problem of mixing between the solutions, which occurs when a solution pushes out the earlier one for the growth of the subsequent layer. Apart from mixing, there could be some grading and variations due to manual operation of solution displacements. Our experiments provide some measure of these aspects. Experiments have been conducted to establish the amounts of P (or Sb) source material used in the solution and the corresponding amount of P (or Sb) incorporated in the epitaxial layer. This was critical in experiments involving synthesis of GaAsP and GaAsSb active layers. Since we need to grow a very thin (50-100 nm) active layer, it was necessary to establish the optimum growth parameters such as growth temperature, solution supersaturation, and growth duration. X-ray diffraction measurements were very useful in characterization of the structures containing these layers, particularly to establish that they were fully strained and pesudomorphic with the GaAs substrate. Ultimate test of these strained active layers being defect free was in the operation of laser devices. These aspects are covered in chapter 4.

In **Chapter 4,** we shall describe electro-optical characterization of heterostructures and laser diodes fabricated from the structures synthesized by us. The spectral measurements of electroluminescence from heterostructures will be presented. These will be compared with the photoluminescence spectra wherever possible. Also presented are the results of L-I and spectral characteristics of laser diodes. Analysis of the spectral peaks is done for the composition of the active layer material by including (i) Al content due to solution mixing and (ii) strain effect in the layer containing P or Sb. Since the layers are fairly thick (~50 nm), quantum confinement effects are neglected. Results of this analysis are compared with the corresponding results obtained from XRD measurements.

Thus, a correspondence between the material composition, strain, photoluminescence and XRD measurements is established. Finally, a comparison is made between the values of liquidus/solidus obtained from phase diagram calculations and the corresponding values obtained from the XRD and electro-luminescence experiments. An interesting dependence of the solidus values on the strain is obtained that seems to be of general significance.

In **Chapter 5**, we shall summarize salient features of the work as listed below and indicate the scope for future work.

(vii) Piston boat is found suitable for low temperature (700^0-400^0C) liquid phase epitaxy and useful for synthesizing device quality heterostructures with undoped, n type (Te), p type (Ge, Mg) AlGaAs and GaAs multilayered structures.

(viii) Thin epitaxial layers (about 50 nm thick), for the active layer of laser diodes can be synthesized reproducibly using LPE.

(ix) Fully-strained, defect-free, thin pesudomorphic layers such as GaAsP and GaAsSb can be synthesized on GaAs substrates using LPE. These layers are of device quality and can be used for the active region of strained-layer laser diodes.

(x) A disadvantage of piston boat is an unavoidable mixing of successive solutions with the preceding ones. About 3-7 % Al is incorporated in GaAs grown from a solution that displaces the solution used for growing $Al_{0.3}Ga_{0.7}As$ layer. This has to be taken into account in the design of a layer, particularly the active layer.

(xi) Emission wavelength of laser diode fabricated from such heterostructure with GaAs active layer is in 820-850 nm range. This variation is due to aluminium incorporation because of solution mixing.

(xii) Incorporation of P produces tensile strain whereas compressive strain is produced by incorporation of Sb. The incorporation of P/Sb, changes the active layer material band gap from that of GaAs and hence different emission wavelengths can be obtained. Thus, with P incorporation lasers emitting at 795, 818, 830 and 833 nm are obtained whereas with Sb incorporation, lasers emitting at 855, 870, 880 and 900 nm are obtained. It is shown by x-ray measurements that the layers are pseudomorphically strained.

(xiii) The thinnest layers grown reproducibly during this work are in 40-50 nm range. It seems desirable to (a) automate the movements of the solutions and (b) improve the saturation/growth temperature control to establish growth of thinner layer (~10 nm) reproducibly. Another aspect would be to incorporate such layers in devices and compare their performance with the devices synthesized using MBE and OMVPE.

(xiv) This work can be extended using GaAs and other substrates, such as InP and GaSb, with active layer of a variety of alloys such as InGaP, InGaAsP, AlGaAsSb, and InGaAsSb to obtain lasers emitting in 650-1600 nm range.

(xv) LPE method is simple, relatively versatile and inexpensive. However, whether it is suitable for scaling up for industrial production of laser diodes emitting in 650-1600 nm range needs to be established.